Superconducting high current magnetic Circuit: Design and Parameter Estimation of a Simulation Model

CERN-THESIS-2017-120
01/08/2017

Bachelor Thesis

Superconducting high current magnetic Circuit: Design and Parameter Estimation of a Simulation Model

Hochschule Offenburg

Alexander Kiefer

Stöcken 1

77770 Durbach

Elektrotechnik/Informationstechnik

Supervised by: Dr. Werner Reich

CERN

European Organisation for Nuclear Research

Geneva, Switzerland

TE-MPE-EE

Supervisor: M.Sc. Mateusz Bednarek

August 2017

Abstract

The Large Hadron Collider (LHC) utilizes superconducting main dipole magnets that bend the trajectory of the particle beams. In order to adjust the not completely homogeneous magnetic field of the main dipole magnets, amongst others, sextupole correctcorrector magnets are used. In one of the 16 corrector magnet circuits placed in the LHC, 154 of these sextupole corrector magnets (MCS) are connected in series. This circuit extends on a 3.35 km tunnel section of the LHC. In 2015, at one of the 16 circuits a fault was detected. The simulation of this circuit is helpful for finding the fault by applying alternating current at different frequencies.

Within this Thesis a PSpice model for the simulation of the superconducting corrector magnet circuit was designed. The physical properties of the circuit and its elements were analyzed and implemented. For the magnets and bus-bars, sub-circuits were created which reflect the parasitic effects of electrodynamics and electrostats. The inductance values and capacitance values of the magnets and the bus-bars were defined by geometric calculation, geometric simulation and evaluation of circuit simulations. PSpice and Matlab are the used software programs for simulations and evaluations.

The real fault in the circuit is defined as a ground fault. By integration of the inductive coupling between the bus-bars, it is also possible to mimic the behavior of the circuit at ground fault conditions. Through the final simulations it was possible to determine the possible position of the real earth fault on a small part in the tunnel section.

Kurzfassung

Der Large Hadron Collider (LHC) nutzt supraleitende Haupt-Dipol-Magnete, welche die Partikelstrahlen in einer Kreisbahn halten. Um das nicht vollständig homogene magnetische Feld der Haupt-Dipol-Magnete nachzujustieren, werden unter anderem Sextupol Korrekturmagnete (MCS) verwendet. In einem der 16 Korrekturmagnet-Stromkreise sind 154 dieser Sextupol Korrekturmagnete (MCS) in Reihe geschaltet. Einer dieser Stromkreis erstreckt sich auf einen 3,35 km langen Tunnelabschnitt des LHC.
In 2015 wurde bei einem dieser 16 Stromkreise ein Fehler erkannt. Für eine Fehlersuche ist es geeignet, den Stromkreis zu simulieren. Hierbei ist das Stromkreisverhalten bei verschiedenen Frequenzen ausschlaggebend.

Im Rahmen dieser Arbeit wurde ein PSpice-Modell für die Simulation eines supraleitenden Korrekturmagnet-Stromkreises entworfen. Die physikalischen Eigenschaften des Stromkreises mit seinen Elementen wurden analysiert und nachgebildet. Für die Magnete und Stromschienen wurden Subcircuits entworfen, welche die parasitären Effekte von Elektrodynamik und Elektrostatik widerspiegeln. Die Werte der Induktivitäten und Kapazitäten von Magneten sowie Stromschienen wurden durch geometrische Berechnung, geometrische Simulation und Auswertung von Stromkreissimulationen definiert. Die zur Simulation und Auswertung verwendeten Softwareprogramme sind PSpice und Matlab.

Der tatsächliche Fehler im realen Stromkreis ist ein Erdschluss. Durch die Integration der induktiven Kopplung zwischen den Stromschienen ist es möglich, auch das Verhalten des Stromkreises bei einem vorhandenen Erdschluss nachzuahmen. Mit den finalen Simulationen war es möglich, die Position des realen Erdschlusses auf einen kleinen Abschnitt des gesamten Magnetstromkreises zu bestimmen.

Acknowledgement

I herewith would like to express my acknowledgements and gratitude towards all the people who offered their support and advice during this Thesis.

A Special thanks goes to my supervisor Mateusz J. Bednarek at CERN. With his extensive experience, he promoted this project significant. Various measurements in the tunnel were made possible with his help.

I also want to thank the "Simulations of Transient Effects in Accelerator Magnets" -team around Marco Prioli, Michal Maciejewski and Lorenzo Bortot, which supported me with every question about simulation and data analysis.

Furthermore, I would also like to thank Krzysztof Stachon and Vasilios Karaventzas, who helped me with uncertainties regarding data collection in PSpice and Matlab.

Finally, I would like to thank the entire TE-MPE team, who has given me the opportunity to write my Bachelor Thesis at CERN.

STATUTORY DECLARATION

Hiermit versichere ich eidesstattlich, dass die vorliegende Bachelor-Thesis von mir selbstständig und ohne unerlaubte fremde Hilfe angefertigt worden ist, insbesondere, dass ich alle Stellen, die wörtlich oder annähernd wörtlich oder dem Gedanken nach aus Veröffentlichungen, unveröffentlichten Unterlagen und Gesprächen entnommen worden sind, als solche an den entsprechenden Stellen innerhalb der Arbeit durch Zitate kenntlich gemacht habe, wobei in den Zitaten jeweils der Umfang der entnommenen Originalzitate kenntlich gemacht wurde. Ich bin mir bewusst, dass eine falsche Versicherung rechtliche Folgen haben wird.

Offenburg, den 18. August 2017

Contents

List of Figures

List of Tables

Chapter 1

Introduction CERN and magnet circuits

The European Organization for Nuclear Research (CERN) is a research organization that operates the largest particle physics laboratory in the world. Established in 1954, the organization has 22 member states and is based in a suburb of Geneva on the France–Swiss border. CERN's main function is to provide particle accelerators of different types like linear- or circular accelerator and other infrastructure needed for high-energy physics research. Numerous experiments have been constructed at CERN as a result of international collaborations. Figure 1.1 illustrates an overview of these experiments and accelerators.

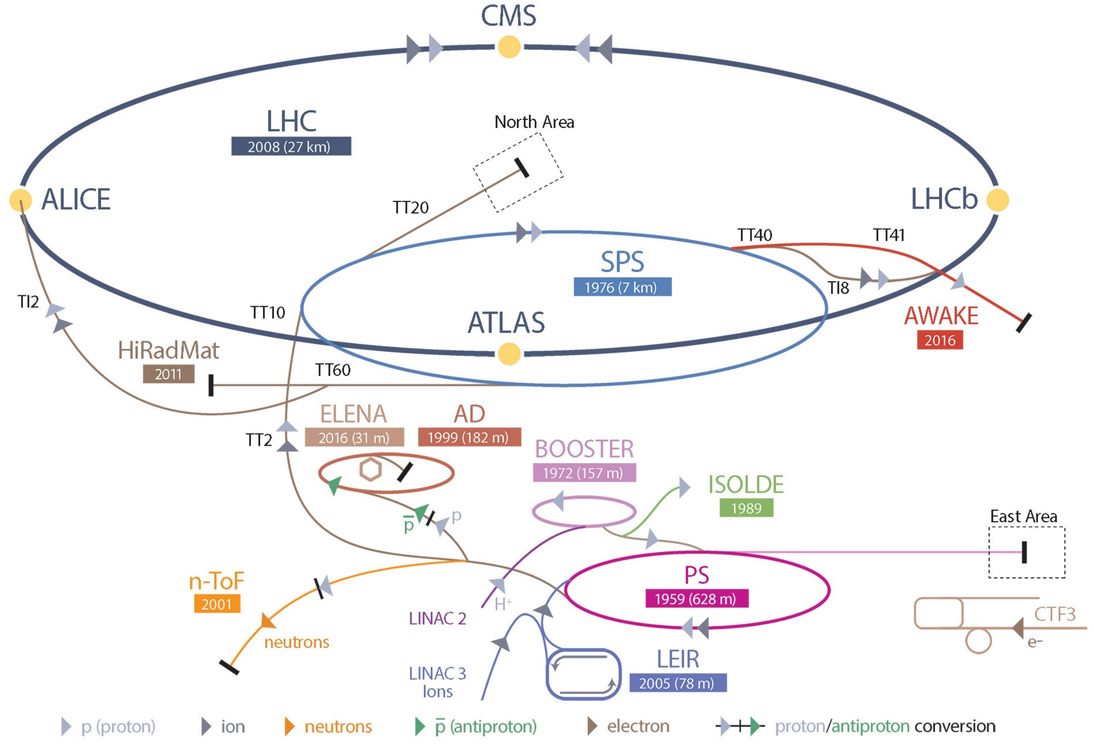

FIGURE 1.1: The up-to-date CERN research complex

1.1 Facts and figures about CERN

Currently there are ten different active accelerators in the CERN laboratory and it operates the world's largest cryostatic plant network. To provide the electrical energy to run the whole complex, it is directly connected to the 400 kV power grid from the State energy provider of France (EDF). The power consumption reaches in peak times the amount of the average consumption of a city with 300.000 residents. 3200 staff members and more than 10.000 visiting scientist are in touch with the CERN laboratory. This organization is financed by the contribution of 22 paying Member States, which results in about one billion Euros per year[1]. The German due is around 20% out of it. One of the main targets is the deep basic research in the composition of matter. Among the greatest milestones in the study of unknown or unseen correlations in particle physics are[1]:

- The discovery of neutral currents in 1973.
- The discovery of W and Z bosons in 1983.
- The determination of the number of light neutrino families in 1989.
- The first creation of antihydrogen atoms in 1995.
- The discovery of direct charge conjugation parity violation in 1999.
- The isolation of 38 atoms of antihydrogen 2010.
- Maintaining antihydrogen for over 15 minutes in 2011.
- The proof of the existence of the Higgs boson in 2012.

1.2 The Large Hadron Collider LHC

The purpose of a particle accelerator is to accelerate charged particles to near light speed and to load them with high energies. During the acceleration a gradual transition takes place causing relativistic effects to become dominant. The acceleration is provided by a series of radiofrequency cavities, in which an alternating electro-magnetic field exerts a driving force on the particles, which are grouped in bunches. At the LHC the strategy is to run particles through the same set of cavities some 11 thousand times per second in a storage ring. In order to keep the particle beams inside the storage ring they need to be constantly bend towards its center, which is achieved using a Lorentz force provided by the magnetic field generated by the main bending dipole magnets. In addition, groups of bending dipoles are alternated with quadrupole and sextupole magnets, which are required to prevent the beams from diverging[2]. In this circular collider bunches of particles in the beams are accelerated in opposite directions in two adjacent circular beams, which cross over at so-called interaction points. At these points the bunches intersect causing some of their particles to collide. Following mass–energy equivalence $E = mc^2$, the kinetic energy of the collision is transformed into a shower of particles including those to be discovered. By analyzing the trajectories physicists are eventually able to discover the existence of new fundamental particles and can determine their properties. Presently the most performing particle accelerator in the world is the LHC at CERN, that is illustrated in Figure 1.2. The circumference of the LHC ring, located in a tunnel complex 40 m up to 140 m under the earth, is about 27 km[2]. In four interactions points the two circulating proton beams intersect. Around these points large detectors named ATLAS, ALICE, CMS and LHCb were built. These detectors are designed and optimized for tracking the debris resulting from the particle collisions. The LHC is constructed of 1232 15-meters-long superconducting main bending magnets, which have a nominal magnetic dipole field of 8.33T when the machine is operating at its maximum collision energy of 14TeV[3].

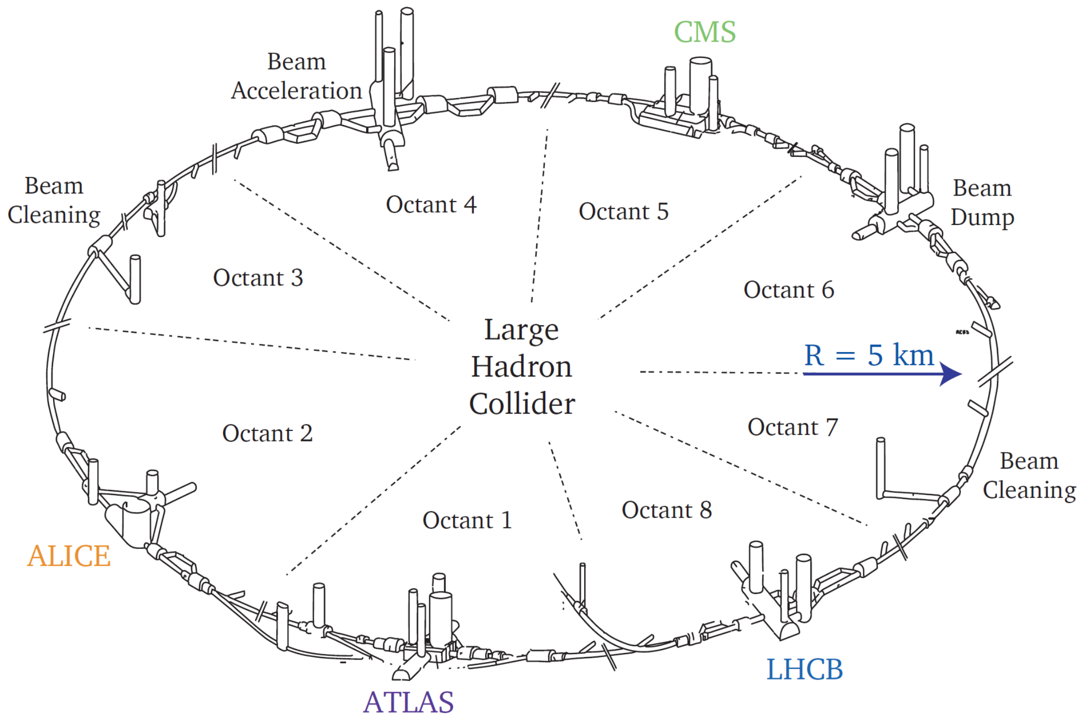

FIGURE 1.2: Tunnel complex of the Large Hadron Collider

1.3 Structure of departments

This project is executed in the Electrical Engineering (EE) section within the Machine Protection and Electrical Integrity Group (MPE), one of the many groups that are present at CERN. The function of the MPE group is to support the Large Hadron Collider operation, maintain and develop state-of-the art technology for magnet circuit protection and interlock systems for the present and future accelerators, magnet test facilities and CERN hosted experiments. The MPE-EE section as part of the Technology Department (TE) mainly provides support for the LHC, and therefore other particle accelerators will be left out of the problem orientation. To get a better overview of the Technology Department structuring, Figure 1.2 is inserted below[4].

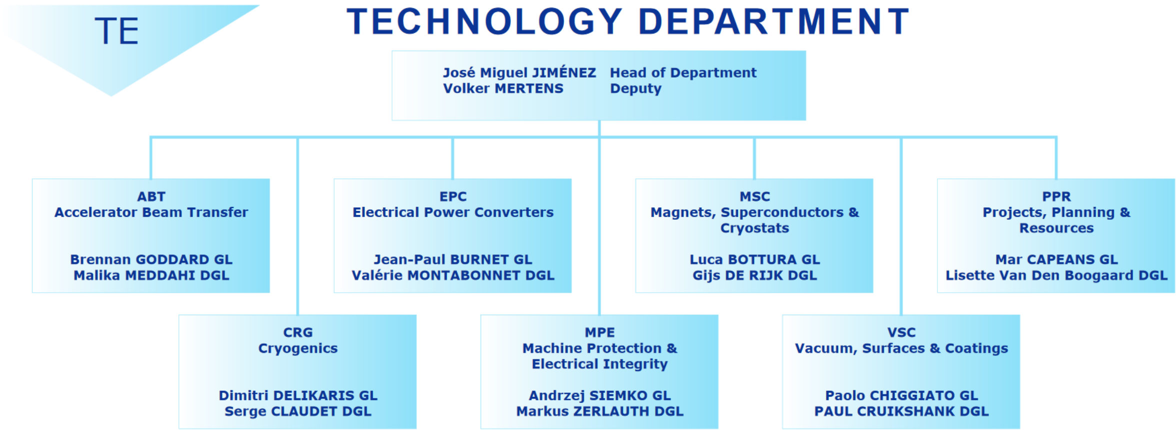

FIGURE 1.3: Structuring of the Technology Department at CERN

1.4 Problem description and main focus

In 2015, a fault in one of the correction magnet circuits was detected during the routine ramp-up of the LHC, and the process was then terminated. It turned out that the faulty circuit is a 600A sextupole magnet circuit with 154 magnets connected in series in Sector 7-8. These 154 magnets are distributed in a 3.35 km part of the arc and the length of the circuit from the electrical point of view is 6.7 km. At every main dipole magnet two of these sextupole magnets are attached. MCS is the acronym for one corrector magnet and stands for Magnet Corrector Sextupole. This particular faulty circuit located in sector 7-8 is named RCS.A78B2.

The main task for the MCS magnets is to compensate persistent current sextupole fields of the main dipole magnets[5]. The MCS is a cold bore magnet with iron yoke. The coils are made of a NbTi conductor, that is cooled to 1.9 K during standard operation. In the original design, the magnet consists of three splice-free sub-coils, which are placed with an automated winding process into pockets of prefabricated support cylinders[5]. Any assembly process of sub-coils with potential misalignment is eliminated[6]. The magnet uses a Kapton-wrapped mini-cable, which allows helium penetration into the vicinity of the conductor, increasing its cryogenic stability[5]. Kapton is a thin polyimide material which can remain stable in a wide range of temperatures (0 K - 673 K). Eliminating all internal splices from the magnet significantly reduces heat loads and the risk of magnet failure during operation. In Table 1.1 the key parameters of the LHC MCS are summarized[6].

TABLE 1.1: Main parameters of the MCS corrector magnet

Attribute	Unit	Value
Field gradient	T/m^2	1657
Integrated field at 10 mm	Tm	0.0187
Nominal current	A	600
Effective length	mm	113
Overall length	mm	160
Bore of magnet	mm	60
Operating temperature	K	1.9

In addition to the high requirements for precision and performance, there is also a clear limitation in the available space directly behind the main dipole magnets. For this reasons, the layout of this magnet, which is point in Figure 1.4, was designed specifically for the LHC[5].

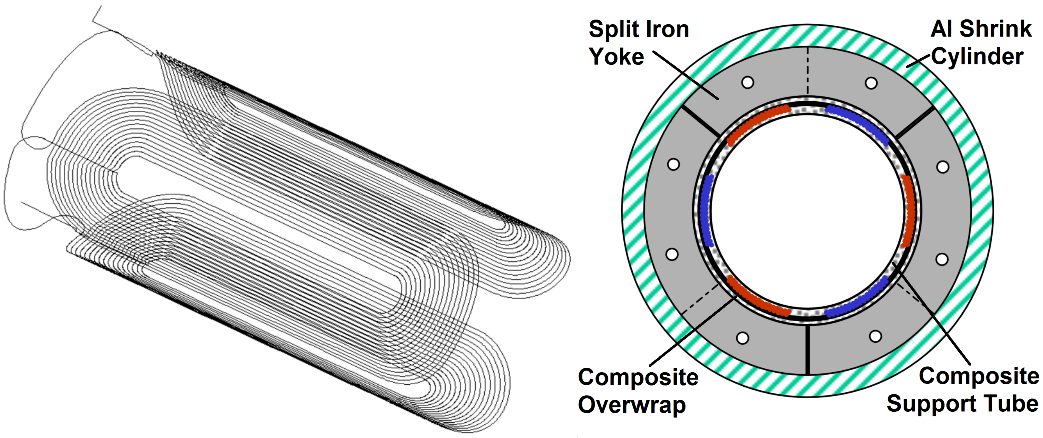

FIGURE 1.4: Coil-cross section and cross section of the MCS magnet

After the detected fault during the LHC operation, the first measurements on the circuit were undertaken promptly. However, after the first analysis of the measured data no meaningful statements about the error could be drawn. Nevertheless three well-founded assumptions could be made with great probability. On one hand, the fault is intermittent and is a function of the current supply of other magnet circuits. On the other hand, it is a low-resistance contact between the circuit and the earth potential. Furthermore the fault is located in the cold part of the magnet chain. This basic conditions compose the fundament of this Thesis with the following aims:

- *Creation of a simulation model:* Since the measurements of the RCS circuit directly in the machine are transfer function measurements (TFM), a simulation model which mirrors the circuit behavior and is suitable for this kind of simulation, needs to be created. PSpice as part of the ORCAD Cadence program bundle and Matlab from MathWorks are suitable software programs for this task.

- *Best possible determination of the fault position:* The final goal is to find the exact position of the failure in the magnet circuit. However, a model is by definition fault-prone and thus can not exactly reproduce the complex circuit and its behavior at different applied frequencies in this case as well.

Chapter 2

Description of physical processes

To create a proper simulation model that represents the behavior of the RCS magnet circuit, a basic knowledge about some electrical and physical processes is required. Looking at the spatial extent of the circuit, the pure size immediately strikes the eye. With a length of 6.7 km as well as the in series connected magnets, the RCS circuit is not a common circuit. As in many electrical circuits, linear components such as resistive resistors, inductances and capacitances form the basic elements and characteristics of the RCS circuit.

During the standard powering with DC voltage, it is not needed to consider its behavior at AC voltage at a few Hertz and beyond. Even the weighting from the imaginary part of the current and the voltage is at standard conditions much lower. Furthermore, the thermal conditions in the cryostat forwards to extraordinary non linear electrical behavior like the magnetization effect.

The most important difference in the comparison of the RCS circuit in the LHC and most of the other high current circuits outside CERN is the circumstance of the superconducting effect. The further implications of an ambient temperature close to the absolute zero point on the electrical behavior are explained in more detail in the following sub-chapters.

2.1 Superconductivity in circuits

Superconductivity is, as the name of the phenomenon suggests, known as a property in certain materials under which the resistivity of said material vanishes completely[7]. This observation was how the effect was first seen. However, another property is of more fundamental importance than the conductivity itself. This physical behavior is called the Meissner effect and it is seen as a superconductor expels an externally applied magnetic field by induced supercurrents on the surface of the material. In addition to characterize the Meissner effect, it is necessary to discuss the critical surface conditions of a superconducting material as well as the difference between a type I and a type II superconductor[8]. Table 2.1 lists some key discoveries related to superconductivity and the associated theories which explain the phenomena[9].

TABLE 2.1: Important discoveries in the superconductivity history

Year	Theory
1908	Liquefaction of Helium, at 4.2 K
1911	Superconductivity discovered in Mercury, at 4.1 K
1933	Meissner–Ochsenfeld effect observed
1950	Ginzburg–Landau theory of superconductivity is formulated
1957	Bardeen–Cooper–Schrieffer (BCS) theory formulated
1962	Josephson effect discovered
1986	High Temperature Superconductivity (HTS) discovered

As a field of science superconductivity arose quickly after Kammerling Onnes managed to liquefy Helium in 1908[9]. The importance of this technological development lies in the fact that first explored simple superconducting materials show merely Low Temperature Superconductivity (LTS).

TABLE 2.2: Critical temperatures of important superconducting materials

Material	Critical temperature T_c in K
NbTi	9.80
Nb_3Sn	18.05
Nb_3Ge	23.20
Nb_3Al	17.50
NbN	16.00
C_{60}	19.20
Hg	4.15
V_3Ga	16.50
V_3Si	17.10
$YBa_2Cu_3O_{6.0}$	90.00
Rb_2CsC_{60}	31.30
MgB_2	39.00

Several materials are now known to be superconducting. It would be worth mentioning that numerous metallic elements exhibit this property. This includes, except from Copper, Silver, Gold and the elements from the first and second main group of the periodic system all metallic elements. Table 2.2 shows a list of some important superconducting alloys[10].

NbTi is used in the superconducting magnets currently installed in the LHC. Nb_3Sn is presently experiencing heavy technological development, in some cases with the intention of replacing the actual use of NbTi. YBCO is an example of a material showing High Temperature Superconductivity (HTS) characteristics. This denotes that the critical temperature T_c is above the maximum temperature of liquid nitrogen from 77K (-196 deg. C) at standard pressure. It was discovered in the late 80's of the 20th century as the first example of such a material. M_gB_2 is another example of superconductor alloy, although at a far lower temperature than YBCO. The interest in this material lies in the low cost, simple structure and relatively high critical temperature T_c[11].

The modern definition of whether or not a material is superconducting is the demonstration of the Meissner–Ochsenfeld effect. This effect manifests in the expulsion of a weak magnetic field from the bulk of the superconductor[12]. Figure 2.1 shows the cross section of a superconducting material and how the field inside behaves as the material is cooled below the critical temperature under application of a small and constant magnetic field. The reason why the magnetic field is expelled from the inner superconductor is the surface current arise on the sphere[10]. This current is not visible mentioned in the Figure.

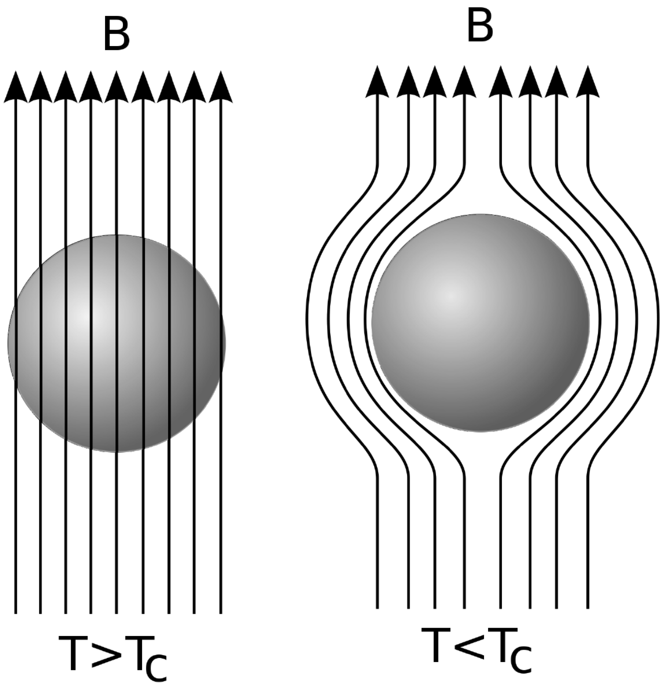

FIGURE 2.1: Demonstration of the Meissner-Ochsenfeld effect

The mathematical description of the Meissner effect is found in the London equation which states that under the application of an external field, there will arise a current density such that the external field is opposed[10].

$$\Delta \times j = -\frac{1}{\mu_0 \lambda_L^2} B \qquad (2.1)$$

$$\lambda_L = \left(\frac{mc^2}{4\pi_s e^2} \right)^{1/2} \tag{2.2}$$

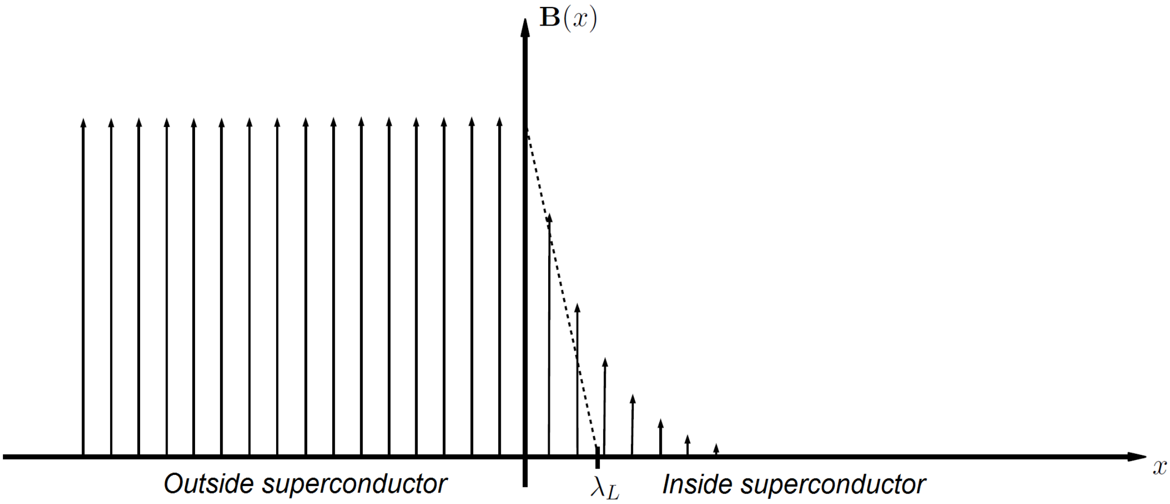

FIGURE 2.2: Penetration depth according to the London equation

The parameter λ_L is called the London penetration depth, and it describes how far into the material bulk the external field is able to penetrate[12]. Figure 2.2 illustrates the exponential screening of the applied field.

The critical temperature $\mathrm{T_c}$ is a threshold above which the superconducting state vanishes. However, also other parameters will determine the viability of the superconducting state of a material. A sufficiently large magnetic field will re-establish the normal state of the material just as a sufficiently large temperature will[10]. This field is usually denoted $\mathrm{H_c}$ as the critical magnetic field. In this context, another basic physical property called the second-order phase transition is explained.

A phase transition is known as a change in the physical presence and behavior of a material. To the first-order transition belong the activities melting and freezing, evaporating and condensation as well as sublimation and re-sublimation[9]. The resulting physical states are solid, liquid or vapour. These examples of transition are also represented by the discontinuity in density of matter and the first derivative of the free energy with respect to a given thermodynamic variable[9]. Second–order phase transitions are continuous in the first derivative, and only exhibits a discontinuity in the second derivative of the free energy with respect to thermodynamic variables[8]. Such transitions will often be characterised by discontinuous heat capacity[13]. The relevant example of such a transition is the superconducting transition. Other examples of second–order phase transitions include the ferromagnetic and ferroelectric phase transitions[9]. It is common to describe them in terms of some critical value of an environmental parameter. In many cases the critical value is the temperature, represented in the curie point for ferroelectric and ferromagnetic transitions or $\mathrm{T_c}$ for the transition from the normal to the superconducting state.

By application of the Ginzburg–Landau model for the superconducting phase transition the relations between T_c and H_c can be point[9].

$$H_c = \frac{\alpha}{\sqrt{\mu_0 \beta}}(T_c - T) \tag{2.3}$$

Regarding the external magnetic field affecting the superconductor, it is needed to note the different trend of the magnetisation curve from type I and type II superconductors. While the superconducting state at the type I superconductors collapse immediately by trespass the critical external magnetic field H_c, the type II superconductors stay superconducting[13]. There are two significant characteristic values for the magnetic field of the latter materials: H_{c1} and H_{c2}. From a field intensity of H_{c1} until H_{c2} the type II superconductor is in a magnetisation state which enables the external magnetic field enter the conducting medium in the form of narrow field tubes[12]. Figure 2.3 presents the comparison of the magnetisation curves for type I and type II superconducting materials.

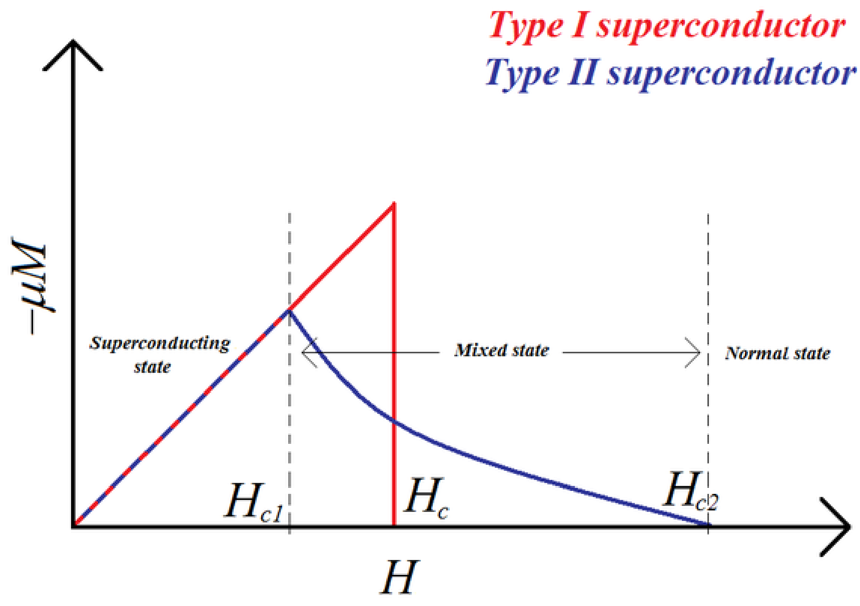

FIGURE 2.3: Magnetisation curves of type I and type II superconducting materials

Alike threatening like a strong external magnetic field or a high temperature are high currents for the ideal superconducting condition. Given by Ampére's law, a conductor carrying an electric current will produce a magnetic field at its surface. This field will penetrate the material a distance given by the penetration depth. As presented in Figure 2.3, a sufficiently high magnetic field will destroy the superconductivity. This means that a sufficiently high current or current density will be able to do the same. Furthermore, electron pairs are formed when the material merges from the normal state into the superconducting state. The BCS theory states, among other things, that if the kinetic energy of the electrons exceeds the binding energy of the electron pairs, the superconducting state breaks down[14]. Following equation highlights this limit circumstance[15].

$$n_{SC} = n_{\infty}\left(1 - \frac{mv^2}{2|\alpha|}\right) \tag{2.4}$$

All in all there are three possibilities to destroy the superconducting state:

- The temperature of the superconducting material exceeds the value of the critical temperature T_c.
- The external magnetic field exceeds the critical magnetic field H_c respectively H_{c2}.
- The value of the leaded current respectively the current density is too high.

2.2 Explanation of a Quench

A quench is the sudden transition of a superconductor to the normal state, occurring when local conditions in terms of temperature, magnetic field, or current density do not allow to continue the superconducting state. Since the heat capacity of all materials is very low at low temperature, even minor perturbations of the order of µJmm$_{-3}$ are sufficient to initiate a transition to the normal state[7]. For comparison, the energy of 4.18 Joule is required to heat one mm$_3$ of water by one Kelvin under normal conditions[13]. The occurrence of a quench is thus part of an operating superconducting magnet. Numerous disturbances occurring in superconducting magnets can lead to a quench such as flux jumps, mechanical events (conductor movement, cracking of epoxy resin), electro-magnetic transients (hysteretic loss, coupling loss, eddy current loss), heat loads (radiation, beam loss), heat leaks, or even loss of primary services like power cuts, loss of coolant or loss of insulation vacuum[16].

Superconducting magnets operate at high magnetic field and can store high magnetic energy, thus the damage potential by overheating is signifcant. Furthermore, their operating current densities are high, hence when in the normal state joule heating will increase the temperature in the coils very quickly. During and after a quench, part of the magnetic energy stored in the magnet, varying from a minimal fraction to its totality, is converted into heat deposited in the winding pack. One of the primary concerns of magnet design is assuring that the temperature reached in the coil hot-spot at the end of the discharge is maintained below the allowable limit. The most common methods for protecting superconducting magnets can be classified according to two characteristics[17]:

- *Discharge mechanism:* protection systems can rely on partly extracting the magnet energy and dissipating it outside the coil or on uniformly spreading the stored energy into the winding pack by forcing a transition to the normal state of a large fraction of the coil.

- *Passive/active systems:* active protection systems require an external trigger to be activated, such as an electronic signal generated after the detection of a quench. Passive protection systems are activated by the occurrence of the quench itself.

Completely passive protection is the simplest, most reliable, and least expensive magnet protection method, because it does not employ additional equipment and does not rely on active triggering which may fail[15]. Once a transition to the normal state occurs, local ohmic heat is generated in the coil hot-spot. The non-superconducting zone then propagates to other sections of the coil by means of thermal conduction. If this process is sufficiently fast, the electrical resistance developed in the normal zone can cause a discharge of the magnet current before the temperature of the coil hot-spot exceeds safe limits[18]. In this condition, most of the magnetic energy stored in the magnet is deposited in the winding pack during the discharge. A superconducting coil can be designed so as to guarantee that the local ohmic heat in a normal zone is smaller than the heat extraction to the cryogen bath at 1.9 K, and hence the superconductor switches back to the superconducting state after a quench. In practice, completely passive self-protection is limited to small coils with low stored energy and low stabilizer current-density[18].

Another passive protection method consists in installing one or multiple by-pass elements across the coil to protect. Valid by-pass elements include resistors, single diodes, back-to-back diodes, or more complex protection schemes composed of combinations of these[17]. Quench protection based on by-pass elements is a good solution for superconducting magnets characterized by low to medium stabilizer current-densities, due to its reliability and its low cost compared to active protection systems[18].

The relatively slow response of passive protection systems make them incompatible with the very fast energy discharge required to protect large but compact superconducting coils with high current density and stored energy. Thus, active systems have to be employed which detect the occurrence of a quench, switch off the circuit power source, and promptly force the discharge of the magnet stored energy[15]. An active protection system relying on an external energy discharge is called an energy-extraction system (EE). Upon quench detection, a switch is activated to divert the circuit current to a collocation of low resistance resistors and largely dimensioned capacitors, in which part of the magnet energy is deposited.

An alternative quench protection strategy is required based on actively transferring the superconductor to the normal state, hence forcing the discharge of the magnet stored energy with the electrical resistance developed in the coil itself. With respect to an external energy-discharge system, active transfer of the superconductor to the normal state also offers a more uniform profile of the voltages and stress within the coil due to the distribution of inductive and resistive components over the conductor length. Conventional active internal-discharge systems rely on quench heaters (QH), consisting of stainless steel strips with thickness of a few tens of micrometer which attached close to coil[15]. During powering the QH's, the stainless steel strips heat up and stoke the magnet coil as well. Nowadays highest performance superconducting magnets are protected by active systems relying on active heating of the conductor.

2.3 Magnetizing effects at low current

In order to represent a superconducting magnet circuit, it requires not only the basic knowledge abut the electro-technical elements of resistance, capacitance and inductance. In the field of superconductors and their circuits, a number of additional properties and phenomena must also be taken into account. Their identification and analysis required several decades. In the following sub-chapters some, sometimes nonlinear phenomena are shown.

2.3.1 Persistent Magnetization

The basis for the persistent magnetization of superconducting circuits is the unintentional generation of permanent currents in the conductors. However, a superconductor has the property that it is able to transfer the electrical current in a barrier-free manner. For this reason, one also speaks of persistent magnetization currents, which generate a permanent magnetic field and an accompanying magnetization after the latter has been induced[19]. This means that the circuit had to be energized from the external side already. That's why this phenomena depends on the history of the magnet circuit, regarded to the supply of electricity. In order to return to zero persistent magnetization, the superconductivity has to be destroyed by heating and subsequently cooling down the circuit.

2.3.2 Eddy currents

Eddy currents are loops of electrical current induced within conductors by a changing magnetic field in the conductor, due to Faraday's law of induction. Eddy currents flow in closed loops within conductors, in planes perpendicular to the magnetic field. They can be induced within nearby stationary conductors by a time-varying magnetic field created by an AC electromagnet or transformer, for example, or by relative motion between a magnet and a nearby conductor[12]. The magnitude of the current in a given loop is proportional to the strength of the magnetic field, the area of the loop, and the rate of change of flux, and inversely proportional to the resistivity of the material[20].

The eddy current loss describes a loss, generated by induced currents owing in normal conducting material in contact with the superconductor, such as added stabilizing material. Any conductor subject to a changing magnetic field will have shielding- respectively eddy currents induced in it, in a direction so such as to oppose the applied field change. If the conductor in question is of a resistive metal such as copper, the eddy currents will decay due to this resistance.

In addition, a changing magnetic field induces eddy currents not only in the cable but also in the copper spacers (wedges) in between the conductor blocks, the magnet collars and the iron yoke[21]. The collars and the iron yoke are made of laminations to reduce the strength of the magnetic field. The eddy currents in the copper spacers cause these parts to behave as secondary inductances that extract energy[12].

Eddy current as part of the dynamic losses contributes to the magnetizing effects and thus the decrease in inductance[21]. The schematic representation of eddy currents are shown in figure 2.4.

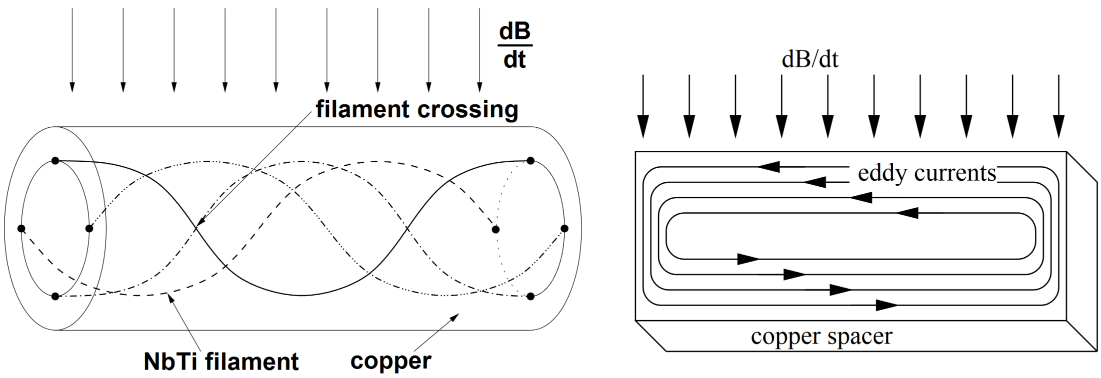

FIGURE 2.4: Schematic representation of eddy currents

2.3.3 Interfilament coupling currents (IFCC)

Due to the presence of a matrix out of copper and superconducting material in the cable, there are eddy currents, specifically referred to as Inter Filament Coupling Currents (IFCC). When the cable is exposed to a changing field, coupling currents flow between filaments with inter-filament cross-contact resistances. This leads to the so-called interfilament coupling loss (IFCL) due to eddy currents in the matrix[22]. The effective transverse resistivity depends on the absolute magnetic field in the matrix due to magneto-resistivity effects, which in turn depend on the electrical resistivity, Residual Resistivity Ratio of copper and the distribution of superconducting material in the matrix[18]. Knowledge of the IFCL in the strands of a cable is necessary for separating the IFCL from the interstrand coupling loss (ISCL) in magnets and bus-bars. Only then can the origin of ramp-rate induced field-distortions and ramp-rate induced quenches in magnets be correctly evaluated. The IFCC has a huge influence on the saturation current of the outer layers of filaments in a strand and the neighbouring strands as well[22].

2.3.4 Interstrand coupling currents (ISCC)

Interstrand coupling currents (ISCCs) contribute to field errors and losses in superconducting cables in the time-transient regime. A field change induces eddy currents in loops formed by the superconducting strands and the resistive matrix of the cable[23]. Two layers of transposed strands in superconducting cables, made of superconducting strands and non superconducting copper are forming loops in which eddy currents can be induced by time-transient fields, e.g., during the ramping of magnets or frequency based measurements[18]. These so called interstrand coupling currents are responsible for additional heat losses and magnetic field errors, also known as interstrand coupling losses (ISCLs)[23]. ISCC and IFCC are very similar to the nature of the phenomenon, but ISCC is viewed from a larger angle of vision. The ability to predict ISCCs is especially important in the context of this Thesis.

Chapter 3

Measurements in the LHC machine

One of the main tasks of this Thesis is to create a simulation model of the RCS.A78B2 circuit. Furthermore, the spatial position of the fault in the circuit is to be determined. For this purpose, it is necessary to have a sufficiently large data base of the characteristics and the behavior of the circuit. On one hand, access to the already recorded measurement data of the RCS circuit and the data sheets of its components such as magnets and bus-bars is used. On the other hand new measurements are inevitable. To make the latter possible, the presence in the LHC tunnel is indispensable. The new measurements were using different approaches and diverse measuring systems for recording, processing and analysing. Different measurements on the RCS.A78B2 circuit are necessary because merely the measurement of the real ground fault is not sufficient. An impedance measurement of the fault-free circuit, in which the current is measured across the entire circuit, can not provide accurate information about the faulty circuit. Even if a simulation model provides very good results for the error-free circuit, the simulation result for the faulty state can yield significantly poorer results. The main part of the RCS circuit is in the superconducting state during the operation of the LHC. This means that there is no information about the circuit in the case of a DC voltage measurement. Even in the presence of the ground fault, a DC voltage measurement does not provide information about the position of the ground fault. Therefore, it is necessary that an analysis of the circuit characteristics is performed by applying different frequencies. The characteristic of the frequency-dependent impedances of inductances and capacitances is taken into consideration. Their almost uniform distribution over the entire circuit is utilized in the analysis of the circuit behavior. For this reasons, various measurements are made under different conditions, which include, among other things, artificially generated ground faults or the change of the measuring system configuration. Further explanations are given in the following sub-chapters.

3.1 Time domain reflectometry measurements

Time Domain Reflectometry (TDR) is one of the most powerful methods used to analyze the integrity of the signal propagating in a transmission line. The method is based on the principle that the wave propagating in the line is reflected at the locations where the impedance of the line changes. The fault points, joints, branches, junctions and abrupt cross-section changes cause such reflections. The time domain reflectometry technique involves the excitation of the circuit under test with a pulse well-defined in duration and amplitude. The pulse reflections of the tested circuit are recorded as a function of time.

The measurement is carried out according to the following procedure. The impulse of defined shape and duration is launched into the circuit under test. The reflected signal is registered and displayed on the screen of the measurement device. Knowing the time elapsed between sending of the input impulse and the arrival of the reflected signal, as well as the velocity of the wave propagation in the cable of the circuit, the distance to the fault can be calculated[24]. In the case of a fast step excitation, the voltage wave reflects at the point of impedance mismatch. On the screen of the measurement device appears an algebraic sum of the reflected- and initial incident wave. The time separation between the incident step and the reflected signal allows to identify the distance to the mismatch. The velocity of the signal propagation v in the cable depends on the relative dielectric constant ε_p of its medium and the velocity of light c according to the subsequent formula[25]:

$$v = \frac{c}{\sqrt{\varepsilon_p}} \tag{3.1}$$

For this measurement in the machine the calculated velocity is at 75% of the speed of light. The determined impulse length was set to eight micro seconds. The measuring method of the TDR is often used for comparing two similar circuits. In fact, there is in the same section of the LHC a further magnet circuit that has under similar circumstances a fault to ground. The RCO.A78B2 circuit behaves like the RCS.A78B2 magnet circuit and its bus-bars are also arranged in the same cryogenic line. For this reason, it is probable that the intermittent ground faults of both circuits are at the same position in the magnet chain. In addition, previous measurements show a strong correlation from these two circuits concerning the faults. With the hope of further inferences relating to the ground fault on RCS.A78B2, a TDR measurement was undertaken on said RCO.A78B2 circuit.

In order to obtain a comparative measurement, the same measurement was also made at the position-equivalent RCO circuit of the second beam RCO.A78B1. These circuits are also corrector magnet circuits with 77 magnets each, which are connected in series. The measurement results are shown in the Figure 3.1.

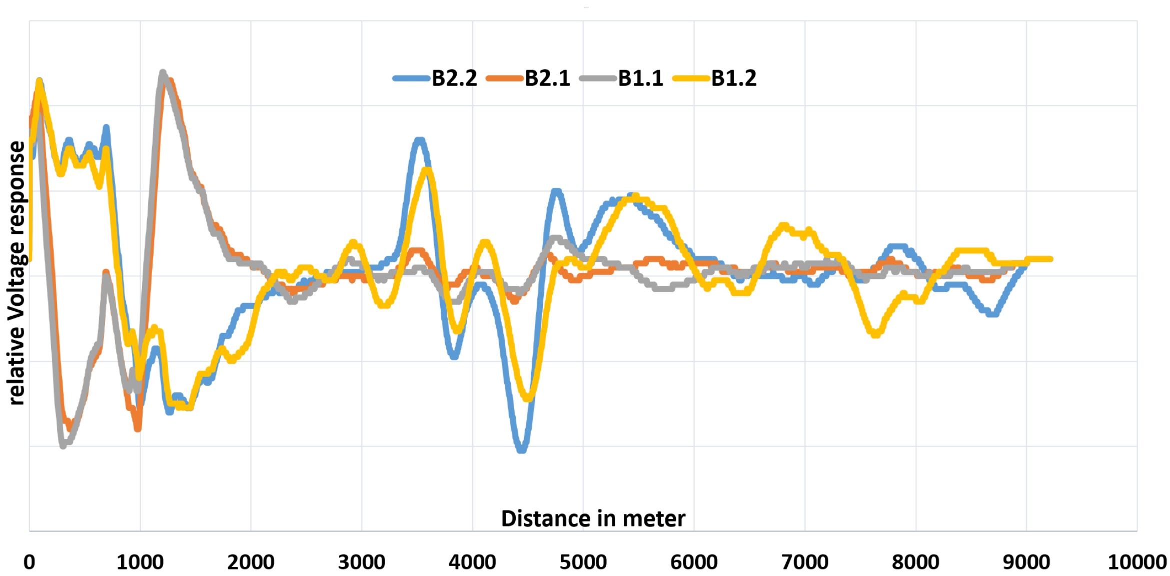

FIGURE 3.1: Time domain reflectometry measurements at RCO circuits in sector 7-8

A measurement at the RCO.A78B2 circuit has given a value of 460 kΩ for the rough impedance identification of the ground fault. This means that the resistance of the ground fault has increased significantly. However, a determination of the error locality is not impossible. Three statements can be made using the TDR measurement shown in Figure 3.1:

- Strong agreement of the two RCO circuits when measured at symmetrical measuring points (B1.1 and B2.1 as well as B1.2 and B2.2).
- No concrete evidence about the influence of the high resistance to ground value on the results of the measurements.
- The Position of the possible inconsistent and impedance-fluctuating ground fault can not be detected. For this reason, no direct inference can be made relating to the ground fault of the RCS.A78B2 circuit.

3.2 Information from previous circuit measurements

The RCS.A78B2 circuit was running perfect until July 2015 when a fault to ground was observed for the first time. The fault occurred a number of times, but high-voltage tests could not reveal the problem. Strong correlation from the fault to ground and the main-dipole circuit powering was observed. Furthermore, the localisation of the fault is to be find and to be fixed as soon as possible. The latest instant of time for the repair is during the long shut-down number two in 2018/2019.

Also with different measurements in the LHC machine is the localisation of the fault particularly difficult because of several factors:

- The fault to ground occurs only when the main-dipole circuits are powered with a current of about 6000 A.
- It accrues merely in the fully superconducting state of the circuit.
- During the required LHC powering no personnel can be present in the tunnel due to safety reasons.
- While the LHC is operating, the cold part of the magnet chain is accessible only via Voltage taps.
- The fault-impedance varies.

A special set-up is being prepared using a PXI (PCI eXtensions for Instrumentation) controlled with a LabVIEW data logging software. In order to isolate the cold part and to minimise the stray capacitance connected to the circuit, the power converter is disconnected by subduction the DC-cables at the beginning of the circuit at the level of the electrical distribution feedbox (DFB). The signal for the diagnostics is provided by an arbitrary function programmable generator connected to the A-lead and ground. 10 Hz to 50 kHz is the frequency range of the frequency sweeps at 1 V peak-amplitude. A 10 Ω series resistor limits the current to 100 mA and shows the overall currents during the frequency sweeps as well. The PXI is powered via an isolating transformer to ensure that the circuit remains grounded at a very well defined point. The connection to the LHC Local Area Network is provided by using WiFi, the access point is connected via a VDSL modem wired to the nearest VDSL socket in the tunnel. Hence a remote control intervention in the measurements is possible.

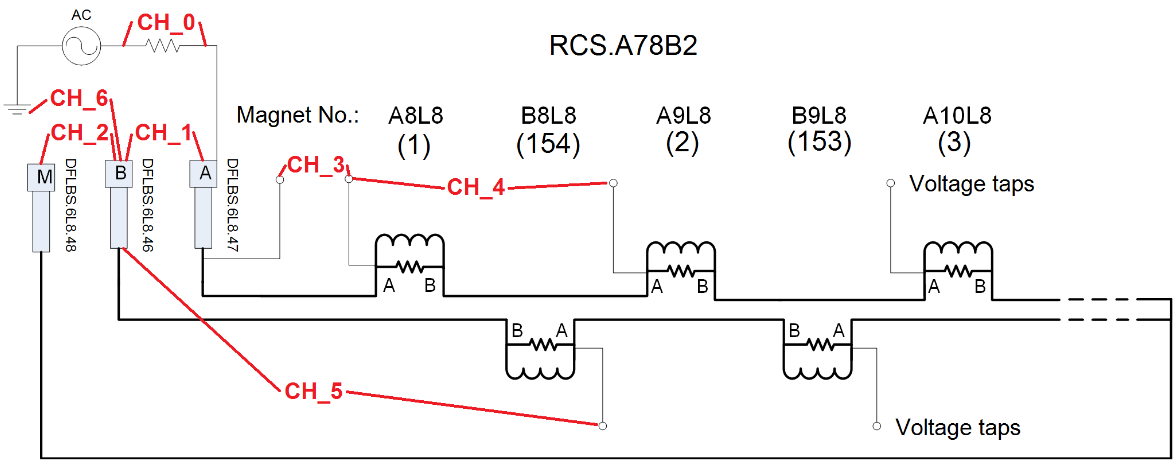

FIGURE 3.2: RCS.A78B2 measurement setup schematic

Figure 3.2 illustrates the connection of the measuring system. During the measurements seven digital multimeter channels of the PXI system are used. The voltage measurement channels are labelled from measuring channel 0 (CH_0) to measuring channel 6 (CH_6). The long distance of CH_3, CH_4 and CH_5 up to 70 meter from the PXI measuring system, which is positioned close to the DFB, requires some long measurement cables. The latter channels are used to obtain closer information about the behavior of one bus-bar piece respectively one magnet while the system is measuring. CH_0, CH_1, CH_2 and CH_6 are supposed to provide information about the behavior of the entire circuit.

The quench protection system is fully connected and operational during the tests. Special current cycles are executed for the measurement in the form of powering the main circuits up to nominal current of 10980 A in several cycles. Therefore according to personnel safety rules no personnel is allowed to be in this part of the tunnel.

3.3 Transfer function measurements

During the past century a number of different ways have evolved to measure transfer functions. Common to all of them is the use of an excitation signal containing all the frequencies of interest to feed the system. The system-response is captured and in some way compared with the original signal. Of course, there is always a certain amount of noise, reducing the informative value of a measurement. Therefore it is desirable to use excitation signals with an adequate high energy so as to achieve a sufficient Signal to Noise Ratio (SNR) over the entire frequency range of interest. Using gating techniques to suppress noise and unwanted reflections further improve the SNR. In practice there is always a certain amount of non-linearity.

One of the most commonly used test functions for a circuit or system is the sine wave[25]. The reason sine waves are important is complex and involve a branch of Mathematics called Fourier Theory. Any signal going into a circuit can be represented by a sum of sine waves of varying frequency and amplitude. At this connection, the form of the signal is irrelevant[24]. Due to the fact that it is possible to represent arbitrarily complex functions using only these very simple function of sine waves, they are important for any Transfer Function Measurements (TFM). There are many ways to analyze the response of a circuit, depending on the mathematical sophistication. A fairly basic explanation uses phasors.

If the input to a Linear Time-Invariant (LTI) system like the RCS.A78B2 circuit is a sinusoid at a particular frequency, then the output of the system is also a sinusoid at the same frequency, but typically with a different amplitude and/or phase. Another way of description is if the input to a system, which describes the transfer function, is $A \cdot sin(\omega \cdot t + \varphi)$, then the output is $M \cdot A \cdot sin(\omega \cdot t + \varphi + \theta)$[18]. This is likewise true for cosine - only the magnitude and phase of the output relative to the input changes. Figure 3.3 shows this relationship.

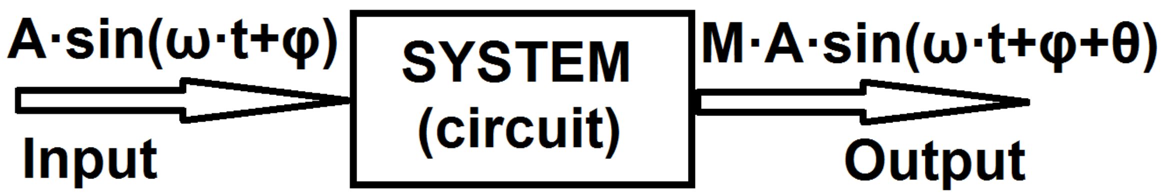

FIGURE 3.3: Scheme of determining system output given input and transfer function

The magnitude of the sinusoid has changed by a factor of M (which is represented as a positive real number) and the phase has changed by a factor of θ (a real number, not necessarily positive)[25]. The task of the measurement is to find the value of M and θ for the particular RCS.A78B2 circuit at particular frequencies ω.

3.3.1 Configuration of the measuring system

The measuring system mentioned in chapter 3.2 is a fully automated measuring system. The PXI system force the frequency generator to provide the desired input frequency with a fixed magnitude to the RCS circuit. While the frequency generator inserts the required alternating voltage into the magnet circuit, the PXI system is measuring the output signals. By dint of the digital multimeter cards of the PXI system, it is possible to detect the sufficiently precise temporal voltage values. These values are recorded in the time domain. This is done by scanning the channels with a maximum of 1.8 million samples per second[26]. At these TFM measurements the focus is placed on a frequency range of 10 Hz to 50 kHz. In this frequency range are 271 different frequencies in logarithmic frequency steps measured and recorded. In order to limit the data volume of the recorded measurements, the maximum possible 1.8 million samples per second is not outbid. The maximum sampling rate of the DMMs is limited to 100 times the frequency which is currently induced by the frequency generator.

For every frequency to be measured, exactly 20 periods of the same frequency are applied to the circuit. For the actual data recording, however, only the last 10 periods are considered. The first ten periods have the purpose to give the circuit sufficient time to engage on the predefined frequency. A further special feature of data recording is that the frequency sweep begins at the highest frequency and ends at 10 Hz. Since the ground fault to be investigated in the RCS circuit is a sporadically occurring ground fault with an unpredictable duration, it is important to obtain as many data points as possible out of the frequency sweep while the ground fault is present. The high frequencies of the frequency sweep can be traversed faster than the low frequencies. In Figure 3.4 the measuring system is shown.

During the frequency sweep a considerable amount of data will be generated in a short period of time. These raw data of the measurement is locally stored on the PXI hard disk. As soon as the PXI is proper connected to the tunnel WiFi network, the raw data are uploaded to the

CERN global storage automatically. Every personal account that has the convenient access authorisation is able to reach these data. With the collected time domain measurement data various evaluations can be made. For further processing of these measured data a LabVIEW program is used, which converts the time domain data into frequency domain data and stores it in a Tab-Separated Values (TSV) file. These TSV files can be opened and edited with many calculation programs such as Matlab or Excel. How the conversion from the time domain data to the frequency domain data takes place is explained next.

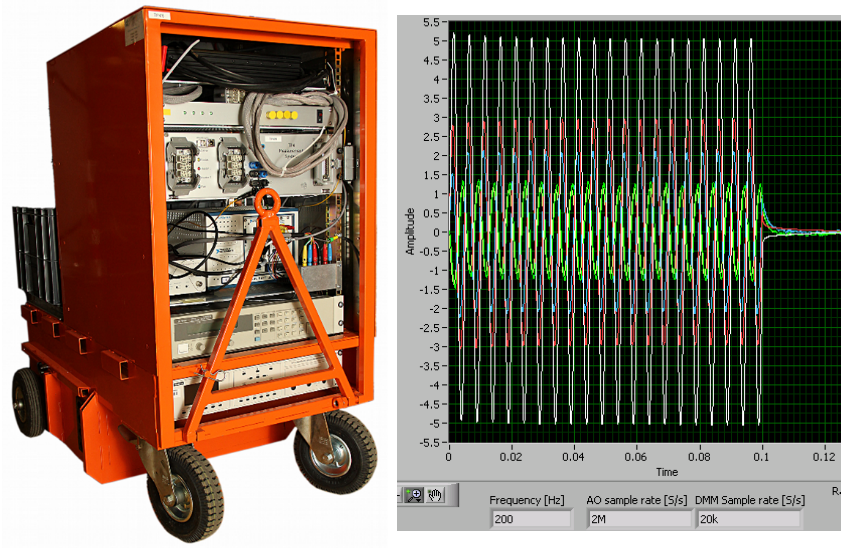

FIGURE 3.4: PXI measuring system and LabVIEW post processing data analysing program

The DMM cards of the PXI measuring system have the task of recording the voltage values at the various measuring points of the RCS circuit. In this case, the voltage values of the frequency generator (Input) and the voltages of the measuring points on the circuit (Output) are recorded at the same instants of time (samples). The phase can be determined by calculating the time offset between Input and Output voltage deviation. When combining inductances, capacitances and resistances as in the RCS circuit, the phase can be between +90 and -90 degrees, depending on the frequency applied on the circuit. A positive phase occurs when the inductive component of the circuit predominates. A negative phase carried out when the capacitive portion of the circuit is preponderant. Since the voltage provided by the frequency generator is as an amplitude value, this is also used to determine the voltages at the measuring points on the circuit. It should be mentioned here that the DMM cards of the PXI measuring system work with a precision of ±10 nV, and thus measure sufficiently precisely[26].

3.3.2 Measurements at warm and cold conditions

In order to obtain the behavior of the RCS circuit when applying different frequencies, some measurements were made on the circuit. However, the temperature conditions were not uniform. Some of the measurements have taken place in the superconducting state at 1.9 K. This includes the measurements from 2015 and the first months of 2016, as well as the measurements in April 2017. In the period from December 2016 to March 2017 the Extended Year-End Technical Stop (EYETS) took place. During this time, the LHC was shut down and sector 7-8 heated to 20 K. Since the NbTi material of bus-bars and magnets leaves the superconducting state above the temperature of 9.3 K, the entire circuit is in the normal-conducting state at this time. During the period in which the sector 7-8 is tempered to 20 K, modified conditions must be taken into account regarding the electrical resistance of the entire circuit. Three basic elements of the circuit must therefore be adapted. These are the parallel resistors of the magnets, the bus-bars and the magnet coils itself. All three elements have a Positive Temperature Coefficient (PTC) temperature behavior and thus increase their electrical resistance[18].

For the purpose of analysing the resistance behavior of a material at temperatures slightly above the absolute zero point, the concept of the Residual-Resistivity Ratio (RRR) should be explained. The RRR is defined as the ratio of the resistivity of a material at room temperature and at 0 K[14].

$$RRR = \frac{\rho_{293K}}{\rho_{0K}} \tag{3.2}$$

Since the RRR can vary quite strongly for a single material depending on the amount of impurities and other crystallographic defects, it serves as a rough index of the purity and overall quality of a sample[13]. As the deep temperature resistance grows with increasing impurity of the conductor material, a large RRR is associated with a pure sample.

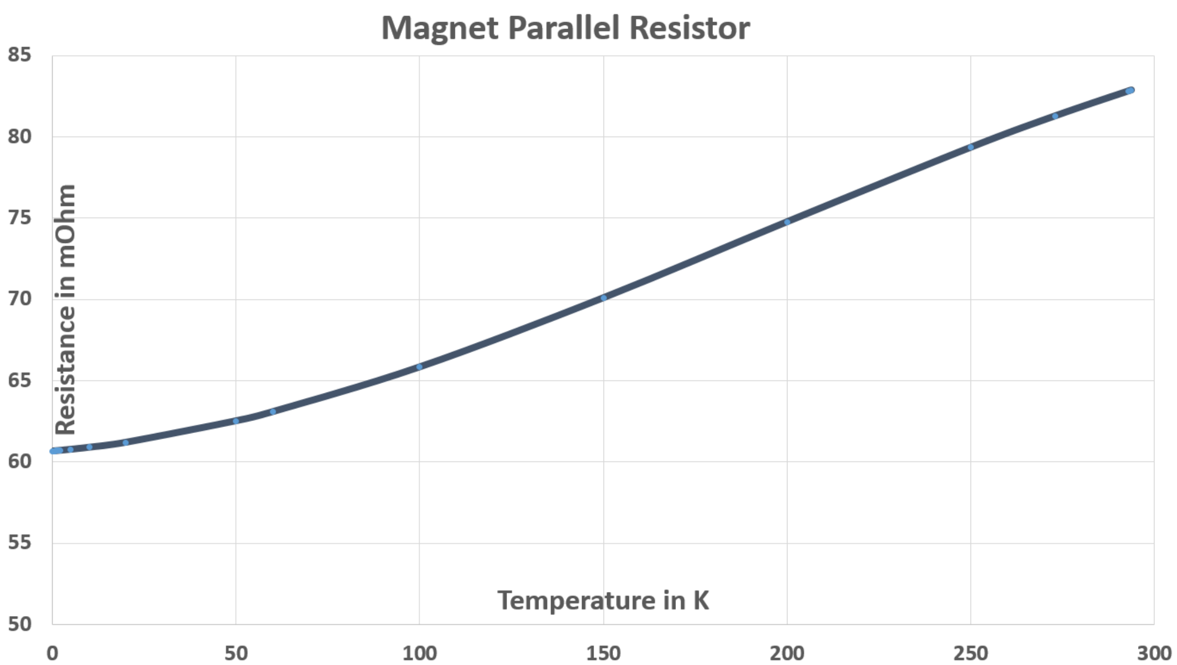

FIGURE 3.5: Resistance measurement of the stainless steal magnet parallel resistor

The parallel resistors of the magnets are made of stainless steel[6]. Since stainless steel is an alloy and by definition not a pure material, the RRR is low. Thus the resistance value of the parallel resistors varies despite the temperature difference of almost 300 K insignificantly. This relationship is shown in Figure 3.5. As can be seen in Figure 3.5 and by dispose Equation 3.2, the RRR of stainless steel is 1.366.

The RRR of the bus-bars and the conductor material in the magnets is clearly different. The main part of the conductor cross-section consists, besides the superconducting material, of high-purity copper[22]. This copper has an Residual-Resistivity Ratio of 80[25]. As the resistivity of the superconductor (NbTi) is significantly higher than the resistivity of copper (more than 30 times at 293 K)[22], the measurements performed above the critical temperature (which for NbTi in zero magnetic field and zero current density is 9.3 K) mainly reflect the properties of the bus-bar copper material. The bus-bar resistance of the entire circuit is calculated to be 146 mΩ. In the same context, the resistance of one magnet at 20 K is estimated to be 16 mΩ. In the circuit model creation, these modified conditions must be taken into account.

3.3.3 Artificial short-cut measurements for reference data

The fault in the RCS.A78B2 circuit, which occurred in 2015, was a ground fault, which occurred at an indeterminate location in sector 7-8. The behavior of the circuit, as a function of the applied frequency and the ground fault, was not known until the beginning of 2017. Of great interest here is the obtaining of measurement data, which contain a ground fault. In order to get these reference data, measurements were made which include a physical ground fault. So-called artificial ground faults were generated at several positions at the RCS circuit in sector 7-8 and each time a TFM measurement was executed. The only access points to the circuit are the Voltage taps, which are shown in Figure 3.2. To create a ground fault, the Voltage taps were connected to the ground potential by a 20 cm long low resistance cable. These measurements took place under 1.9 K temperature conditions and were undertaken at 28 positions in the circuit.

Chapter 4

Model design in PSpice

The RCS.A78B2 circuit is not a common circuit. This is shown by the following properties:

- The circuit is operating at up to 600 A.
- The 154 magnets are connected in series.
- The circuit is spread over more than 3 km.
- The peak field in the magnet coil is at 1.9 T.
- The total length of the bus-bars is around 10 km.
- The circuit is only operating with DC voltage during normal operation.
- The standard operating temperature is with 1.9 K near the absolute zero point.
- During proper operation, the major part of the circuit is in the superconducting state.

It is possible to describe the complete RCS.A78B2 circuit only by three fundamental elements of electrical engineering. These are resistors (R), inductances (L) and capacitances (C). R describes the ohmic resistance of the element under consideration. L describes the inductance and C the capacitance of the element under consideration. The inductance of the RCS circuit is mainly represented by the magnets. However, the bus-bars also contribute to the total inductance since the inductance depends on the magnetic flux loop that is penetrating the bus-bars as well[18]. All the capacitances are parasitic effects and the determination of them is not trivial. On the one hand, the capacitance to ground is observed. It appears on the magnets and the bus-bars. On the other hand, the parasitic capacitances between the RCS bus-bars must be taken into account. The latter is also called coupling capacitance[22].

As can be seen in Figure 5.1, the three RCS.A78B2 bus-bar lines are bundled parallel within a five-line package called splice bus-bars. This package is embedded in the bus-bar network of the main quadrupole magnets. The three bus-bars of the RCS circuit consist of two main bus-bars (20 and 19) and one reserve bus-bar (18). The last-mentioned bus-bar is thus not used under regular operation and has no direct function from the electrotechnical viewpoint. It is connected exactly at the middle of the magnet circuit between the 77th and the 78th magnet. This is also the geometric end point of the RCS.A78B2 tunnel segment. The other end of the reserve bus-bar is not directly connected to a circuit or potential.

For the reason that the circuit consists of many similar components, which gradually recur, it makes sense to create sub-circuits for some elements. These include the sextupole magnets as well as the bus-bars.

4.1 Model of the magnets

The behavior of a magnet is not completely inductive due to the presence of magnetization effects, eddy currents, and coil-to-ground parasitic capacitances[18]. Moreover these are frequency dependent effects. In many applications, magnets are used in non-DC conditions and are subject to current ramping. The necessary consideration of dynamic effects during transient faults is to be mentioned as well. To understand the effect of parasitic capacitances and the magnetization on magnets which are mentioned in Chapter 2.3, as well as the frequency dependent electrical characteristics of magnet systems itself, it is necessary to accurately determine the electrical characteristics of superconducting magnets over the entire operational frequency range.

A MCS sextupole magnet, shown in Figure 1.4, includes a central tube providing a path for particle beams, a superconducting coil for conducting high density current to generate the magnetic field, a laminated collar for holding the magnet together, a laminated steel yoke forming the magnetic field path and a cryogenic shell required for low temperature operation[6]. When the magnet is superconducting, the DC resistivity of the coil disappears. Therefore the magnet behaves as an inductor at low frequencies. If the magnet current contains AC components, however, eddy currents will be induced in the central tube, the magnet coil, and other metallic elements. These eddy currents impose a resistive component in the impedance[23]. The electrical characteristics of the magnet are therefore frequency dependent. When the formation of the magnet becomes in terms of the geometric structure the complexity of a sextupole magnet, the model is an approximation.

The magnetizing effects can be represented by the coupled inductive circuit shown in Figure 4.1. The primary inductance L_1 represents the superconducting coil, the secondary inductance L_2 and the resistor R_b represent the parasitic effects itself.

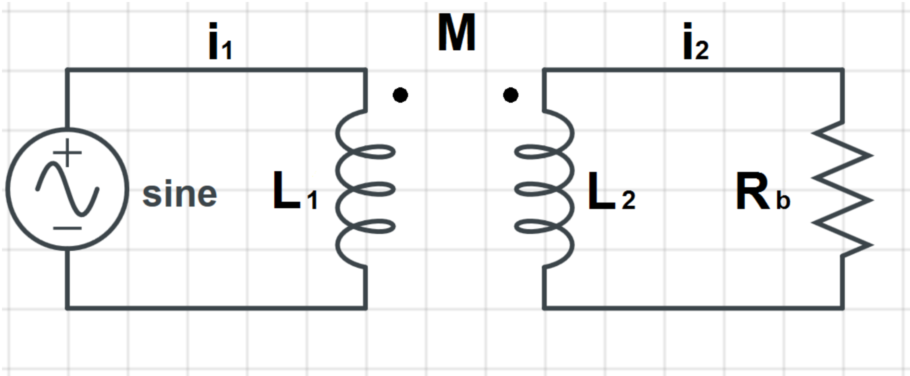

FIGURE 4.1: Transformer similar MCS representation according to the parasitic effects

Suppose the mutual inductance is M, the coupling coefficient is $\sqrt{k} = \frac{M}{\sqrt{L_1 L_2}}$ and the complex variable in the frequency domain is $s = \sigma + j\omega$, the impedance of the magnet is therefore obtained as[18]:

$$Z = sL_1 - sM \frac{sM}{R_b + sL_2} \tag{4.1}$$

If the number of coil turns is disregarded and $L_2 = kL_1$, $R = R_b$ as well as considering the connection of $Ri_2 = sMi_1 - sL_2 i_2$, the impedance function changed to[18],[20]:

$$Z = sL_1(1-k) + \frac{skL_1R}{R + skL_1} \tag{4.2}$$

The Equation 4.2 leads to the in Figure 4.2 shown circuit, which can be implemented in a basic PSpice model.

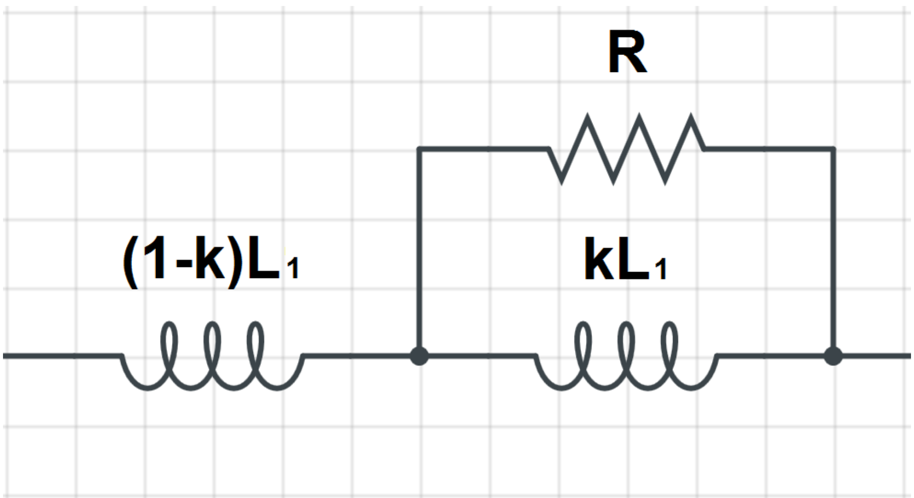

FIGURE 4.2: Basic representation of a MCS Magnet in PSpice

Further, with coil-to-ground capacitance taken into account, a magnet equivalent circuit is obtained as shown in Figure 4.3, where C represents the summed effect of the coil-to-ground parasitic capacitance.

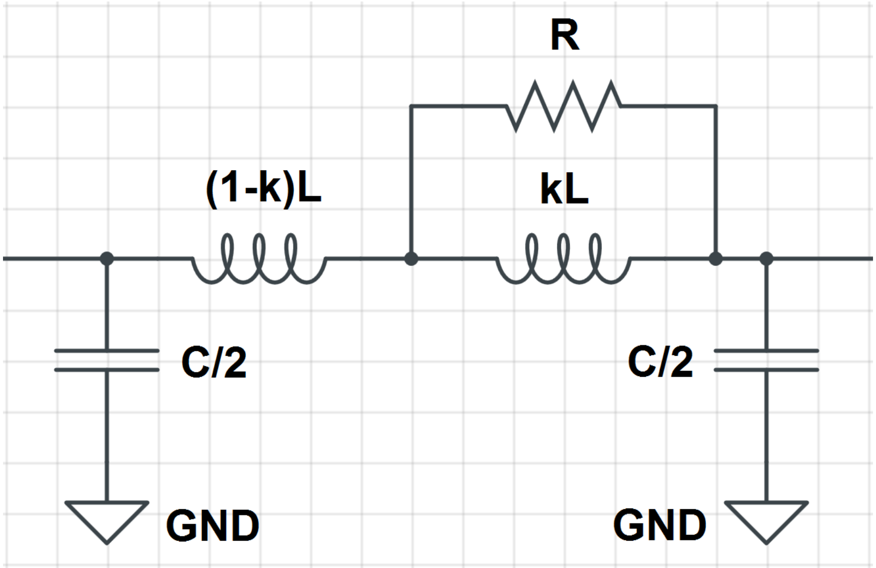

FIGURE 4.3: Additional capacitances to ground in the MCS magnet representation

The impedance of the magnet circuit is therefore[21]:

$$Z(s) = \frac{sL\left(1 + \frac{s}{R/(k(1-k)L)}\right)}{\left(1 + \frac{s}{R/(kL)}\right)\left(1 + R\frac{C}{4}s + (1-k)L\frac{C}{4}s^2\right)} \tag{4.3}$$

Of course, it is important to provide a model for the magnets of the RCS circuit to simulate its actual behavior. However, what makes this circuit also an unusual magnet circuit is the fact that each magnet is staged with a parallel resistor. Its temperature-dependent resistance is explained in chapter 3.3.2. The nominal inductance value L of a MCS magnet is 80 mH. Its inductive reactance can be calculated with the basic equation: $X_L = 2\pi f L$. Thus, the inductive reactance of the MCS magnet has already at 0.12 Hz the same value as the ohmic resistance of the parallel resistor. This means that the contribution of the magnets in the TFM measurements at higher frequencies is almost irrelevant, because they are nearly perfectly bridged. Simply the capacitance to ground is relevant for the model.

The main focus on the model of the whole circuit is thus not the as at the first glance assumed most important elements, the magnets, but rather the bus-bars, which make the series connection of the magnets possible.

With the aim of limiting the duration of the entire RCS circuit simulation in PSpice, the use of a magnet model, which is essentially limited to self-inductance, has been selected on the basis of the aforementioned reasons. This magnet model can be seen in Figure 4.4.

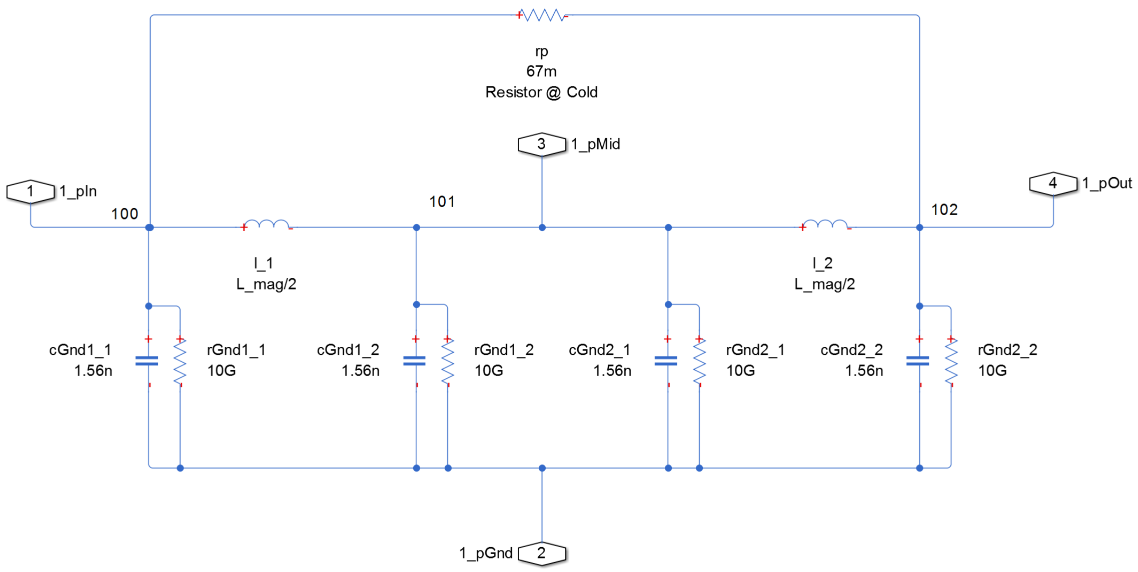

FIGURE 4.4: Simplified model of the MCS magnet

4.2 Model of the bus-bars

In an adapted manner, the same physical effects apply to the bus-bars as to the magnets. Thus the parasitic magnetization effects also play an influencing role in the bus-bar simulation[22]. In addition to the parasitic capacitances to ground and the self-inductance, the coupling capacitances between the bus-bars must also be included. In order to obtain an impression of the frequency-dependent inductance curve of the entire RCS.A78B2 circuit, the result of this TFM measurement can be seen in Figure 4.5.

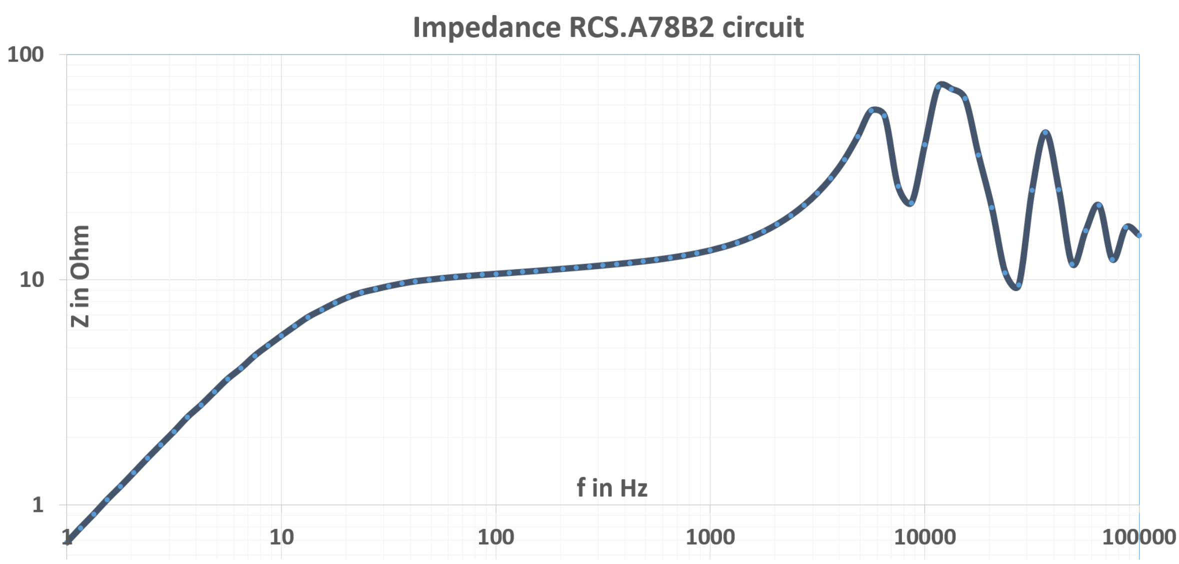

FIGURE 4.5: Impedance curve of the RCS.A78B2 circuit as a function of frequency

As can be seen primarily in the higher frequencies, the interplay of resistances, inductances and capacitances, which are distributed over the entire circuit, can not be easily determined. Several minima and maxima of the impedance curve are evidence of multiple resonance frequencies. Due to the fact that the influence of the magnets on the impedance profile is limited by their parallel resistors, the bus-bars are the main actors.

Figure 3.2 illustrates, that in addition to the two magnets connecting bus-bars, a third bus-bar, which can be seen as the lower line in the diagram, belongs to the entire circuit. This bus-bar (M) must also be included in the model of the entire circuit, since it is at one end directly connected to the magnet chain. Even if the other end of this bus-bar does not have a direct connection to other contact points and is thus half-floating, the potential adjustment due to the one-sided link results in potential differences across the tunnel section. Conditioned by these possible potential differences, the capacitances to ground as well as the coupling capacitances to the rest of the RCS.A78B2 circuit also play a role.

The sub-circuit model of the three parallel bus-bars consists of three similar inductive conductor lines, where each end of them can be connected to any node in PSpice. In the tunnel itself this sub-circuit stands for a 36 m long bus-bar section, which describes the electrical distance from one to the next magnet. The bunched bus-bar model is illustrated in Figure 4.6.

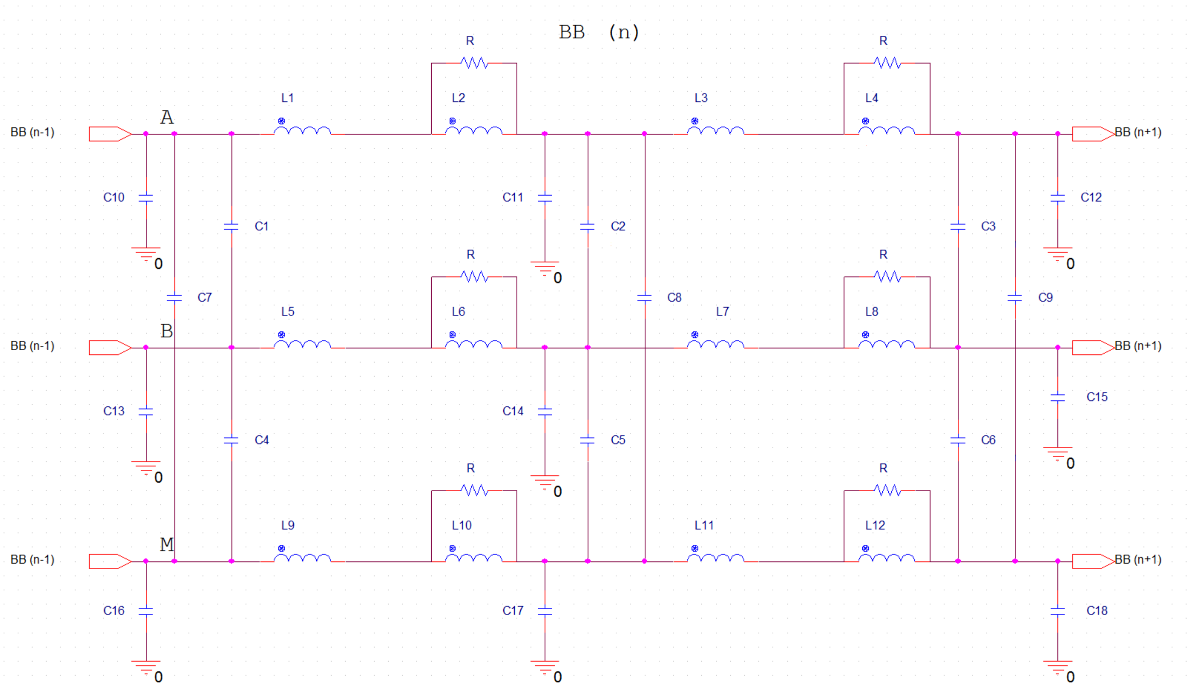

FIGURE 4.6: Bus-bar equivalent model for PSpice as sub-circuit

This model is merely a simplification of the actual geometrical RCS.A78B2 order. In the tunnel, the magnets of the back and forth bus-bars are arranged alternately to one another. However, this fact plays only a subordinate role. The short distances of the branches to the 16 cm long MCS magnets are negligible compared to the size of the entire magnet circuit of around seven kilometers. The third bus-bar line (M) does not contain magnets and therefore no branches, as opposed to the other two bus-bar lines A and B.

Since a plurality of additional parasitic currents can be formed by the consideration of the coupling capacitances, the prediction of the circuit behavior by variation of the frequency becomes more difficult.

4.3 Representation of the circuit

To handle the amount of elements which has to consider in a simulation model of the RCS circuit, the often used simulation program PSpice suits. A huge part of the PSpice program includes the "Simulation Program with Integrated Circuit Emphasis" (SPICE) itself. SPICE is a well known circuit simulator computer program[27]. The SPICE solver is the core part of the program and the part that solves the circuit equations. It is command line driven and is thus regarded as difficult to use[28]. Consequently, several commercial versions are available which provide a graphical interface and up to date component libraries which involve models of commercially available electrical components mainly provided by their manufacturers[27]. PSpice is such a commercial implementation for Microsoft Windows and is sold by OrCAD. It has a schematic graphical user interface input and an oscilloscope-like output interface. The schematic input lets users draw circuits to be simulated on the screen and the oscilloscope-like output allows to interactively plot traces after a simulation run. In between this input and output works the original SPICE solver. It reads the circuit definitions from a netlist and runs the circuit simulation. A netlist is a text file which describes the circuit by specifying components, their values and their interconnections. It is possible to specify circuits by writing the netlist by hand in a text editor and this netlist file is effectively the input to the simulator. PSpice create the netlist automatically from the drawn graphical user interface circuit schematic[28]. Up to a certain size, it may be easier to draw a circuit than to write it in a text editor. Also a graphical visualization of the circuit is much more intuitive.

Due to the size of the RCS circuit, it is impractical to represent the entire circuit in the graphical user interface of PSpice. Therefore, the use of the netlist-based creation of the circuit is selected. The correct sequence of the entire circuit substantially comprises the following elements:

- The arbitrary function programmable generator.
- The shunt resistor.
- The transition track from the normal- to the superconducting part of the circuit.
- The first half of the alternating order of bus-bars and magnets.

- The direct resistance-free connection to the M bus-bar.
- The second half of the alternating order of bus-bars and magnets.
- The transition track from the superconducting to the normal conducting part of the circuit.
- The connection to ground or to the PXI measuring System.

The components required for the representation of the entire circuit are essentially constituted by the elements of resistance, capacitance and inductance. Figure 4.7 shows how these elements are specified in the text file belonging to the netlist.

```
%Element      %Node(Input Output) %Value
R_example     (100 101)           1000
```

FIGURE 4.7: Code example for resistor definition

In the second line of Figure 4.7, the first part (R_example) shows the type of the element and its name. The first letter signals to the solver what type of component it is exactly. For a resistor, the first letter is reserved with R or r. Capacitors and inductors are indicated by C or c, respectively L or l for the first letter. The directly afterwards added letters complete the name of the component. This name may be present in the final netlist file only once. The two figures inside the brackets in the same raw stand for the input and output nodes to which the component is connected. These nodes can propagate through the netlist and be used following the users needs[27]. The name of the nodes may also be assigned once. The solver does not recognize the use of a node at two completely different positions in the circuit as an error. The exact description must therefore be taken into account when using nodes. It is irrelevant for the circuit generation whether the name of the nodes consists of letters or numbers or a mix of both. However, some functions integrated in PSpice work only with nodes whose names are composed solely of digits[28].

The last element in this line describes the value of the component. The resistance value of the example is indicated as 1000 Ω. The unit is automatically set by PSpice and does not have to be specified. With the scientific notation, very large or very small numerical values can be represented compactly.

In order to define a suitable arrangement of the entire circuit, which connects the subcircuits to each other, a further circuit-file was created. This circuit-file is intuitively titled with RCS_MCSChain. It is mainly responsible for the correct connection of the nodes between bus-bars and magnets.

Chapter 5

Parameter estimation and simulation of the circuit

In Figure 5.1 one can see the cryodipole cross-section of the Large Hadron Collider[2]. At the upper part of the iron yoke are the bus-bars of the main quadrupole magnet circuit placed. On the left part of the Figure some attached smaller bus-bars are visible. These bus-bars are among the 120 A and 600 A corrector magnet circuits like the RCS circuit. The real bus-bars from the RCS circuit are numbered with 18 (M), 19 (B) and 20 (A), which is also taken into account in Figure 5.1.

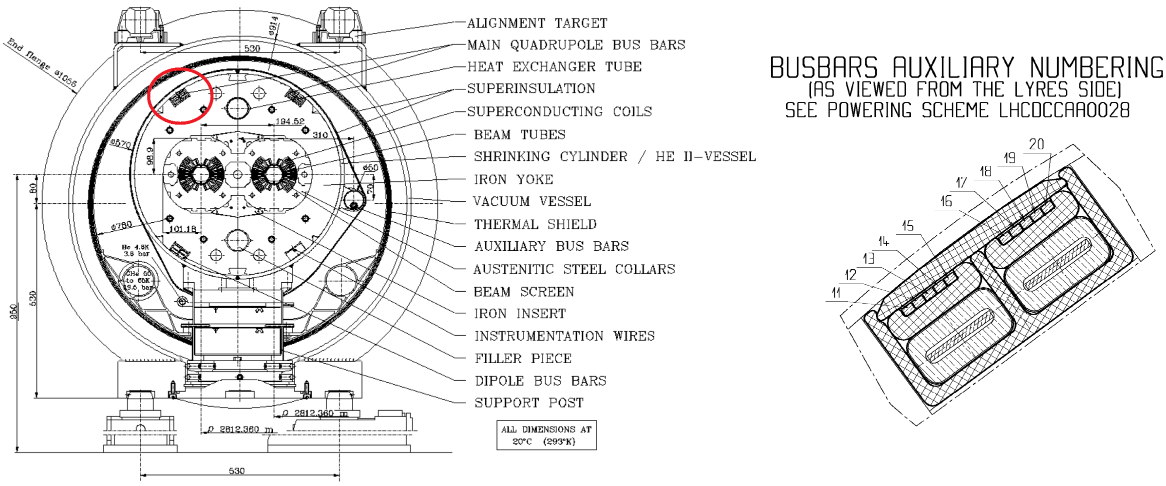

FIGURE 5.1: Cross-section of cryodipole and bus-bars

A relevant task is to find proper electrical values for the magnets and the bus-bars of the RCS circuit model. The major effort is needed to search for the parasitic properties which plays an important role in the Transfer Function Measurements. This includes parasitic capacitances to ground as well as parasitic capacitances between the bus-bars. Furthermore the bus-bar inductance and the inductive coupling between them has to be considered.

In order to determine the parasitic capacitances, a high voltage measurement has been undertaken on the entire RCS circuit. In this case, the circuit is loaded with rapidly rising voltage ramps of 200 V each. During the rising voltage of the circuit relating to ground, there is a leakage current through the parasitic capacitances visible. The following two pictures illustrate the measurements of this test procedure.

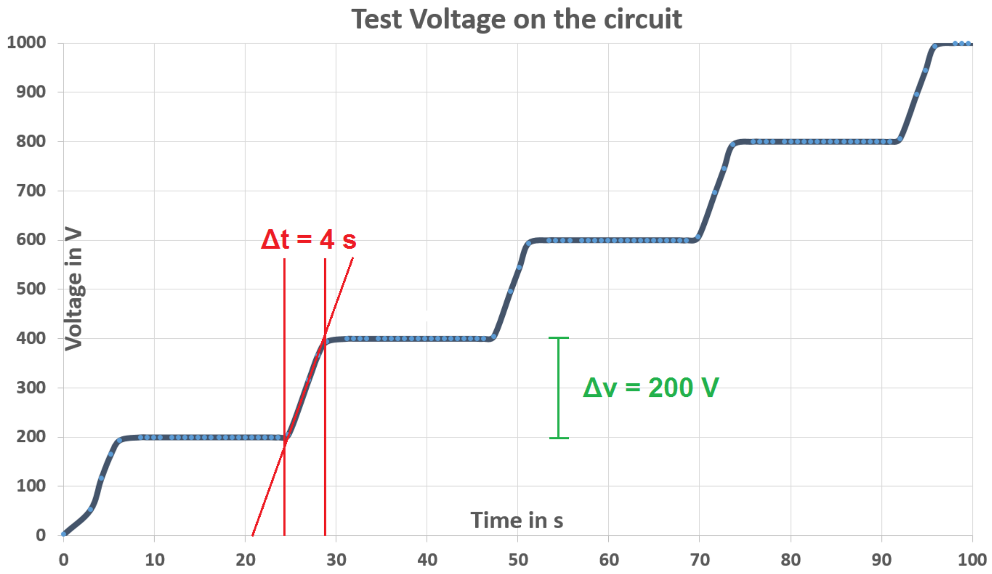

FIGURE 5.2: Voltage ramps for ground current through capacitances analysis

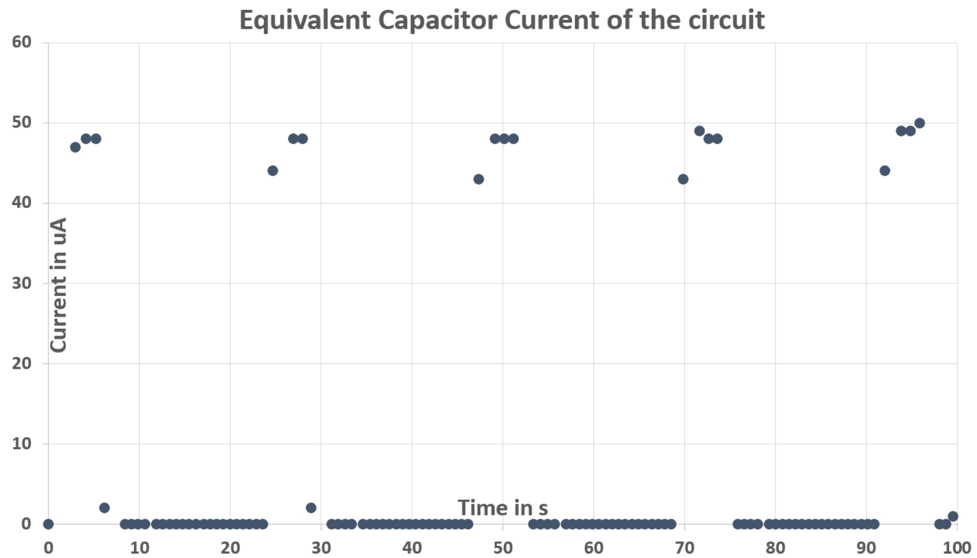

FIGURE 5.3: Resulting parasitic capacitance to ground current

Owing to the measured current through the parasitic capacitances to ground during voltage level variations, the total value of the capacitance to ground C_{GNDtot} is computable.

$$C_{GNDtot} = \frac{i}{\dot{u}} \tag{5.1}$$

As can be seen from Figure 5.2 and Figure 5.3, the first derivative of the voltage $\dot{u} = \frac{\triangle v}{\triangle t}$ is 50 V per second and i is 48 µA. The result of C_{GNDtot} is therefore 960 nF. For the estimation of the parasitic resistance to ground of the entire circuit a similar measurement has been executed. During the embossing of a constant voltage of 1000 V on the RCS circuit the leakage current to ground is measured. With the help of $R_{GNDtot} = \frac{u}{i}$ the total resistance to ground is definable to 8.04 GΩ due to the leakage current of 124 nA.

5.1 Parameters of the magnets

As shown in Figure 1.4, the MCS magnet has a round shape and a compact design compared to other magnets. The insulation material of the coils has on the outer face a thickness of 60 µm. Furthermore, this insulation material is in contact with a grounded metal frame at the other side. On the inner face of the coil, the same insulation material is with 260 µm much thicker and is attached on a grounded metal shield as well. The approach of the magnet capacitance to ground takes place with the geometry of two plate capacitors. With the outside surface of the superconducting coils of 106 cm^2 and the inside surface of 107 cm^2 is the missing part for the Equation 5.3 the material-specific relative permittivity of the synthetic insulation material. Its amount is 3.23.
Before comparing the parasitic capacitances to ground of measurements and assessments, it is worth to reflect which values are expected. Based on the fact that the magnets have a not negligible capacitance to ground, the share of the magnets in the entire capacitance to ground should be recognizable. With Equation 5.3, the capacitance to ground of a single MCS magnet is 6.24 nF. For 154 magnets in the entire circuit, the capacitance to ground of 960 nF is obtained. This is by far the largest share of the entire capacitance to ground. However, it must be taken into account that this is merely a geometrical approximation.

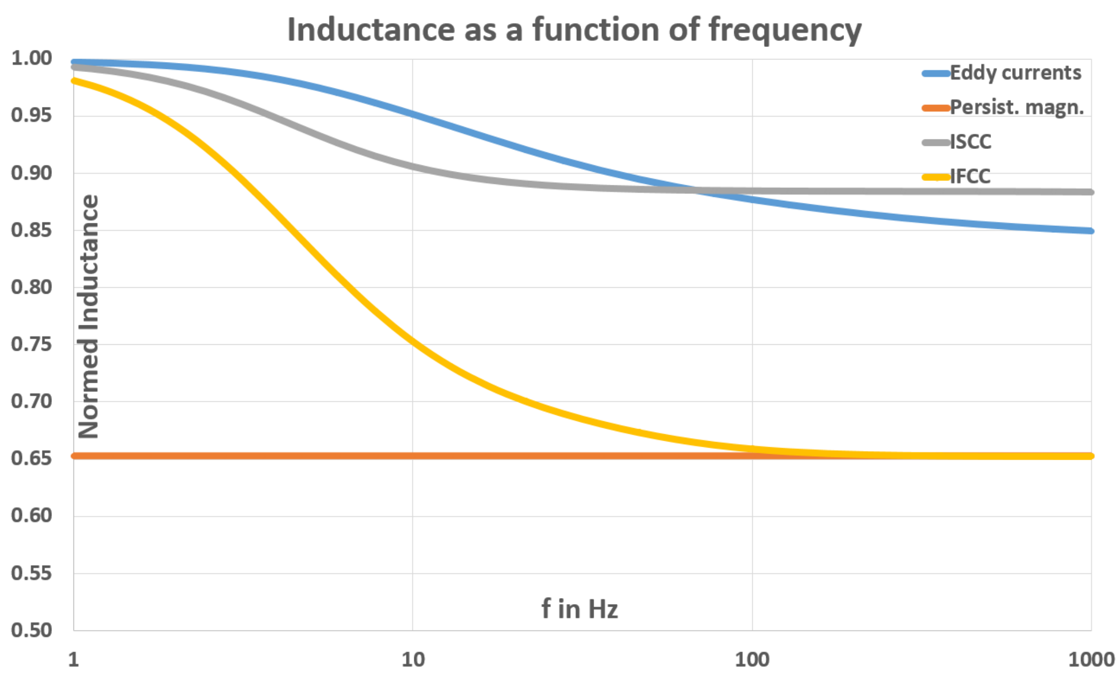

FIGURE 5.4: Qualitative representation of magnetizing effects on magnets

Based on the data sheet and the measurement shown in Chapter 3.3.2, the parallel resistors have a resistance of 67 mΩ each. The same also applies to the inductance of one MCS magnet, which is accurately defined of a nominal value of 80 mH. The latter value, however, is to be considered with caution because of the parasitic effects which are illuminated in Chapter 2.3 and can deviate with increasing frequency. A qualitative representation of these effects can be found in the following Figure 5.4.

5.2 Parameters of the bus-bars

For use in the RCS circuit, the perfect bus-bar should have neither resistance nor capacitance, inductance or other parasitic properties. In order to guarantee survivability in case of a quench, the bus-bar is sheathed with high-purity copper. In the event of a sudden quench of the bus-bar, this serves to allow the circuit current to flow around the NbTi material in the non-superconducting copper that acts as a heat sink[15]. Due to the compact design of the bus-bars, the following features must be taken into account when designing the model.

5.2.1 Parameters according to the spatial dimensions

The following basic sizes of the RCS bus-bars are known: The length, the position, the interspace and the shape and size of the cross-section. As can be seen in Chapter 5.1, the ground-capacitance of the circuit is mainly borne by the magnets. Nevertheless, the parasitic capacitance of the circuit can not be ignored. Same also applies to the coupling capacitances of the bus-bars. In order to estimate the size range of these two values, the simplification of a bus-bar to a half of a pipe-capacitor C_{pipe} and a plate capacitor C_{plate} is assumed. The formulas of the two capacitor types are depict below[18].

$$C_{pipe} = \frac{\epsilon_0 \epsilon_r l 2\pi (r - \frac{d_r}{2})}{d} \tag{5.2}$$

$$C_{plate} = \frac{\epsilon_0 \epsilon_r A}{d} \tag{5.3}$$

From the dielectric constant ϵ_0 and the material-specific relative permittivity of the synthetic insulation material ϵ_r of 2.25 as well as the length of a 36 meter bus-bar piece l, the 7 mm radius r and the insulation thickness d of 6 mm, results the parasitic capacitance to ground of 1.5 nF per bus-bar piece. With the side surface of a bus-bar piece of 0.103 m^2 and the distance of 60 µm from bus-bar to bus-bar as well as the changed relative permittivity value of 3.4 for the direct insulation tape, it results in 13 nF coupling capacitance between the adjacent bus-bars.

Due to the geometrical data of the bus-bars cross-section from 3.35 mm in width, 2.7 mm in height and the length of 36 m, the inductance of one bus-bar piece is estimated as 50 µH. The unmitigated bus-bar chain inductance is at 7.65 mH.

5.2.2 Two dimensional FEM-model parameters

Overall, the goal is to evaluate the parasitic capacitance to ground and between the bus-bars, than to compare these with the measured values explained at the beginning of chapter 5. Considering that the parasitic capacitances from the bus-bars are supposed to be of the same order of magnitude as the ones in the sextupole MCS magnet itself, these bus-bar parasitic capacitances cannot be neglected in any evaluation of the total parasitic capacitance. Therefore, a Finite-Element-Method (FEM) model has been developed in order to calculate them. To calculate the parasitic capacitance of the RCS bus-bar, a geometric representation of the cross section was created in COMSOL. The geometric forms are drawn from Figure 5.1 and the model comprises of two symmetric ordered bus bar elements. Each of them consists of a larger bus-bar for the main quadrople magnet circuit, three smaller bus-bars for the sextupole corrector magnet circuit RCS and two unused reserve bus-bars of the same dimensions. The bus-bars are surrounded by polyimide insulation and glass-fiber[5]. Around this is an iron yoke, and underneath one has the main steel collar of the beam tube[2].

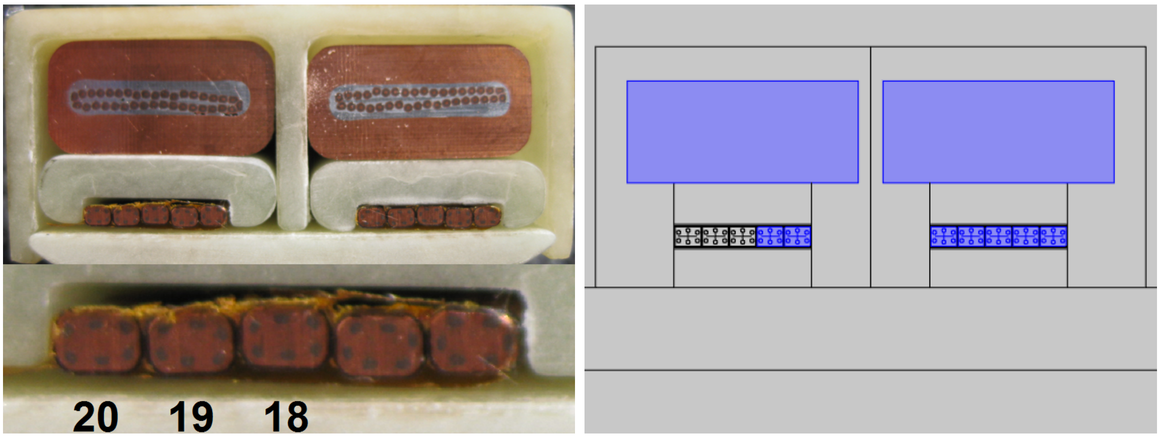

FIGURE 5.5: Cross-section of the bus-bars and the corresponding model

The challenging aspect of evaluating parasitic capacitances in this problem is that the bus-bars are equipotential over the cross section, although one does not have any information of their value. When these metallic parts are left unassigned, COMSOL creates fields across the bus-bars that are not equipotential. Furthermore, the charge accumulated on the terminals are not accessible numerically to the user and thus the other capacitances, which depend on this charge, can not be evaluated. In addition, not only the grounded iron yoke and stainless steel collar is given zero potential, but also all the metallic bus-bars which is point in Figure 5.5.

Subsequently, the capacitances are calculated by running four different simulations. Gradually, each of the three bus-bars is supplied with a potential of 10 V. Both other bus-bars of this RCS bus-bar segment are at the zero potential like the rest of the model bus-bars. The complete capacitance to ground value is estimated by supplying 10 V on all the three RCS bus-bars (18, 19 and 20) at the same time. The results of this simulations are shown in Table 5.1.

TABLE 5.1: Capacitance values of the COMSOL simulation in [F/m]

	20	19	18	GND
20	-	4.07e-10	5.47E-12	3.90E-11
19	4.07E-10	-	4.04E-10	1.21E-11
18	5.47E-12	4.04E-10	-	1.06E-11
GND	3.90E-11	1.21E-11	1.06E-11	-

By comparison of the results of the COMSOL simulations and the capacitances according to the spatial dimension calculation shown in Chapter 5.2.1, the results of the bus-bar 20 and its capacitance to ground match. Looking at the other bus-bars concerning the capacitances to ground, it differs since the result of the COMSOL simulation is significantly lower. With the focus on the coupling capacitance between the bus-bars, the results of the calculation and simulation agree very well.

5.3 Simulation and adaptation of the circuit

The first simulations were carried out with the data obtained from Chapter 5.1 and 5.2. Chapter 3 describes how the comparison data of simulation and measurement were obtained in the form of measurements in the LHC machine. The resulting data from the PSpice circuit simulation are stored in a probe document (.dat format). The data from this probe document are extracted with the help of Matlab. For this purpose, an already existing algorithm is used that extracts from the probe document the required nodes whose voltage profiles has to be analyzed. This algorithm is used in the DatRead function and belongs to the standard PSpice and Matlab repertoire of the section. To be more precise, this algorithm extracts the real and imaginary values of the measurement points.

If the PSpice solver is not instructed to restrict the simulation data, it analyzes all existing nodes and stores their voltage- and current profiles in the probe document. The calculation and data storage of all node data requires time and also memory space. In order not to unnecessarily require the calculation resources, only the data of the nodes which are measured by the measuring channels on the real circuit are stored in the resulting probe document. This is made possible in the main circuit file by the .PROBE instruction and the subsequent calling of the required nodes as well as their voltage analysis. An example is as follows: .PROBE V(100 101).

The voltage profiles extracted by the DatRead Matlab function are stored in the Matlab-struct variable outputPSpice. For a graphical comparison of simulation to measurement, the magnitude of the voltage out of the real part and the imaginary part, corresponding to the respective frequency value must be formed. These voltage magnitudes are calculated using the following formula:

$$|V_i| = \sqrt{(Re\{V_i\})^2 + (Im\{V_i\})^2} \tag{5.4}$$

The realization of this formula in the Matlab code is shown in Figure 5.6.

```
vch_0 = ((outputPspice.Real (:,1)).^2 + (outputPspice.Imag (:,2)).^2).^(1/2);
vch_1 = ((outputPspice.Real (:,3)).^2 + (outputPspice.Imag (:,4)).^2).^(1/2);
vch_2 = ((outputPspice.Real (:,1)).^2 + (outputPspice.Imag (:,2)).^2).^(1/2);
vch_6 = ((outputPspice.Real (:,3)).^2 + (outputPspice.Imag (:,4)).^2).^(1/2);
```

FIGURE 5.6: Calculation of the voltage magnitude in Matlab

5.3.1 Adjustment of the circuit parameters

It is necessary to check the impedance progression of the entire RCS circuit. This is done by comparing measurement data to simulation data. The reference measurement data, which serve as the basis for the comparison of simulation and measurement, are recorded directly on the LHC machine. In this case, a 1 Ω resistor is connected in series to the RCS.A78B2 circuit. The voltage generator generates an alternating voltage with the amplitude of 1.5 V. The other end of the circuit is directly connected to the ground potential. In order to obtain the impedance behavior of the entire RCS.A78B2 circuit over a wide range, the frequency range to be investigated was selected from 1 Hz to 100 kHz. Figure 5.7 points out the impedance profile of the simulation and measurement.

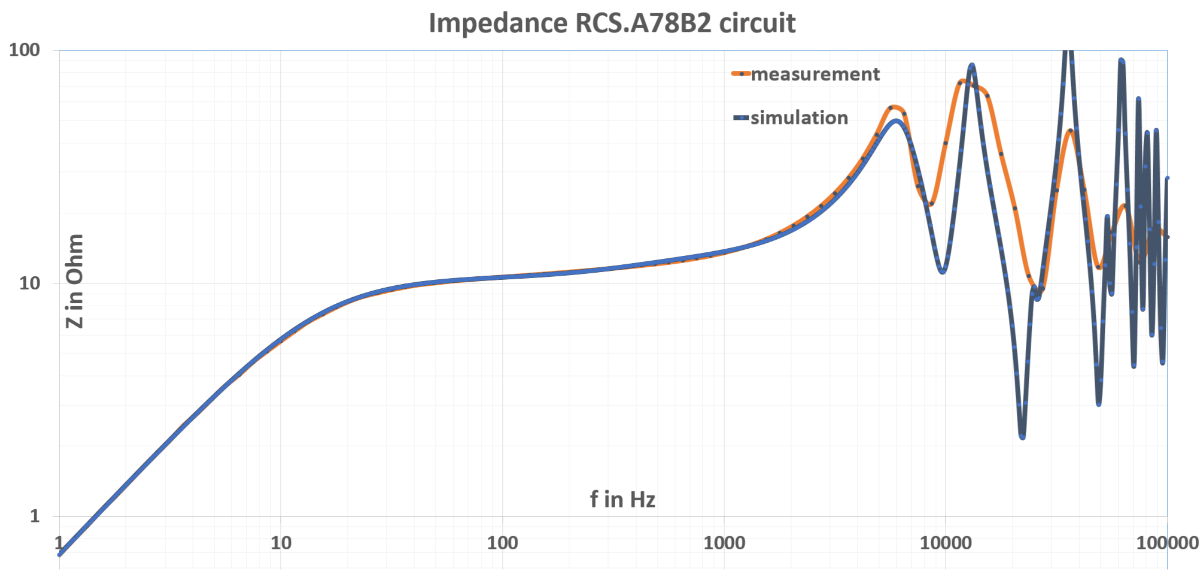

FIGURE 5.7: Simulation and measurement of the RCS.A78B2 circuit impedance curve as a function of frequency

Figure 5.7 shows that the simulation model almost perfectly matches the real measurement of the impedance behavior up to around 1 kHz. At higher frequencies, however, the differences between simulation and real measurement are clearly visible. In the low frequencies below 100 Hz, where the parasitic effects of the capacitances are barely effective, the approximated calculation of the complex circuit impedance is possible with the following formula[18].

$$Z_i = Re\{Z_i\} + jIm\{Z_i\} = \frac{RX_L^2}{R^2 + X_L^2} + j\frac{R^2 X_L}{R^2 + X_L^2} \tag{5.5}$$

With this formula the circuit is merely approximated. In this case, the circuit is assumed to be simplified as a series connection of 154 magnets and their parallel resistors. Other unwanted effects such as magnetization are not taken into account. Since the measurement have been made in the superconducting state of the cryostat, the resistances of the bus-bars are not present. In addition, the inductance of the bus-bars is also neglected.
The magnitude of the impedance is obtained by:

$$|Z_i| = \sqrt{(Re\{Z_i\})^2 + (Im\{Z_i\})^2} \tag{5.6}$$

A further simulation has the purpose to validate the parasitic capacitances of the RCS.A78B2 circuit model. In this case, the generator is connected to the circuit with the same system as in the previous impedance measurement. The entire circuit has no low-resistance connection to ground potential. A connection to the ground potential consists only of the high-resistance (>10 GΩ) digital multimeter card channels of the PXI measuring system an the parasitic capacitances. Thus, with the voltage drop of the shunt resistor, the current to ground via the parasitic capacitances can be determined. Here, too, the voltage of the shunt resistor is measured as a function of frequency.

As can be seen on the logarithmic scaled voltage measurement in Figure 5.8, there is a constant offset between real measurement and simulation. Since the simulation has a higher voltage compared to the measurement, which can especially be seen in CH_0, CH_1 and CH_2, a higher current flows in the simulation. Higher current results in this measurement mainly due to too large parasitic capacitances to ground. It is excluded that this is an ohmic resistance which is too small assumed in the circuit. This is due to the fact that the resistance value of an ohmic resistance does not vary with the frequency. However, this can be clearly seen in Figure 5.8.

In order to optimize the value of the capacitances to ground, some simulations have been made and the value of the capacitances has been adapted after each simulation. It is not

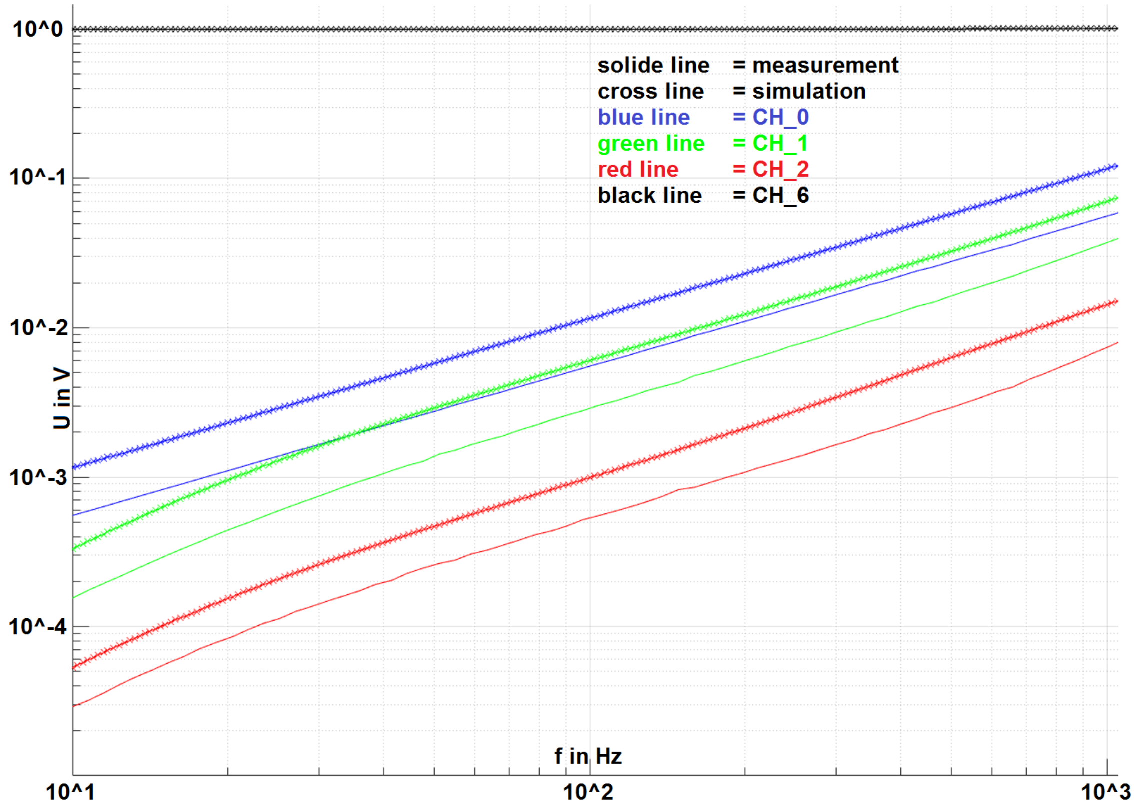

FIGURE 5.8: Voltage of the model with unchanged values for C to GND

enough to change only the capacitances to ground of the bus-bars. The largest part of the capacitances to ground contribute, as in Chapter 5.1 mentioned, the magnets. After consultation with a magnet expert of the group, the parasitic capacitances to ground should not deviate greatly from the calculations. The maximum deviation is defined as ±25%. Also, the value of the capacitances to ground at the bus-bars has been changed. Despite the variation of these two values by -22% and -50%, it is not possible to adjust the simulation of the measurements satisfactorily.

A significant improvement is shown by the additional change in the coupling capacitances between the bus-bars. By increasing their values by a factor of 3.5, a nearly perfect overlapping of the simulation and measurement results. Figure 5.9 shows this result with the last mentioned adjustments. On the basis of these findings it is to be assumed that the capacitances changed in the model are merely limited suitable for the real circuit.

What is also very clear in Figure 5.9 is the fact that the above-mentioned adaptations of the capacitances have significantly less influence on the voltage characteristic of CH_2. This channel measures the voltage between the beginning of the M bus-bar and the end of the magnet chain. However, it is important to note that Figure 5.9 has a logarithmic scale of the y-axis. The original CH_2 voltage measurement on the machine is more than the factor 16 smaller compared to the measurements of CH_0. Thus, the approximation of simulation to measurement of the CH_2 is more severe.

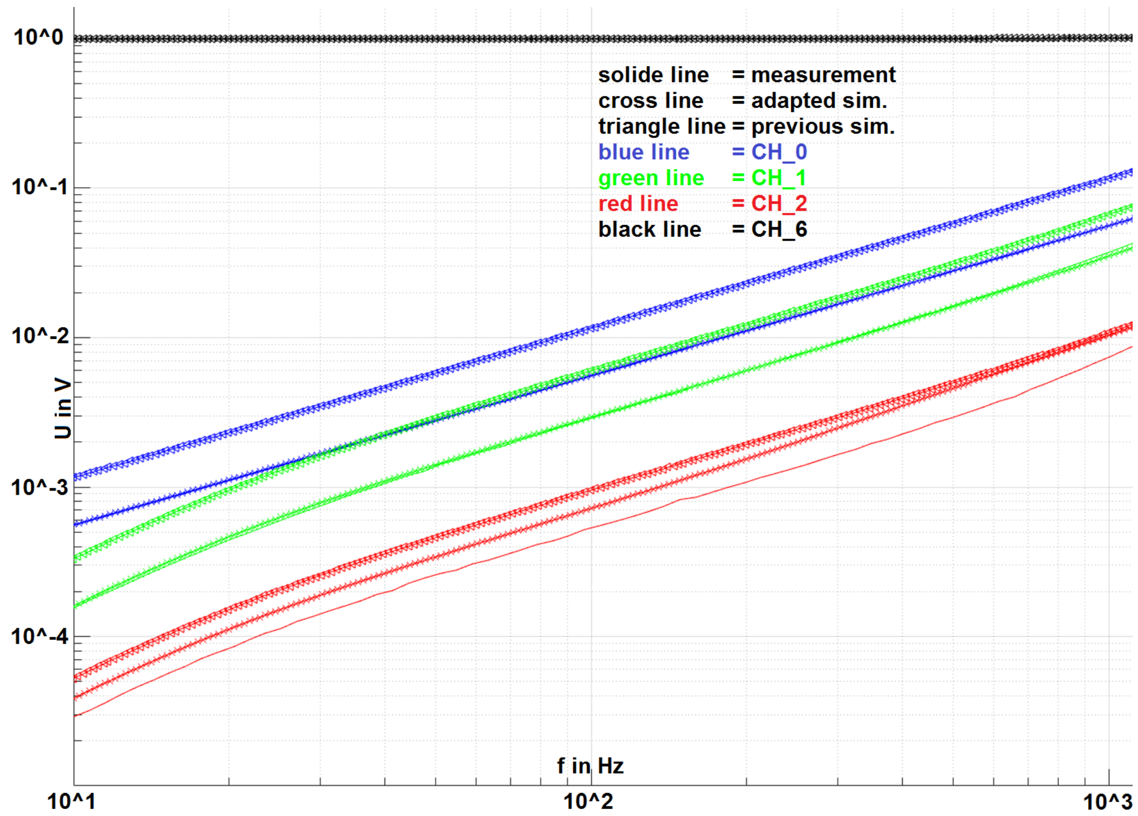

FIGURE 5.9: Voltage of the model with changed and unchanged values for C to GND

5.3.2 Insertion of the inductive coupling

With the obtaining of reference measurements by means of artificial ground faults, whose generation procedure is explained in Chapter 3.3.3, further simulations are undertaken. In the following simulations ground faults are feigned. This artificially generated ground fault is produced at one of the RCS.A78B2 Voltage taps. In this case, the voltage tap, which is directly connected to the circuit, is intentionally connected to the ground potential. This ground potential connection is produced by a low-resistance copper cable whose resistance value lies in the lower mΩ range. Thus, a nearly perfect ground fault is given by the voltage-tap position on the circuit and the ground potential.

Figure 5.10 shows the measurement and simulation of the RCS.A78B2 circuit with a short cut to ground at Voltage tap 35, which is also the input side of magnet number 35. In this simulation, the RCS model is used with the same parameters of the simulation from Figure 5.9. Up to a frequency of 1 kHz show except from CH_6 all simulated channels the same movement as the measured ones. However, the voltage courses of simulation and measurement are different from a frequency of 1 kHz. At the higher frequencies starting at 1 kHz, on the shunt-resistor, which is connected in series to the RCS circuit, falls significantly less voltage.

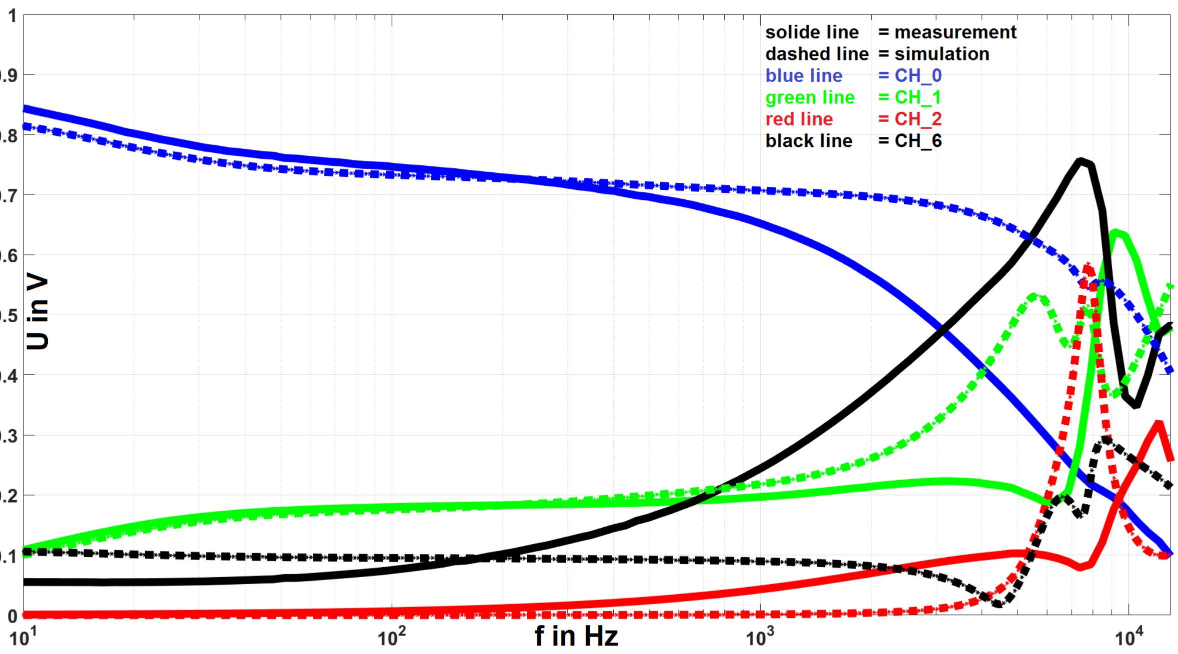

FIGURE 5.10: Voltage of the model without inductive coupling of the bus-bars

This means that less current flows through the circuit and thus the impedance of the circuit must be higher at these frequencies. The impedance of the entire circuit is thus also frequency-dependent. By increasing the bus-bar inductance, the impedance of the circuit at higher frequencies can be raised. This adaptation results in an improvement on the approximation from simulation to measurement at CH_0. However, this change also affects the other channels.

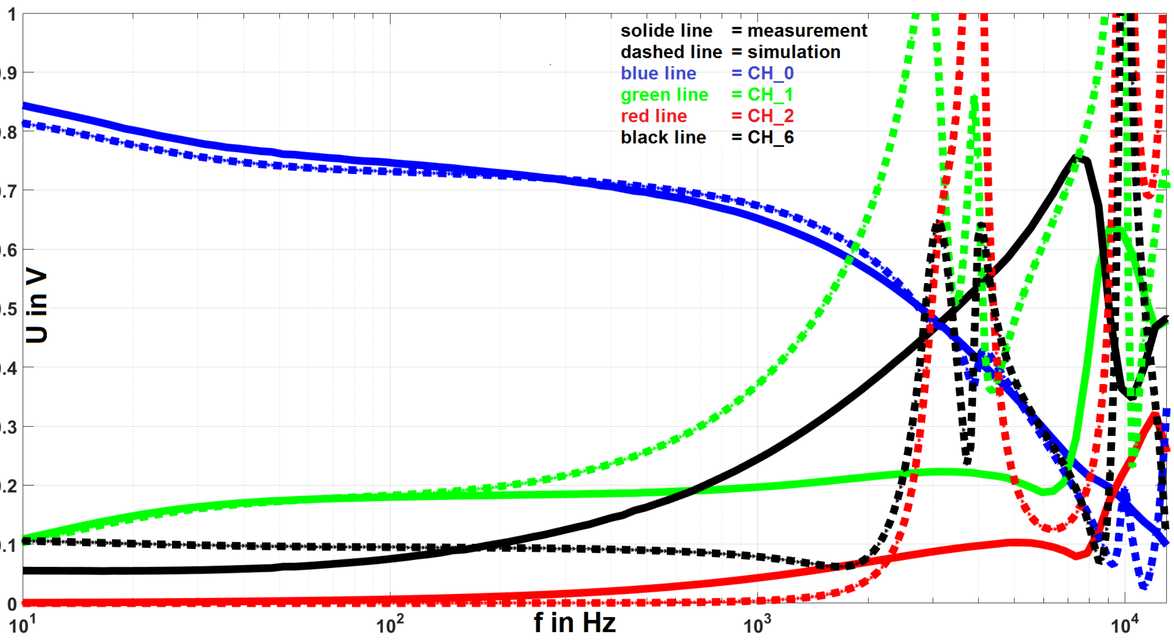

FIGURE 5.11: Voltage of the model without inductive coupling and increased inductance of the bus-bars

As can be seen in Figure 5.11, the overlapping of measurement and simulation at CH_0 has increased after the raise of the bus-bar inductance. In this case, the bus-bar inductance is increased by a factor of four. However, by comparison of simulation and measurement in Figure 5.11, the negative changes at CH_1, CH_2 and CH_6 can be seen well after the adaptation of the inductance. Due to the fact that the simulated current through the circuit and thus also the impedance of the entire RCS circuit with the ground fault at magnet 35 almost coincides with the measurement, there must be another constraint on the RCS circuit.

In the hitherto existing model of the RCS circuit, no parasitic inductive couplings are considered. The goal is therefore to change the bus-bar model to the extent that it can simulate the inductive coupling between the bus-bars. In this case, the parallel bus-bars communicate with one another through the induction law. The principle is the same as for a transformer in which the primary and secondary coils agitate with one another.

To realize the inductive coupling, the bus-bar model offers a suitable template. In this model, the respective partial inductances of the bus-bar sections are arranged according to the reality in the cryostat. This extension of the bus-bar model is done with the following code, which can be seen in Figure 5.12. The left column (K...) shows the name of the respective inductive coupling. With the letter K in the first place, the inductive coupling is indicated. The brackets contain the names of the two respective partial inductances communicating with one another. The variable containing the amount of inductive coupling per se is contained in the curved brackets. It can take the amount from 0 to 1. The closer the value of the variable is to 1, the higher is the inductive coupling between the aforementioned inductances in the circuit.

```
K_11_21 (l1_1 l2_1)  {Ind_coupling_A_B}
K_12_22 (l1_2 l2_2)  {Ind_coupling_A_B}
K_13_23 (l1_3 l2_3)  {Ind_coupling_A_B}
K_14_24 (l1_4 l2_4)  {Ind_coupling_A_B}

K_11_31 (l1_1 l3_1)  {Ind_coupling_A_M}
K_12_32 (l1_2 l3_2)  {Ind_coupling_A_M}
K_13_33 (l1_3 l3_3)  {Ind_coupling_A_M}
K_14_34 (l1_4 l3_4)  {Ind_coupling_A_M}

K_21_31 (l2_1 l3_1)  {Ind_coupling_B_M}
K_22_32 (l2_2 l3_2)  {Ind_coupling_B_M}
K_23_33 (l2_3 l3_3)  {Ind_coupling_B_M}
K_24_34 (l2_4 l3_4)  {Ind_coupling_B_M}
```

FIGURE 5.12: Code of the inductive coupling in the bus-bar

5.3.3 Further parameter definition after adjustment of the circuit

With the addition of the inductive coupling between the bus-bars, there is now a further, not precisely determined parameter in the bus-bar model. In addition to the inductive coupling, the inaccurately defined parameters also include the coupling capacitances between the bus-bars and the capacitances to ground. Some have already been defined in the previous chapters, but the ground fault simulation requires an adjustment of these parameters. The large differences between measurement and simulations, as shown in Figure 5.10 and Figure 5.11, confirm this. Since the value of the inductive coupling between the bus-bars can vary, this parameter is divided into:

- inductive coupling between A-lead and B-lead of the RCS.A78B2 circuit.
- inductive coupling between B-lead and M-lead of the RCS.A78B2 circuit.
- inductive coupling between A-lead and M-lead of the RCS.A78B2 circuit.

Thus there are now six parameters in the bus-bar model which are not exactly determined. The change by hand of these parameters before each simulation can be a very lengthy matter. This also depends on the number of simulations which are required for finding suitable parameter values.

In order to obtain the best possible simulation result with this circuit model, a large number of simulations as well as their comparison with the measurements have to be provided. Since six parameters of the bus-bar model should be determined at the same time, it is a six-dimensional function for finding the smallest error between simulation and measurement. The implementation of an algorithm, which automatically determines the optimal parameters according to the principle of the extreme value, becomes difficult. Furthermore, the error function may have countless local minima. For this reason, another method is used for adapting the bus-bar parameters. The parameters are modified according to the grid scheme. This means that for each of the six parameters, a value range and the step size in which the parameter per iteration is changed must be determined.

The resulting number of simulations following from the multiplication of the iteration steps of the respective parameter value range. An important part here is the useful selection of the value ranges of the searched parameters. For this purpose, the process is repeated several times, beginning with large ranges of values and large step sizes, both of which gradually become smaller and thus more precise.

To compare the individual resulting simulations per iteration step, the simulation results are compared with the measurements. This comparison takes a Matlab function and outputs an error value in the form of a scalar. The resulting error value can be compared with the error values of the other simulations. The following code section in Figure 5.13 shows how the uniform error value generation is implemented.

```
ch0_meas_resamp_y = spline ( freqmeas, mag_ch0_1, newFreqs);
ch0_sim_resamp_y = spline ( freqsim, vch0, newFreqs);
for q= 1: 1 : Iterations
error = error + (((ch0_meas_resamp_y(1,q) - ch0_sim_resamp_y(1,q))^2)^(1/2));
end
```

FIGURE 5.13: Code section for uniform error value generation

The resulting error value, which essentially indicates the deviation from simulation to measurement, is stored together with the bus-bar parameters used for this simulation in a further text file. This is also done by Matlab. All further simulation results are stored in the same text file and can be compared after the finish of all iterations. Microsoft Excel makes sense for this task.

Before each further simulation with PSpice, the parameters at the bus-bar model have to be changed. The PSpice bus-bar model is written in a text file, which is stored as a PSpice Model Library (.lib) file. This Library file can be opened with the "fopen" statement in Matlab and then edited. How the change of the six parameters at the bus-bar model is implemented in Matlab is shown in Figure 5.14.

```
fid = fopen(fileNameOrigBusBar);
txt = '';
tline = fgetl(fid);
while ischar(tline)
    tline = fgetl(fid);
    txt = [txt tline '\n'];
end
fclose(fid);
for(k = 1:length(p))
    txt = strrep(txt,['varParam(',num2str(k),')'],num2str(p(k)));
end
fid = fopen(fileName2owBusBar, 'w');
fprintf(fid,txt);
fclose(fid);
```

FIGURE 5.14: Code section for the bus-bar model changing

Now a variety of simulations can be executed and evaluated one after the other automatically. With this proceeding, the result was markedly improved as compared with that shown in Figure 5.11. One can see the clearly improved approach from simulation to measurement in Figure 5.15.

CH_0 and CH_6 show a visible distance from simulation to measurement in the lower frequencies at about 10 Hz in Figure 5.15. Since it can be assumed that this distance is also present in the case of a DC voltage, it must be a difference in the ohmic resistance of the measured RCS circuit. By adjusting the grounding resistance at Voltage tap 35 to 850 mΩ, the gaps from simulation to measurement can be reduced. This change can be seen in Figure 5.16.

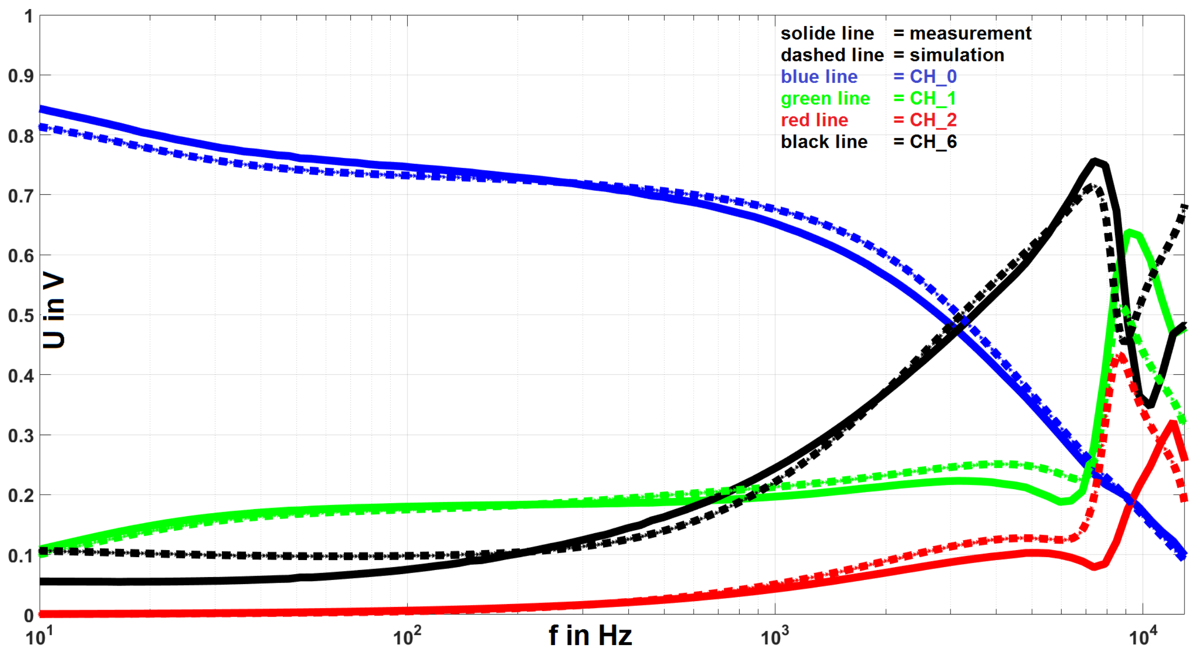

FIGURE 5.15: Voltage of the model with inductive coupling of the bus-bars

Furthermore, further measurements with artificial ground faults as mentioned in Chapter 3.3.3 are used to improve the RCS model. The connections between the measuring system and RCS.A78B2 have been slightly modified. The changed adjustment of the measuring system is shown in Figure 5.17.

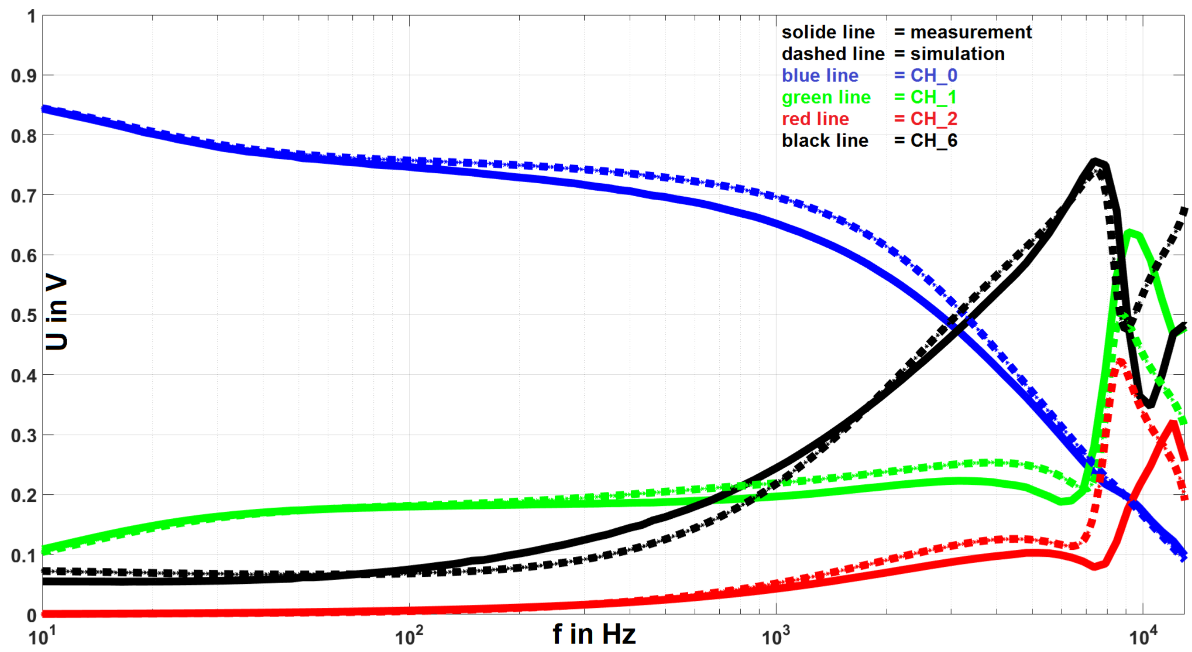

FIGURE 5.16: Voltage of the model with inductive coupling of the bus-bars and changed short-cut resistance

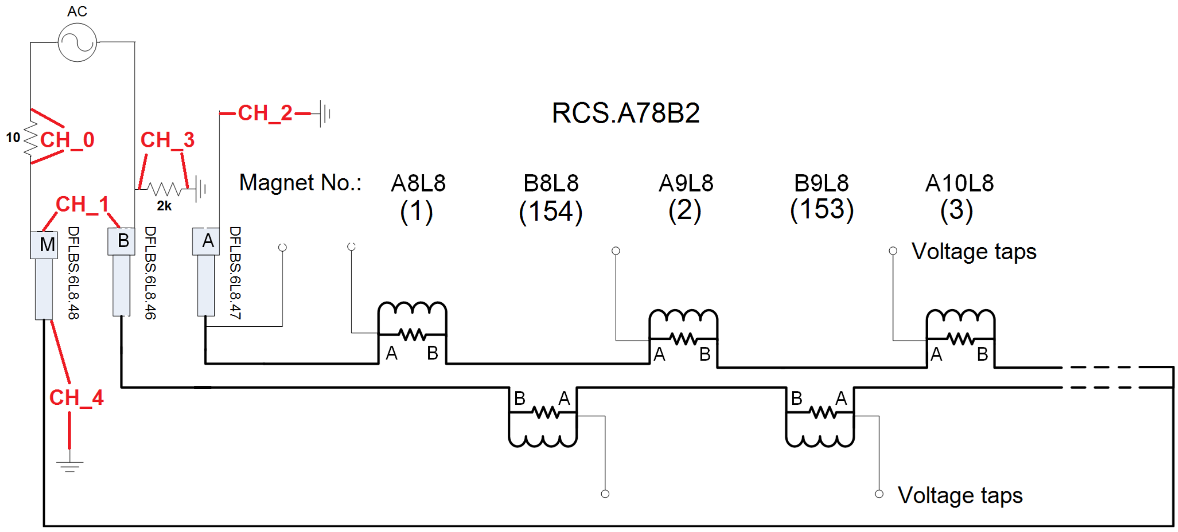

FIGURE 5.17: Changed RCS.A78B2 measurement setup schematic

The changed conditions are now:

- The entire measurement setup with circuit is almost in the floating state. A connection to ground is available only through the 2 kΩ resistor. The voltage drop at the 2 kΩ resistor is measured via CH_3.
- The influence of parasitic capacitances to ground at higher frequencies is reduced by the floating of the circuit.
- The AC generator is connected between the beginnings of M-lead and B-lead.
- Due to the 2 kΩ resistance from circuit to ground potential, the impedance value of the real or artificially generated ground fault plays a lesser role.
- Five measurement channels record the voltage curves at the points shown in Figure 5.17.

The previous mentioned procedure of this chapter is also applied to the last-shown configuration in Figure 5.17. The matching of simulation and measurement of the exemplary ground-fault position 35 are also given here with the same bus-bar model. In order to analyze how the model of the entire circuit behaves when the ground fault position changes, the ground fault position in the main-circuit PSpice file must be adjusted. The adaptation of the ground-fault positions in the main-circuit PSpice file is done with the same procedure as shown in Figure 5.14.

Not all measurements from the different positions of the artificial generated ground faults coincide with the simulations consistently good. Nevertheless, with the help of the last-mentioned model of the RCS circuit it is being attempted to determine the position of the real ground fault. For this purpose, the appropriate reference measurements are available, with which the simulations of the individual ground faults can be compared.

Final, an ground fault in the RCS model is generated successively at each Voltage tap and the behavior of the entire circuit is simulated. Into these 154 resulting simulations, the measurement of the real ground fault is inserted and displayed graphically. By combining the 154 resulting graphics in a PDF document, it is possible to get the best approximation of a simulation and the measurement of the real ground fault rapidly. The best match, which is at magnet position 42, is shown in Figure 5.18.

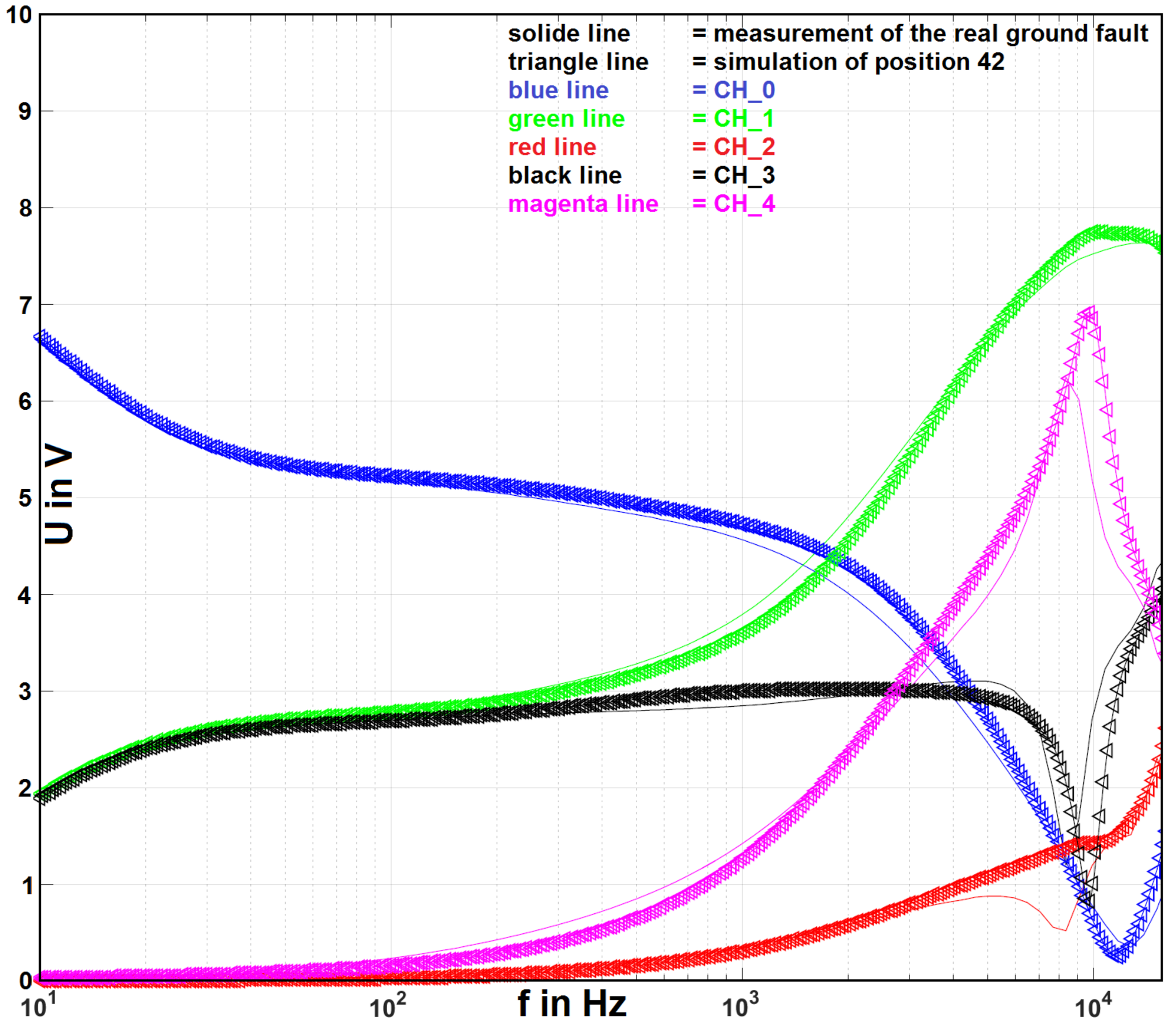

FIGURE 5.18: Best approximation of a simulation and the measurement of the real ground fault

In the RCS model generation, the characteristics and the behavior of the real circuit were approximated by several steps. This includes the consideration of parasitic capacitances to ground as well as between the bus-bars. With the introduction of inductive couplings between the bus-bars, it was possible to mimic the circuit under ground fault condition. The model parameters of the bus-bars have been optimized by multi-simulation and the automatic evaluation. Due to the fact that the model can not perfectly reflect the real circuit, the prediction of the real earth fault position with its infinite number of possible forms of appearance is not given. The synergies of simulations and measurements are indispensable for its determination.

The following statements can be made:

- A ground fault at the M-lead or B-lead can be excluded.
- The real ground fault is in the A-lead in the proximity of magnet 42.
- The model cannot identify the exact fault all-alone due to the infinite amount of fault position and fault impedance magnitude combinations.
- The simulation model is of great support for the measurement campaigns to validate or exclude hypotheses.

Chapter 6

Conclusion and outlook

6.1 Conclusion of the simulations

One of the main objectives of this thesis was the model design of the RCS magnet circuit. The RCS circuit is a circuit which is geometrically large and shows widely scattered physical effects. These physical and electrical properties could not be reproduced perfectly, but in the basic principles. With the help of sub-circuits of the bus bars and magnets, the complex design of the RCS magnet circuit could be presented in a simplified and practical form.

The other main goal was to determine the fault in the circuit as precisely as possible. For this, the parameters of the model were calculated and adapted so that the simulations match the test measurements as well as possible. The parameters were calculated using the geometrical approximation of the circuit elements as well as the simulation with COMSOL. Matlab enabled the using of an automated procedure to find the best parameters for the circuit in ground fault condition. The proof that the parameters used in the model, in particular the parameters of the bus-bars, are the same as the real parameters of the RCS circuit, is not made. The position of the real ground fault could not be determined exactly, but a variety of possibilities could be excluded. Thus, the position of the real ground fault is limited to a small part of the RCS circuit.

An alternative approach would be in retrospect to focus on the model of the bus-bars and to replicate their exact course throughout the entire circuit. It also seems sensible to prioritize the creation of an algorithm that allows the quick and efficient definition of the best possible parameters for the RCS circuit model.

A very reasonable method is the automatic parameter change in the circuit- and library files by Matlab. The uniform comparison of measurements with the help of Matlab has also proved to be efficient. Furthermore, the recording of various measurements in the tunnel with different configurations of the measuring system was a good decision in order to obtain a broad spectrum of reference data.

6.2 Outlook

The topic of the circuit simulation offers several possibilities of supplement. For the RCS simulation further adjustments of the models would be conceivable, which would represent the behavior of the entire circuit even better. It would also be possible to use an improved model to predict what happens in the event of further circuit faults and what measurements are to be expected. An example of this would be the error of a double ground fault.

Also, the use of the structure of this circuit model could be helpful for building a model of other magnet circuits with similar structure. The creation of universal libraries and functions in PSpice and Matlab supports this. It is also possible to work with graphical user interfaces, which makes the handling of the involved software more user-friendly. A further expansion step would be the connection of PSpice, Matlab and LabVIEW to a simulation software bundle. Thus, the main programs for circuit measurement and circuit simulation were networked efficiently and in a structured manner.

Bibliography

[1] CERN. The history of CERN. *access: 18.07.2017*, page 4, 2017. URL https://timeline.web.cern.ch/timelines/The-history-of-CERN.

[2] Lucio Rossi (CERN); Oliver Brüning (CERN). *The High Luminosity Large Hadron Collider: The new machine for illuminating the mysteries of Universe*. Hackensack, NJ World Scientific, 2015. ISBN 978-9814675468.

[3] Scott M. Rowan. LHC Main Dipole Magnet Circuits: Sustaining Near-Nominal Beam Energies. University of Glasgow, November 2016. Dissertation.

[4] TE Department CERN. Organisation. *access: 08.06.2017*, 2017. URL https://edms.cern.ch/ui/file/1764265/1/TE_June_2017_cdr_cpdf.pdf.

[5] R. B. Meinke, W. M. Hinson, M. Senti; Advanced Magnet Lab Inc, Palm Bay, Florida. W.J. Op de Beeck, C. De Ryck; SMCE NV Heist-op-den Berg, Belgium. SEXTUPOLE CORRECTION MAGNETS FOR THE LARGE HADRON COLLIDER. *IEEE*, pages 3212–3214, 1999. ISSN 0-7803-5573-3.

[6] M. Allitt, A. Ijspeert, M. Karppinen, J. Mazet, J. Perez, J. Salminen, S. Bapna, M. Karmarkar, A. Puntambekar, K. Ruwali, A. Thipsay. FURTHER DEVELOPMENT OF THE SEXTUPOLE AND DECAPOLE SPOOL CORRECTOR MAGNETS FOR THE LHC. Technical report, LHC Project Report 353, CERN, September 1999.

[7] Martin N. Wilson. *Superconducting magnets, Monographs on Cryogenics*. Clarendon Press, 1983. ISBN 0198548052.

[8] CERN. Superconductivity. *access: 13.07.2017*, 2017. URL https://home.cern/about/engineering/superconductivity.

[9] J.F. Annett. *Superconductivity, Superfluids and Condensates*. OUP Oxford, 2004. ISBN 9780198507567.

[10] C. Kittel. *Introduction to Solid State Physics*. Wiley, 2004. ISBN 9780471415268.

[11] K. Vinod, R. G. Abhilash Kumar, U. Syamaprasad; Regional Research Laboratory (CSIR), India. Prospects for mgb2 superconductors for magnet application. *SUPERCONDUCTOR SCIENCE AND TECHNOLOGY*, pages R1 – R13, December 2006. doi: 10.1088/0953-2048/20/1/R01.

[12] Y. Iwasa. *Case Studies in Superconducting Magnets: Design and Operational Issues*. Springer US, 2010. ISBN 9781441935397.

[13] H. Nishimori, G. Ortiz. *Elements of Phase Transitions and Critical Phenomena*. OUP Oxford, 2010. ISBN 9780191035531.

[14] C.P. Poole. *Superconductivity*. Superconductivity Series, Elsevier Science, 2007. ISBN 9780080550480.

[15] E. Ravaioli. *CLIQ: A new quench protection technology for superconducting magnets*. University of Twente, The Netherlands, 2015. ISBN 978-90-365-3908-1.

[16] L. Bottura. Cable stability. *CERN Yellow Report*, pages 401–451, May 2014. doi: 10.5170/CERN-2014-005.401.

[17] J.H. Schultz. Protection of superconducting magnets. *IEEE Transactions on Applied Superconductivity, vol. 12*, page no. 1, March 2002. doi: 10.1109/TASC.2002.1018662.

[18] K.-H. Mess, P. Schmueser, S. Wolf. *Superconducting Accelerator Magnets*. World Scientific, 1996. ISBN 981-02-2790-6.

[19] Thitipong Satiramatekul, Frédéric Bouillault. Magnetization of Coupled and Noncoupled Superconducting Filaments With Dependence of Current Density on Applied Field. *IEEE TRANSACTIONS ON MAGNETICS, VOL. 41*, pages 3751 – 3753, October 2005. doi: 10.1109/INTMAG.2005.1464021.

[20] R. L. Stoll. *The analysis of eddy currents*. Oxford University Press, 1974. ISBN 9780198593119.

[21] E. Ravaioli, B. Auchmann, A. P. Verweij. Fast method to quantify the collective magnetization in superconducting magnets. *IEEE Transactions on Applied Superconductivity, V23 I3*, pages 4700204 – 4700204, June 2013. doi: 10.1109/TASC.2012.2227649.

[22] A.P. Verweij. *ELECTRODYNAMICS OF SUPERCONDUCTING CABLES IN ACCELERATOR MAGNETS*. University Twente, Netherlands, 1995. ISBN 90-9008555-6.

[23] B. Auchmann, R. de Maria, S. Russenschuck. Comparative study of inter-strand coupling current models for accelerator magnets. *European Particle Accelerator Conference 2006*, pages 2631 – 2633, June 2006.

[24] Benjamin Crabtree. Build your own time-domain reflectometer. *access: 03.07.2017*, 2015. URL https://edms.cern.ch/ui/file/1764265/1/TE_June_2017_cdr_cpdf.pdf.

[25] L. Heinhold, R. Stubbe. *Power Cables and Their Applications*. Siemens Aktiengesellschaft, 1990. ISBN 978-3800915354.

[26] National Instruments. *SPECIFICATIONS PXI-4071*, 371371M-01 edition, January 2017.

[27] Muhammad H. Rashid, Hasan M. Rashid. *SPICE for Power Electronics and Electric Power*. CRC Press, 2005. ISBN 9780849334184.

[28] Cadence PCB Systems Division. *PSpice Reference Guide*. Cadence Design Systems, Inc., Second online edition, May 2000.

Appendix A

PSpice and Matlab Code

A.1 PSpice Code for circuit generation

A.1.1 Main circuit file

```
* PSPICE RCS Standard TEST Simulation File
* 08/2017 CERN
* Alexander Kiefer

*** Libraries --------------------------------------------------
*Pspice custom components Library
.LIB "C:\\RCS_Sim\\Library\\RCS_MCS_SuperCondState.lib"
.LIB "C:\\RCS_Sim\\Library\\RCS_BbWithIron_SuperCondState.lib"
.INCLUDE "C:\\RCS_Sim\\Library\\RCS_MCSChain.cir"

*** Main circuit -----------------------------------------------
v_in    (leadOut PS_out) ac 8 dc 0
r_2kMeas (leadOut node_GND) 2000
v_GndPS (node_GND 0) 0
v_simulation1 (PS_out 7998) 0
r_simulationADD (7998 7999) 0.12
r_shunt  (7999 N7775) 10
v_simulation2 (N7775 8000) 0
v_simulation2_1 (8000 N7776) 0
r_leadIn (N7776 x_MagChain.x_BusBar_1.300) 50e-6

*Inner Busbar
x_Bb_In  ( BB_In0 BB_Out0 BB_Out154 MAG_Out154)
    RCS_BusBar_NoIron_Inner

*Magnet chain
```

```
v1_bbIn_PH  (BB_Out0 MAG_In1) 0
x_MagChain  (MAG_In1 MAG_Out154) RCS_MCSChain

*ADDITIONAL V_Simulations for nodes .PROBE
V_simulation3 (BB_In0 8001) 0
r_simulation4 (8001 node_GND) 100000000
V_simulation5 (leadOut 8002) 0
r_simulation6 (8002 node_GND) 100000000

*Automated Selection for the whole circuit*********************
V_test4automatedSelection1 (x_MagChain.MAG_In5 11001) 0
V_test4automatedSelection2 (x_MagChain.MAG_In11 11002) 0
V_test4automatedSelection3 (x_MagChain.MAG_In17 11003) 0
V_test4automatedSelection4 (x_MagChain.MAG_In23 11004) 0
V_test4automatedSelection5 (x_MagChain.MAG_In29 11005) 0
V_test4automatedSelection6 (x_MagChain.MAG_In35 11006) 0
V_test4automatedSelection7 (x_MagChain.MAG_In42 11007) 0
V_test4automatedSelection8 (x_MagChain.MAG_In47 11008) 0
V_test4automatedSelection9 (x_MagChain.MAG_In52 11009) 0
V_test4automatedSelection10 (x_MagChain.MAG_In57 11010) 0
V_test4automatedSelection11 (x_MagChain.MAG_In64 11011) 0
V_test4automatedSelection12 (x_MagChain.MAG_In70 11012) 0
V_test4automatedSelection13 (x_MagChain.MAG_In75 11013) 0
V_test4automatedSelection14 (x_MagChain.MAG_In78 11014) 0
V_test4automatedSelection15 (x_MagChain.MAG_In80 11015) 0
V_test4automatedSelection16 (x_MagChain.MAG_In85 11016) 0
V_test4automatedSelection17 (x_MagChain.MAG_In91 11017) 0
V_test4automatedSelection18 (x_MagChain.MAG_In97 11018) 0
V_test4automatedSelection19 (x_MagChain.MAG_In103 11019) 0
V_test4automatedSelection20 (x_MagChain.MAG_In108 11020) 0
V_test4automatedSelection21 (x_MagChain.MAG_In114 11021) 0
V_test4automatedSelection22 (x_MagChain.MAG_In120 11022) 0
V_test4automatedSelection23 (x_MagChain.MAG_In126 11023) 0
V_test4automatedSelection24 (x_MagChain.MAG_In132 11024) 0
V_test4automatedSelection25 (x_MagChain.MAG_In138 11025) 0
V_test4automatedSelection26 (x_MagChain.MAG_In144 11026) 0
V_test4automatedSelection27 (x_MagChain.MAG_In150 11027) 0

R_test4automatedSelection29 (x_MagChain.MAG_In154 11000) 10000000
V_test4automatedSelection29 (11000 0) 0

*TEST Shortcut
r_testShortCut (varParamNode node_GND) 0.5

* Outer circuit to PS
```

```
r_leadOut   (BB_Out154 leadOut) 50e-6

r_exchange_PXI_CH_6_Voltage_Measurement (leadOut node_GND) 1000000

*** Solver -------------------------------------------------------
.AC dec 100 500Hz 20000Hz

*** Post Processing ----------------------------------------------
.PROBE V(7999,8000) V(8000,8002) V(8001,0) V(8002,0) V(8000,0)
*      CH0         CH1         CH2       CH3       CH4

.END
```

A.1.2 Superconducting corrector magnet

```
.subckt RCS_MCS_Corrector   1_pIn 1_pMid  1_pOut 1_pGND
+ PARAMS:
+ L_mag=0.8e-3 rGnd1=10e09 rGnd2=10e09 rGnd3=10e09 rGnd4=10e09

.PARAM CtoGnd=4.875e-9

*Inner Busbar
v1_bbIn_PlaceHolder (1_pIn 100) 0

*Poles
l_1 (100 101) {L_mag/2}
l_2 (101 102) {L_mag/2}

*Midport for picking up voltage across each aperture
v1_bbMid_PlaceHolder (101 1_pMid) 0

*Resistor in parallel
rp (100 102) 65.5e-3

*GND circuit
cGnd1_1    (100 1_pGND) {CtoGnd/4}
rGnd1_1    (100 1_pGND) {rGnd1}

cGndPar1_2 (101 1_pGND) {CtoGnd/2}
rGndPar1_2 (101 1_pGND) {(rGnd2*rGnd3)/(rGnd2+rGnd3)}

cGnd2_2    (102 1_pGND) {CtoGnd/4}
rGnd2_2    (102 1_pGND) {rGnd4}

*Outer Busbar
```

```
v1_bbOut_PlaceHolder (102 1_pOut) 0

.ends
```

A.1.3 Superconducting bus-bar segment

```
.subckt RCS_BusBar_WithIron 2_pIn 2_pOut 1_pIn 1_pOut 3_pIn 3_pOut

.PARAM L_change_factor = varParam(1)
.PARAM Ind_coupling_A_B = varParam(2)
.PARAM Ind_coupling_B_M = varParam(3)
.PARAM Ind_coupling_A_M = varParam(4)
.PARAM C_coupling_change_factor = varParam(5)
.PARAM C_ToGND_change_factor = varParam(6)
.PARAM R_eddy_change_factor = 1
.PARAM Coupling = 1

* Position 1 Params ***************************************
.PARAM L_aut_1  = 0.942e-6
.PARAM length_1 = 35
.PARAM k_1      = 0.3235
.PARAM rEddy_1  = {(1/Coupling*0.47e-3) * R_eddy_change_factor}
.PARAM C_1Gnd   = {1.445e-9 * C_ToGND_change_factor}
.PARAM C_12     = {15.9e-9 * C_coupling_change_factor}

* Position 2 Params ***************************************
.PARAM L_aut_2  = 0.942e-6
.PARAM length_2 = {length_1}
.PARAM k_2      = {k_1}
.PARAM rEddy_2  = {rEddy_1}
.PARAM C_2Gnd   = {0.4445e-9 * C_ToGND_change_factor}
.PARAM C_21     = 3e-9
.PARAM C_23     = {C_12}

* Position 3 Params ***************************************
.PARAM L_aut_3  = 0.942e-6
.PARAM length_3 = {length_1}
.PARAM k_3      = {k_1}
.PARAM rEddy_3  = {rEddy_1}
.PARAM C_32     = 3e-9
.PARAM C_3Gnd   = {0.3885e-9 * C_ToGND_change_factor}
.PARAM C_13   = {C_12/2}

* Mutual Params *******************************************
.PARAM L_bb1 = {L_aut_1-M_12}
```

```
.PARAM L_bb2 = {L_aut_2-M_21}
.PARAM L_bb3 = {L_aut_3-M_21}

* Position 1 *********************************************
v1_In_PH (1_pIn 100) 0

l1_1     (100 101) {((1-k_1) * L_bb1 * length_1/2) *
    L_change_factor }
l1_2     (101 102) {((k_1)   * L_bb1 * length_1/2) *
    L_change_factor }
l1_3     (102 103) {((1-k_1) * L_bb1 * length_1/2) *
    L_change_factor }
l1_4     (103 104) {((k_1)   * L_bb1 * length_1/2) *
    L_change_factor }

*Eddy currents
r1_1     (101 102) {rEddy_1}
r1_2     (103 104) {rEddy_1}

*Parasitic Capacitances
c_1Gnd_1 (100 0) {C_1Gnd/4}
c_1Gnd_2 (102 0) {C_1Gnd/2}
c_1Gnd_4 (104 0) {C_1Gnd/4}

c_12_1   (100 200) {C_12/4}
c_12_2   (102 202) {C_12/2}
c_12_4   (104 204) {C_12/4}

v1_Out_PH (104 1_pOut) 0

* Position 2 *********************************************
v2_In_PH (2_pIn 200) 0

l2_1     (200 201) {((1-k_2) * L_bb2 * length_2/2) *
    L_change_factor }
l2_2     (201 202) {((k_2)   * L_bb2 * length_2/2) *
    L_change_factor }
l2_3     (202 203) {((1-k_2) * L_bb2 * length_2/2) *
    L_change_factor }
l2_4     (203 204) {((k_2)   * L_bb2 * length_2/2) *
    L_change_factor }

*Eddy currents
r2_1     (201 202) {rEddy_2}
r2_2     (203 204) {rEddy_2}
```

```

*Parasitic Capacitances
c_2Gnd_1 (200 0) {C_2Gnd/4}
c_2Gnd_2 (202 0) {C_2Gnd/2}
c_2Gnd_4 (204 0) {C_2Gnd/4}

c_23_1   (200 300) {C_23/4}
c_23_2   (202 302) {C_23/2}
c_23_4   (204 304) {C_23/4}

v2_Out_PH (204 2_pOut) 0

* Position 3 ***********************************************
v3_In_PH (3_pIn 300) 0

l3_1    (300 301) {((1-k_3) * L_bb3 * length_3/2) * L_change_factor  }
l3_2    (301 302) {((k_3)   * L_bb3 * length_3/2) * L_change_factor  }
l3_3    (302 303) {((1-k_3) * L_bb3 * length_3/2) * L_change_factor  }
l3_4    (303 304) {((k_3)   * L_bb3 * length_3/2) * L_change_factor  }

*Eddy currents
r3_1    (301 302) {rEddy_3}
r3_2    (303 304) {rEddy_3}

*Parasitic Capacitances
c_3Gnd_1 (300 0) {C_3Gnd/4}
c_3Gnd_2 (302 0) {C_3Gnd/2}
c_3Gnd_4 (304 0) {C_3Gnd/4}

c_31_1   (100 300) {C_13/4}
c_31_2   (102 302) {C_13/2}
c_31_4   (104 304) {C_13/4}

v3_Out_PH (304 3_pOut) 0

* Mutuals **************************************************

K_11_21 (l1_1 l2_1)  {Ind_coupling_A_B}
K_12_22 (l1_2 l2_2)  {Ind_coupling_A_B}
K_13_23 (l1_3 l2_3)  {Ind_coupling_A_B}
K_14_24 (l1_4 l2_4)  {Ind_coupling_A_B}
```

```
K_11_31 (l1_1 l3_1) {Ind_coupling_A_M}
K_12_32 (l1_2 l3_2) {Ind_coupling_A_M}
K_13_33 (l1_3 l3_3) {Ind_coupling_A_M}
K_14_34 (l1_4 l3_4) {Ind_coupling_A_M}

K_21_31 (l2_1 l3_1) {Ind_coupling_B_M}
K_22_32 (l2_2 l3_2) {Ind_coupling_B_M}
K_23_33 (l2_3 l3_3) {Ind_coupling_B_M}
K_24_34 (l2_4 l3_4) {Ind_coupling_B_M}

.ends
```

A.1.4 Creation of the circuit order

```
.subckt RCS_MCSChain  MAG_In1 MAG_Out154

*Magnets Series
x_MCS1  ( MAG_In1 MAG_Mid1 MAG_Out1 0 ) RCS_MCS_Corrector
+  PARAMS: L_mag=0.6972e-3 rGnd1=100e09 rGnd2=100e09 rGnd3=100e09
    rGnd4=100e09
x_MCS2  ( MAG_In2 MAG_Mid2 MAG_Out2 0 ) RCS_MCS_Corrector
+  PARAMS: L_mag=0.6972e-3 rGnd1=100e09 rGnd2=100e09 rGnd3=100e09
    rGnd4=100e09
x_MCS3  ( MAG_In3 MAG_Mid3 MAG_Out3 0 ) RCS_MCS_Corrector
+  PARAMS: L_mag=0.6972e-3 rGnd1=100e09 rGnd2=100e09 rGnd3=100e09
    rGnd4=100e09
x_MCS4  ( MAG_In4 MAG_Mid4 MAG_Out4 0 ) RCS_MCS_Corrector
+  PARAMS: L_mag=0.6972e-3 rGnd1=100e09 rGnd2=100e09 rGnd3=100e09
    rGnd4=100e09
x_MCS5  ( MAG_In5 MAG_Mid5 MAG_Out5 0 ) RCS_MCS_Corrector
+  PARAMS: L_mag=0.6972e-3 rGnd1=100e09 rGnd2=100e09 rGnd3=100e09
    rGnd4=100e09
x_MCS6  ( MAG_In6 MAG_Mid6 MAG_Out6 0 ) RCS_MCS_Corrector
+  PARAMS: L_mag=0.6972e-3 rGnd1=100e09 rGnd2=100e09 rGnd3=100e09
    rGnd4=100e09
x_MCS7  ( MAG_In7 MAG_Mid7 MAG_Out7 0 ) RCS_MCS_Corrector
+  PARAMS: L_mag=0.6972e-3 rGnd1=100e09 rGnd2=100e09 rGnd3=100e09
    rGnd4=100e09
x_MCS8  ( MAG_In8 MAG_Mid8 MAG_Out8 0 ) RCS_MCS_Corrector
+  PARAMS: L_mag=0.6972e-3 rGnd1=100e09 rGnd2=100e09 rGnd3=100e09
    rGnd4=100e09
x_MCS9  ( MAG_In9 MAG_Mid9 MAG_Out9 0 ) RCS_MCS_Corrector
+  PARAMS: L_mag=0.6972e-3 rGnd1=100e09 rGnd2=100e09 rGnd3=100e09
    rGnd4=100e09
```

```
x_MCS10  ( MAG_In10 MAG_Mid10 MAG_Out10 0 ) RCS_MCS_Corrector
+  PARAMS: L_mag=0.6972e-3 rGnd1=100e09 rGnd2=100e09 rGnd3=100e09 rGnd4=100e09
x_MCS11  ( MAG_In11 MAG_Mid11 MAG_Out11 0 ) RCS_MCS_Corrector
+  PARAMS: L_mag=0.6972e-3 rGnd1=100e09 rGnd2=100e09 rGnd3=100e09 rGnd4=100e09
x_MCS12  ( MAG_In12 MAG_Mid12 MAG_Out12 0 ) RCS_MCS_Corrector
+  PARAMS: L_mag=0.6972e-3 rGnd1=100e09 rGnd2=100e09 rGnd3=100e09 rGnd4=100e09
x_MCS13  ( MAG_In13 MAG_Mid13 MAG_Out13 0 ) RCS_MCS_Corrector
+  PARAMS: L_mag=0.6972e-3 rGnd1=100e09 rGnd2=100e09 rGnd3=100e09 rGnd4=100e09
x_MCS14  ( MAG_In14 MAG_Mid14 MAG_Out14 0 ) RCS_MCS_Corrector
+  PARAMS: L_mag=0.6972e-3 rGnd1=100e09 rGnd2=100e09 rGnd3=100e09 rGnd4=100e09
x_MCS15  ( MAG_In15 MAG_Mid15 MAG_Out15 0 ) RCS_MCS_Corrector
+  PARAMS: L_mag=0.6972e-3 rGnd1=100e09 rGnd2=100e09 rGnd3=100e09 rGnd4=100e09
x_MCS16  ( MAG_In16 MAG_Mid16 MAG_Out16 0 ) RCS_MCS_Corrector
+  PARAMS: L_mag=0.6972e-3 rGnd1=100e09 rGnd2=100e09 rGnd3=100e09 rGnd4=100e09
x_MCS17  ( MAG_In17 MAG_Mid17 MAG_Out17 0 ) RCS_MCS_Corrector
+  PARAMS: L_mag=0.6972e-3 rGnd1=100e09 rGnd2=100e09 rGnd3=100e09 rGnd4=100e09
x_MCS18  ( MAG_In18 MAG_Mid18 MAG_Out18 0 ) RCS_MCS_Corrector
+  PARAMS: L_mag=0.6972e-3 rGnd1=100e09 rGnd2=100e09 rGnd3=100e09 rGnd4=100e09
x_MCS19  ( MAG_In19 MAG_Mid19 MAG_Out19 0 ) RCS_MCS_Corrector
+  PARAMS: L_mag=0.6972e-3 rGnd1=100e09 rGnd2=100e09 rGnd3=100e09 rGnd4=100e09
x_MCS20  ( MAG_In20 MAG_Mid20 MAG_Out20 0 ) RCS_MCS_Corrector
+  PARAMS: L_mag=0.6972e-3 rGnd1=100e09 rGnd2=100e09 rGnd3=100e09 rGnd4=100e09
x_MCS21  ( MAG_In21 MAG_Mid21 MAG_Out21 0 ) RCS_MCS_Corrector
+  PARAMS: L_mag=0.6972e-3 rGnd1=100e09 rGnd2=100e09 rGnd3=100e09 rGnd4=100e09
x_MCS22  ( MAG_In22 MAG_Mid22 MAG_Out22 0 ) RCS_MCS_Corrector
+  PARAMS: L_mag=0.6972e-3 rGnd1=100e09 rGnd2=100e09 rGnd3=100e09 rGnd4=100e09
x_MCS23  ( MAG_In23 MAG_Mid23 MAG_Out23 0 ) RCS_MCS_Corrector
+  PARAMS: L_mag=0.6972e-3 rGnd1=100e09 rGnd2=100e09 rGnd3=100e09 rGnd4=100e09
x_MCS24  ( MAG_In24 MAG_Mid24 MAG_Out24 0 ) RCS_MCS_Corrector
+  PARAMS: L_mag=0.6972e-3 rGnd1=100e09 rGnd2=100e09 rGnd3=100e09 rGnd4=100e09
```

```
x_MCS25 ( MAG_In25 MAG_Mid25 MAG_Out25 0 ) RCS_MCS_Corrector
+ PARAMS: L_mag=0.6972e-3 rGnd1=100e09 rGnd2=100e09 rGnd3=100e09 rGnd4=100e09
x_MCS26 ( MAG_In26 MAG_Mid26 MAG_Out26 0 ) RCS_MCS_Corrector
+ PARAMS: L_mag=0.6972e-3 rGnd1=100e09 rGnd2=100e09 rGnd3=100e09 rGnd4=100e09
x_MCS27 ( MAG_In27 MAG_Mid27 MAG_Out27 0 ) RCS_MCS_Corrector
+ PARAMS: L_mag=0.6972e-3 rGnd1=100e09 rGnd2=100e09 rGnd3=100e09 rGnd4=100e09
x_MCS28 ( MAG_In28 MAG_Mid28 MAG_Out28 0 ) RCS_MCS_Corrector
+ PARAMS: L_mag=0.6972e-3 rGnd1=100e09 rGnd2=100e09 rGnd3=100e09 rGnd4=100e09
x_MCS29 ( MAG_In29 MAG_Mid29 MAG_Out29 0 ) RCS_MCS_Corrector
+ PARAMS: L_mag=0.6972e-3 rGnd1=100e09 rGnd2=100e09 rGnd3=100e09 rGnd4=100e09
x_MCS30 ( MAG_In30 MAG_Mid30 MAG_Out30 0 ) RCS_MCS_Corrector
+ PARAMS: L_mag=0.6972e-3 rGnd1=100e09 rGnd2=100e09 rGnd3=100e09 rGnd4=100e09
x_MCS31 ( MAG_In31 MAG_Mid31 MAG_Out31 0 ) RCS_MCS_Corrector
+ PARAMS: L_mag=0.6972e-3 rGnd1=100e09 rGnd2=100e09 rGnd3=100e09 rGnd4=100e09
x_MCS32 ( MAG_In32 MAG_Mid32 MAG_Out32 0 ) RCS_MCS_Corrector
+ PARAMS: L_mag=0.6972e-3 rGnd1=100e09 rGnd2=100e09 rGnd3=100e09 rGnd4=100e09
x_MCS33 ( MAG_In33 MAG_Mid33 MAG_Out33 0 ) RCS_MCS_Corrector
+ PARAMS: L_mag=0.6972e-3 rGnd1=100e09 rGnd2=100e09 rGnd3=100e09 rGnd4=100e09
x_MCS34 ( MAG_In34 MAG_Mid34 MAG_Out34 0 ) RCS_MCS_Corrector
+ PARAMS: L_mag=0.6972e-3 rGnd1=100e09 rGnd2=100e09 rGnd3=100e09 rGnd4=100e09
x_MCS35 ( MAG_In35 MAG_Mid35 MAG_Out35 0 ) RCS_MCS_Corrector
+ PARAMS: L_mag=0.6972e-3 rGnd1=100e09 rGnd2=100e09 rGnd3=100e09 rGnd4=100e09
x_MCS36 ( MAG_In36 MAG_Mid36 MAG_Out36 0 ) RCS_MCS_Corrector
+ PARAMS: L_mag=0.6972e-3 rGnd1=100e09 rGnd2=100e09 rGnd3=100e09 rGnd4=100e09
x_MCS37 ( MAG_In37 MAG_Mid37 MAG_Out37 0 ) RCS_MCS_Corrector
+ PARAMS: L_mag=0.6972e-3 rGnd1=100e09 rGnd2=100e09 rGnd3=100e09 rGnd4=100e09
x_MCS38 ( MAG_In38 MAG_Mid38 MAG_Out38 0 ) RCS_MCS_Corrector
+ PARAMS: L_mag=0.6972e-3 rGnd1=100e09 rGnd2=100e09 rGnd3=100e09 rGnd4=100e09
x_MCS39 ( MAG_In39 MAG_Mid39 MAG_Out39 0 ) RCS_MCS_Corrector
+ PARAMS: L_mag=0.6972e-3 rGnd1=100e09 rGnd2=100e09 rGnd3=100e09 rGnd4=100e09
```

```
x_MCS40  ( MAG_In40 MAG_Mid40 MAG_Out40 0 ) RCS_MCS_Corrector
+  PARAMS: L_mag=0.6972e-3 rGnd1=100e09 rGnd2=100e09 rGnd3=100e09 rGnd4=100e09
x_MCS41  ( MAG_In41 MAG_Mid41 MAG_Out41 0 ) RCS_MCS_Corrector
+  PARAMS: L_mag=0.6972e-3 rGnd1=100e09 rGnd2=100e09 rGnd3=100e09 rGnd4=100e09
x_MCS42  ( MAG_In42 MAG_Mid42 MAG_Out42 0 ) RCS_MCS_Corrector
+  PARAMS: L_mag=0.6972e-3 rGnd1=100e09 rGnd2=100e09 rGnd3=100e09 rGnd4=100e09
x_MCS43  ( MAG_In43 MAG_Mid43 MAG_Out43 0 ) RCS_MCS_Corrector
+  PARAMS: L_mag=0.6972e-3 rGnd1=100e09 rGnd2=100e09 rGnd3=100e09 rGnd4=100e09
x_MCS44  ( MAG_In44 MAG_Mid44 MAG_Out44 0 ) RCS_MCS_Corrector
+  PARAMS: L_mag=0.6972e-3 rGnd1=100e09 rGnd2=100e09 rGnd3=100e09 rGnd4=100e09
x_MCS45  ( MAG_In45 MAG_Mid45 MAG_Out45 0 ) RCS_MCS_Corrector
+  PARAMS: L_mag=0.6972e-3 rGnd1=100e09 rGnd2=100e09 rGnd3=100e09 rGnd4=100e09
x_MCS46  ( MAG_In46 MAG_Mid46 MAG_Out46 0 ) RCS_MCS_Corrector
+  PARAMS: L_mag=0.6972e-3 rGnd1=100e09 rGnd2=100e09 rGnd3=100e09 rGnd4=100e09
x_MCS47  ( MAG_In47 MAG_Mid47 MAG_Out47 0 ) RCS_MCS_Corrector
+  PARAMS: L_mag=0.6972e-3 rGnd1=100e09 rGnd2=100e09 rGnd3=100e09 rGnd4=100e09
x_MCS48  ( MAG_In48 MAG_Mid48 MAG_Out48 0 ) RCS_MCS_Corrector
+  PARAMS: L_mag=0.6972e-3 rGnd1=100e09 rGnd2=100e09 rGnd3=100e09 rGnd4=100e09
x_MCS49  ( MAG_In49 MAG_Mid49 MAG_Out49 0 ) RCS_MCS_Corrector
+  PARAMS: L_mag=0.6972e-3 rGnd1=100e09 rGnd2=100e09 rGnd3=100e09 rGnd4=100e09
x_MCS50  ( MAG_In50 MAG_Mid50 MAG_Out50 0 ) RCS_MCS_Corrector
+  PARAMS: L_mag=0.6972e-3 rGnd1=100e09 rGnd2=100e09 rGnd3=100e09 rGnd4=100e09
x_MCS51  ( MAG_In51 MAG_Mid51 MAG_Out51 0 ) RCS_MCS_Corrector
+  PARAMS: L_mag=0.6972e-3 rGnd1=100e09 rGnd2=100e09 rGnd3=100e09 rGnd4=100e09
x_MCS52  ( MAG_In52 MAG_Mid52 MAG_Out52 0 ) RCS_MCS_Corrector
+  PARAMS: L_mag=0.6972e-3 rGnd1=100e09 rGnd2=100e09 rGnd3=100e09 rGnd4=100e09
x_MCS53  ( MAG_In53 MAG_Mid53 MAG_Out53 0 ) RCS_MCS_Corrector
+  PARAMS: L_mag=0.6972e-3 rGnd1=100e09 rGnd2=100e09 rGnd3=100e09 rGnd4=100e09
x_MCS54  ( MAG_In54 MAG_Mid54 MAG_Out54 0 ) RCS_MCS_Corrector
+  PARAMS: L_mag=0.6972e-3 rGnd1=100e09 rGnd2=100e09 rGnd3=100e09 rGnd4=100e09
```

```
x_MCS55  ( MAG_In55 MAG_Mid55 MAG_Out55 0 ) RCS_MCS_Corrector
+  PARAMS: L_mag=0.6972e-3 rGnd1=100e09 rGnd2=100e09 rGnd3=100e09 rGnd4=100e09
x_MCS56  ( MAG_In56 MAG_Mid56 MAG_Out56 0 ) RCS_MCS_Corrector
+  PARAMS: L_mag=0.6972e-3 rGnd1=100e09 rGnd2=100e09 rGnd3=100e09 rGnd4=100e09
x_MCS57  ( MAG_In57 MAG_Mid57 MAG_Out57 0 ) RCS_MCS_Corrector
+  PARAMS: L_mag=0.6972e-3 rGnd1=100e09 rGnd2=100e09 rGnd3=100e09 rGnd4=100e09
x_MCS58  ( MAG_In58 MAG_Mid58 MAG_Out58 0 ) RCS_MCS_Corrector
+  PARAMS: L_mag=0.6972e-3 rGnd1=100e09 rGnd2=100e09 rGnd3=100e09 rGnd4=100e09
x_MCS59  ( MAG_In59 MAG_Mid59 MAG_Out59 0 ) RCS_MCS_Corrector
+  PARAMS: L_mag=0.6972e-3 rGnd1=100e09 rGnd2=100e09 rGnd3=100e09 rGnd4=100e09
x_MCS60  ( MAG_In60 MAG_Mid60 MAG_Out60 0 ) RCS_MCS_Corrector
+  PARAMS: L_mag=0.6972e-3 rGnd1=100e09 rGnd2=100e09 rGnd3=100e09 rGnd4=100e09
x_MCS61  ( MAG_In61 MAG_Mid61 MAG_Out61 0 ) RCS_MCS_Corrector
+  PARAMS: L_mag=0.6972e-3 rGnd1=100e09 rGnd2=100e09 rGnd3=100e09 rGnd4=100e09
x_MCS62  ( MAG_In62 MAG_Mid62 MAG_Out62 0 ) RCS_MCS_Corrector
+  PARAMS: L_mag=0.6972e-3 rGnd1=100e09 rGnd2=100e09 rGnd3=100e09 rGnd4=100e09
x_MCS63  ( MAG_In63 MAG_Mid63 MAG_Out63 0 ) RCS_MCS_Corrector
+  PARAMS: L_mag=0.6972e-3 rGnd1=100e09 rGnd2=100e09 rGnd3=100e09 rGnd4=100e09
x_MCS64  ( MAG_In64 MAG_Mid64 MAG_Out64 0 ) RCS_MCS_Corrector
+  PARAMS: L_mag=0.6972e-3 rGnd1=100e09 rGnd2=100e09 rGnd3=100e09 rGnd4=100e09
x_MCS65  ( MAG_In65 MAG_Mid65 MAG_Out65 0 ) RCS_MCS_Corrector
+  PARAMS: L_mag=0.6972e-3 rGnd1=100e09 rGnd2=100e09 rGnd3=100e09 rGnd4=100e09
x_MCS66  ( MAG_In66 MAG_Mid66 MAG_Out66 0 ) RCS_MCS_Corrector
+  PARAMS: L_mag=0.6972e-3 rGnd1=100e09 rGnd2=100e09 rGnd3=100e09 rGnd4=100e09
x_MCS67  ( MAG_In67 MAG_Mid67 MAG_Out67 0 ) RCS_MCS_Corrector
+  PARAMS: L_mag=0.6972e-3 rGnd1=100e09 rGnd2=100e09 rGnd3=100e09 rGnd4=100e09
x_MCS68  ( MAG_In68 MAG_Mid68 MAG_Out68 0 ) RCS_MCS_Corrector
+  PARAMS: L_mag=0.6972e-3 rGnd1=100e09 rGnd2=100e09 rGnd3=100e09 rGnd4=100e09
x_MCS69  ( MAG_In69 MAG_Mid69 MAG_Out69 0 ) RCS_MCS_Corrector
+  PARAMS: L_mag=0.6972e-3 rGnd1=100e09 rGnd2=100e09 rGnd3=100e09 rGnd4=100e09
```

```
x_MCS70  ( MAG_In70 MAG_Mid70 MAG_Out70 0 ) RCS_MCS_Corrector
+  PARAMS: L_mag=0.6972e-3 rGnd1=100e09 rGnd2=100e09 rGnd3=100e09
    rGnd4=100e09
x_MCS71  ( MAG_In71 MAG_Mid71 MAG_Out71 0 ) RCS_MCS_Corrector
+  PARAMS: L_mag=0.6972e-3 rGnd1=100e09 rGnd2=100e09 rGnd3=100e09
    rGnd4=100e09
x_MCS72  ( MAG_In72 MAG_Mid72 MAG_Out72 0 ) RCS_MCS_Corrector
+  PARAMS: L_mag=0.6972e-3 rGnd1=100e09 rGnd2=100e09 rGnd3=100e09
    rGnd4=100e09
x_MCS73  ( MAG_In73 MAG_Mid73 MAG_Out73 0 ) RCS_MCS_Corrector
+  PARAMS: L_mag=0.6972e-3 rGnd1=100e09 rGnd2=100e09 rGnd3=100e09
    rGnd4=100e09
x_MCS74  ( MAG_In74 MAG_Mid74 MAG_Out74 0 ) RCS_MCS_Corrector
+  PARAMS: L_mag=0.6972e-3 rGnd1=100e09 rGnd2=100e09 rGnd3=100e09
    rGnd4=100e09
x_MCS75  ( MAG_In75 MAG_Mid75 MAG_Out75 0 ) RCS_MCS_Corrector
+  PARAMS: L_mag=0.6972e-3 rGnd1=100e09 rGnd2=100e09 rGnd3=100e09
    rGnd4=100e09
x_MCS76  ( MAG_In76 MAG_Mid76 MAG_Out76 0 ) RCS_MCS_Corrector
+  PARAMS: L_mag=0.6972e-3 rGnd1=100e09 rGnd2=100e09 rGnd3=100e09
    rGnd4=100e09
x_MCS77  ( MAG_In77 MAG_Mid77 MAG_Out77 0 ) RCS_MCS_Corrector
+  PARAMS: L_mag=0.6972e-3 rGnd1=100e09 rGnd2=100e09 rGnd3=100e09
    rGnd4=100e09
x_MCS78  ( MAG_In78 MAG_Mid78 MAG_Out78 0 ) RCS_MCS_Corrector
+  PARAMS: L_mag=0.6972e-3 rGnd1=100e09 rGnd2=100e09 rGnd3=100e09
    rGnd4=100e09
x_MCS79  ( MAG_In79 MAG_Mid79 MAG_Out79 0 ) RCS_MCS_Corrector
+  PARAMS: L_mag=0.6972e-3 rGnd1=100e09 rGnd2=100e09 rGnd3=100e09
    rGnd4=100e09
x_MCS80  ( MAG_In80 MAG_Mid80 MAG_Out80 0 ) RCS_MCS_Corrector
+  PARAMS: L_mag=0.6972e-3 rGnd1=100e09 rGnd2=100e09 rGnd3=100e09
    rGnd4=100e09
x_MCS81  ( MAG_In81 MAG_Mid81 MAG_Out81 0 ) RCS_MCS_Corrector
+  PARAMS: L_mag=0.6972e-3 rGnd1=100e09 rGnd2=100e09 rGnd3=100e09
    rGnd4=100e09
x_MCS82  ( MAG_In82 MAG_Mid82 MAG_Out82 0 ) RCS_MCS_Corrector
+  PARAMS: L_mag=0.6972e-3 rGnd1=100e09 rGnd2=100e09 rGnd3=100e09
    rGnd4=100e09
x_MCS83  ( MAG_In83 MAG_Mid83 MAG_Out83 0 ) RCS_MCS_Corrector
+  PARAMS: L_mag=0.6972e-3 rGnd1=100e09 rGnd2=100e09 rGnd3=100e09
    rGnd4=100e09
x_MCS84  ( MAG_In84 MAG_Mid84 MAG_Out84 0 ) RCS_MCS_Corrector
+  PARAMS: L_mag=0.6972e-3 rGnd1=100e09 rGnd2=100e09 rGnd3=100e09
    rGnd4=100e09
```

```
x_MCS85 ( MAG_In85 MAG_Mid85 MAG_Out85 0 ) RCS_MCS_Corrector
+ PARAMS: L_mag=0.6972e-3 rGnd1=100e09 rGnd2=100e09 rGnd3=100e09
    rGnd4=100e09
x_MCS86 ( MAG_In86 MAG_Mid86 MAG_Out86 0 ) RCS_MCS_Corrector
+ PARAMS: L_mag=0.6972e-3 rGnd1=100e09 rGnd2=100e09 rGnd3=100e09
    rGnd4=100e09
x_MCS87 ( MAG_In87 MAG_Mid87 MAG_Out87 0 ) RCS_MCS_Corrector
+ PARAMS: L_mag=0.6972e-3 rGnd1=100e09 rGnd2=100e09 rGnd3=100e09
    rGnd4=100e09
x_MCS88 ( MAG_In88 MAG_Mid88 MAG_Out88 0 ) RCS_MCS_Corrector
+ PARAMS: L_mag=0.6972e-3 rGnd1=100e09 rGnd2=100e09 rGnd3=100e09
    rGnd4=100e09
x_MCS89 ( MAG_In89 MAG_Mid89 MAG_Out89 0 ) RCS_MCS_Corrector
+ PARAMS: L_mag=0.6972e-3 rGnd1=100e09 rGnd2=100e09 rGnd3=100e09
    rGnd4=100e09
x_MCS90 ( MAG_In90 MAG_Mid90 MAG_Out90 0 ) RCS_MCS_Corrector
+ PARAMS: L_mag=0.6972e-3 rGnd1=100e09 rGnd2=100e09 rGnd3=100e09
    rGnd4=100e09
x_MCS91 ( MAG_In91 MAG_Mid91 MAG_Out91 0 ) RCS_MCS_Corrector
+ PARAMS: L_mag=0.6972e-3 rGnd1=100e09 rGnd2=100e09 rGnd3=100e09
    rGnd4=100e09
x_MCS92 ( MAG_In92 MAG_Mid92 MAG_Out92 0 ) RCS_MCS_Corrector
+ PARAMS: L_mag=0.6972e-3 rGnd1=100e09 rGnd2=100e09 rGnd3=100e09
    rGnd4=100e09
x_MCS93 ( MAG_In93 MAG_Mid93 MAG_Out93 0 ) RCS_MCS_Corrector
+ PARAMS: L_mag=0.6972e-3 rGnd1=100e09 rGnd2=100e09 rGnd3=100e09
    rGnd4=100e09
x_MCS94 ( MAG_In94 MAG_Mid94 MAG_Out94 0 ) RCS_MCS_Corrector
+ PARAMS: L_mag=0.6972e-3 rGnd1=100e09 rGnd2=100e09 rGnd3=100e09
    rGnd4=100e09
x_MCS95 ( MAG_In95 MAG_Mid95 MAG_Out95 0 ) RCS_MCS_Corrector
+ PARAMS: L_mag=0.6972e-3 rGnd1=100e09 rGnd2=100e09 rGnd3=100e09
    rGnd4=100e09
x_MCS96 ( MAG_In96 MAG_Mid96 MAG_Out96 0 ) RCS_MCS_Corrector
+ PARAMS: L_mag=0.6972e-3 rGnd1=100e09 rGnd2=100e09 rGnd3=100e09
    rGnd4=100e09
x_MCS97 ( MAG_In97 MAG_Mid97 MAG_Out97 0 ) RCS_MCS_Corrector
+ PARAMS: L_mag=0.6972e-3 rGnd1=100e09 rGnd2=100e09 rGnd3=100e09
    rGnd4=100e09
x_MCS98 ( MAG_In98 MAG_Mid98 MAG_Out98 0 ) RCS_MCS_Corrector
+ PARAMS: L_mag=0.6972e-3 rGnd1=100e09 rGnd2=100e09 rGnd3=100e09
    rGnd4=100e09
x_MCS99 ( MAG_In99 MAG_Mid99 MAG_Out99 0 ) RCS_MCS_Corrector
+ PARAMS: L_mag=0.6972e-3 rGnd1=100e09 rGnd2=100e09 rGnd3=100e09
    rGnd4=100e09
```

```
x_MCS100 ( MAG_In100 MAG_Mid100 MAG_Out100 0 ) RCS_MCS_Corrector
+ PARAMS: L_mag=0.6972e-3 rGnd1=100e09 rGnd2=100e09 rGnd3=100e09 rGnd4=100e09
x_MCS101 ( MAG_In101 MAG_Mid101 MAG_Out101 0 ) RCS_MCS_Corrector
+ PARAMS: L_mag=0.6972e-3 rGnd1=100e09 rGnd2=100e09 rGnd3=100e09 rGnd4=100e09
x_MCS102 ( MAG_In102 MAG_Mid102 MAG_Out102 0 ) RCS_MCS_Corrector
+ PARAMS: L_mag=0.6972e-3 rGnd1=100e09 rGnd2=100e09 rGnd3=100e09 rGnd4=100e09
x_MCS103 ( MAG_In103 MAG_Mid103 MAG_Out103 0 ) RCS_MCS_Corrector
+ PARAMS: L_mag=0.6972e-3 rGnd1=100e09 rGnd2=100e09 rGnd3=100e09 rGnd4=100e09
x_MCS104 ( MAG_In104 MAG_Mid104 MAG_Out104 0 ) RCS_MCS_Corrector
+ PARAMS: L_mag=0.6972e-3 rGnd1=100e09 rGnd2=100e09 rGnd3=100e09 rGnd4=100e09
x_MCS105 ( MAG_In105 MAG_Mid105 MAG_Out105 0 ) RCS_MCS_Corrector
+ PARAMS: L_mag=0.6972e-3 rGnd1=100e09 rGnd2=100e09 rGnd3=100e09 rGnd4=100e09
x_MCS106 ( MAG_In106 MAG_Mid106 MAG_Out106 0 ) RCS_MCS_Corrector
+ PARAMS: L_mag=0.6972e-3 rGnd1=100e09 rGnd2=100e09 rGnd3=100e09 rGnd4=100e09
x_MCS107 ( MAG_In107 MAG_Mid107 MAG_Out107 0 ) RCS_MCS_Corrector
+ PARAMS: L_mag=0.6972e-3 rGnd1=100e09 rGnd2=100e09 rGnd3=100e09 rGnd4=100e09
x_MCS108 ( MAG_In108 MAG_Mid108 MAG_Out108 0 ) RCS_MCS_Corrector
+ PARAMS: L_mag=0.6972e-3 rGnd1=100e09 rGnd2=100e09 rGnd3=100e09 rGnd4=100e09
x_MCS109 ( MAG_In109 MAG_Mid109 MAG_Out109 0 ) RCS_MCS_Corrector
+ PARAMS: L_mag=0.6972e-3 rGnd1=100e09 rGnd2=100e09 rGnd3=100e09 rGnd4=100e09
x_MCS110 ( MAG_In110 MAG_Mid110 MAG_Out110 0 ) RCS_MCS_Corrector
+ PARAMS: L_mag=0.6972e-3 rGnd1=100e09 rGnd2=100e09 rGnd3=100e09 rGnd4=100e09
x_MCS111 ( MAG_In111 MAG_Mid111 MAG_Out111 0 ) RCS_MCS_Corrector
+ PARAMS: L_mag=0.6972e-3 rGnd1=100e09 rGnd2=100e09 rGnd3=100e09 rGnd4=100e09
x_MCS112 ( MAG_In112 MAG_Mid112 MAG_Out112 0 ) RCS_MCS_Corrector
+ PARAMS: L_mag=0.6972e-3 rGnd1=100e09 rGnd2=100e09 rGnd3=100e09 rGnd4=100e09
x_MCS113 ( MAG_In113 MAG_Mid113 MAG_Out113 0 ) RCS_MCS_Corrector
+ PARAMS: L_mag=0.6972e-3 rGnd1=100e09 rGnd2=100e09 rGnd3=100e09 rGnd4=100e09
x_MCS114 ( MAG_In114 MAG_Mid114 MAG_Out114 0 ) RCS_MCS_Corrector
+ PARAMS: L_mag=0.6972e-3 rGnd1=100e09 rGnd2=100e09 rGnd3=100e09 rGnd4=100e09
```

```
x_MCS115  ( MAG_In115 MAG_Mid115 MAG_Out115 0 ) RCS_MCS_Corrector
+  PARAMS: L_mag=0.6972e-3 rGnd1=100e09 rGnd2=100e09 rGnd3=100e09 rGnd4=100e09
x_MCS116  ( MAG_In116 MAG_Mid116 MAG_Out116 0 ) RCS_MCS_Corrector
+  PARAMS: L_mag=0.6972e-3 rGnd1=100e09 rGnd2=100e09 rGnd3=100e09 rGnd4=100e09
x_MCS117  ( MAG_In117 MAG_Mid117 MAG_Out117 0 ) RCS_MCS_Corrector
+  PARAMS: L_mag=0.6972e-3 rGnd1=100e09 rGnd2=100e09 rGnd3=100e09 rGnd4=100e09
x_MCS118  ( MAG_In118 MAG_Mid118 MAG_Out118 0 ) RCS_MCS_Corrector
+  PARAMS: L_mag=0.6972e-3 rGnd1=100e09 rGnd2=100e09 rGnd3=100e09 rGnd4=100e09
x_MCS119  ( MAG_In119 MAG_Mid119 MAG_Out119 0 ) RCS_MCS_Corrector
+  PARAMS: L_mag=0.6972e-3 rGnd1=100e09 rGnd2=100e09 rGnd3=100e09 rGnd4=100e09
x_MCS120  ( MAG_In120 MAG_Mid120 MAG_Out120 0 ) RCS_MCS_Corrector
+  PARAMS: L_mag=0.6972e-3 rGnd1=100e09 rGnd2=100e09 rGnd3=100e09 rGnd4=100e09
x_MCS121  ( MAG_In121 MAG_Mid121 MAG_Out121 0 ) RCS_MCS_Corrector
+  PARAMS: L_mag=0.6972e-3 rGnd1=100e09 rGnd2=100e09 rGnd3=100e09 rGnd4=100e09
x_MCS122  ( MAG_In122 MAG_Mid122 MAG_Out122 0 ) RCS_MCS_Corrector
+  PARAMS: L_mag=0.6972e-3 rGnd1=100e09 rGnd2=100e09 rGnd3=100e09 rGnd4=100e09
x_MCS123  ( MAG_In123 MAG_Mid123 MAG_Out123 0 ) RCS_MCS_Corrector
+  PARAMS: L_mag=0.6972e-3 rGnd1=100e09 rGnd2=100e09 rGnd3=100e09 rGnd4=100e09
x_MCS124  ( MAG_In124 MAG_Mid124 MAG_Out124 0 ) RCS_MCS_Corrector
+  PARAMS: L_mag=0.6972e-3 rGnd1=100e09 rGnd2=100e09 rGnd3=100e09 rGnd4=100e09
x_MCS125  ( MAG_In125 MAG_Mid125 MAG_Out125 0 ) RCS_MCS_Corrector
+  PARAMS: L_mag=0.6972e-3 rGnd1=100e09 rGnd2=100e09 rGnd3=100e09 rGnd4=100e09
x_MCS126  ( MAG_In126 MAG_Mid126 MAG_Out126 0 ) RCS_MCS_Corrector
+  PARAMS: L_mag=0.6972e-3 rGnd1=100e09 rGnd2=100e09 rGnd3=100e09 rGnd4=100e09
x_MCS127  ( MAG_In127 MAG_Mid127 MAG_Out127 0 ) RCS_MCS_Corrector
+  PARAMS: L_mag=0.6972e-3 rGnd1=100e09 rGnd2=100e09 rGnd3=100e09 rGnd4=100e09
x_MCS128  ( MAG_In128 MAG_Mid128 MAG_Out128 0 ) RCS_MCS_Corrector
+  PARAMS: L_mag=0.6972e-3 rGnd1=100e09 rGnd2=100e09 rGnd3=100e09 rGnd4=100e09
x_MCS129  ( MAG_In129 MAG_Mid129 MAG_Out129 0 ) RCS_MCS_Corrector
+  PARAMS: L_mag=0.6972e-3 rGnd1=100e09 rGnd2=100e09 rGnd3=100e09 rGnd4=100e09
```

```
x_MCS130 ( MAG_In130 MAG_Mid130 MAG_Out130 0 ) RCS_MCS_Corrector
+ PARAMS: L_mag=0.6972e-3 rGnd1=100e09 rGnd2=100e09 rGnd3=100e09
    rGnd4=100e09
x_MCS131 ( MAG_In131 MAG_Mid131 MAG_Out131 0 ) RCS_MCS_Corrector
+ PARAMS: L_mag=0.6972e-3 rGnd1=100e09 rGnd2=100e09 rGnd3=100e09
    rGnd4=100e09
x_MCS132 ( MAG_In132 MAG_Mid132 MAG_Out132 0 ) RCS_MCS_Corrector
+ PARAMS: L_mag=0.6972e-3 rGnd1=100e09 rGnd2=100e09 rGnd3=100e09
    rGnd4=100e09
x_MCS133 ( MAG_In133 MAG_Mid133 MAG_Out133 0 ) RCS_MCS_Corrector
+ PARAMS: L_mag=0.6972e-3 rGnd1=100e09 rGnd2=100e09 rGnd3=100e09
    rGnd4=100e09
x_MCS134 ( MAG_In134 MAG_Mid134 MAG_Out134 0 ) RCS_MCS_Corrector
+ PARAMS: L_mag=0.6972e-3 rGnd1=100e09 rGnd2=100e09 rGnd3=100e09
    rGnd4=100e09
x_MCS135 ( MAG_In135 MAG_Mid135 MAG_Out135 0 ) RCS_MCS_Corrector
+ PARAMS: L_mag=0.6972e-3 rGnd1=100e09 rGnd2=100e09 rGnd3=100e09
    rGnd4=100e09
x_MCS136 ( MAG_In136 MAG_Mid136 MAG_Out136 0 ) RCS_MCS_Corrector
+ PARAMS: L_mag=0.6972e-3 rGnd1=100e09 rGnd2=100e09 rGnd3=100e09
    rGnd4=100e09
x_MCS137 ( MAG_In137 MAG_Mid137 MAG_Out137 0 ) RCS_MCS_Corrector
+ PARAMS: L_mag=0.6972e-3 rGnd1=100e09 rGnd2=100e09 rGnd3=100e09
    rGnd4=100e09
x_MCS138 ( MAG_In138 MAG_Mid138 MAG_Out138 0 ) RCS_MCS_Corrector
+ PARAMS: L_mag=0.6972e-3 rGnd1=100e09 rGnd2=100e09 rGnd3=100e09
    rGnd4=100e09
x_MCS139 ( MAG_In139 MAG_Mid139 MAG_Out139 0 ) RCS_MCS_Corrector
+ PARAMS: L_mag=0.6972e-3 rGnd1=100e09 rGnd2=100e09 rGnd3=100e09
    rGnd4=100e09
x_MCS140 ( MAG_In140 MAG_Mid140 MAG_Out140 0 ) RCS_MCS_Corrector
+ PARAMS: L_mag=0.6972e-3 rGnd1=100e09 rGnd2=100e09 rGnd3=100e09
    rGnd4=100e09
x_MCS141 ( MAG_In141 MAG_Mid141 MAG_Out141 0 ) RCS_MCS_Corrector
+ PARAMS: L_mag=0.6972e-3 rGnd1=100e09 rGnd2=100e09 rGnd3=100e09
    rGnd4=100e09
x_MCS142 ( MAG_In142 MAG_Mid142 MAG_Out142 0 ) RCS_MCS_Corrector
+ PARAMS: L_mag=0.6972e-3 rGnd1=100e09 rGnd2=100e09 rGnd3=100e09
    rGnd4=100e09
x_MCS143 ( MAG_In143 MAG_Mid143 MAG_Out143 0 ) RCS_MCS_Corrector
+ PARAMS: L_mag=0.6972e-3 rGnd1=100e09 rGnd2=100e09 rGnd3=100e09
    rGnd4=100e09
x_MCS144 ( MAG_In144 MAG_Mid144 MAG_Out144 0 ) RCS_MCS_Corrector
+ PARAMS: L_mag=0.6972e-3 rGnd1=100e09 rGnd2=100e09 rGnd3=100e09
    rGnd4=100e09
```

```
x_MCS145  ( MAG_In145 MAG_Mid145 MAG_Out145 0 ) RCS_MCS_Corrector
+  PARAMS: L_mag=0.6972e-3 rGnd1=100e09 rGnd2=100e09 rGnd3=100e09 rGnd4=100e09
x_MCS146  ( MAG_In146 MAG_Mid146 MAG_Out146 0 ) RCS_MCS_Corrector
+  PARAMS: L_mag=0.6972e-3 rGnd1=100e09 rGnd2=100e09 rGnd3=100e09 rGnd4=100e09
x_MCS147  ( MAG_In147 MAG_Mid147 MAG_Out147 0 ) RCS_MCS_Corrector
+  PARAMS: L_mag=0.6972e-3 rGnd1=100e09 rGnd2=100e09 rGnd3=100e09 rGnd4=100e09
x_MCS148  ( MAG_In148 MAG_Mid148 MAG_Out148 0 ) RCS_MCS_Corrector
+  PARAMS: L_mag=0.6972e-3 rGnd1=100e09 rGnd2=100e09 rGnd3=100e09 rGnd4=100e09
x_MCS149  ( MAG_In149 MAG_Mid149 MAG_Out149 0 ) RCS_MCS_Corrector
+  PARAMS: L_mag=0.6972e-3 rGnd1=100e09 rGnd2=100e09 rGnd3=100e09 rGnd4=100e09
x_MCS150  ( MAG_In150 MAG_Mid150 MAG_Out150 0 ) RCS_MCS_Corrector
+  PARAMS: L_mag=0.6972e-3 rGnd1=100e09 rGnd2=100e09 rGnd3=100e09 rGnd4=100e09
x_MCS151  ( MAG_In151 MAG_Mid151 MAG_Out151 0 ) RCS_MCS_Corrector
+  PARAMS: L_mag=0.6972e-3 rGnd1=100e09 rGnd2=100e09 rGnd3=100e09 rGnd4=100e09
x_MCS152  ( MAG_In152 MAG_Mid152 MAG_Out152 0 ) RCS_MCS_Corrector
+  PARAMS: L_mag=0.6972e-3 rGnd1=100e09 rGnd2=100e09 rGnd3=100e09 rGnd4=100e09
x_MCS153  ( MAG_In153 MAG_Mid153 MAG_Out153 0 ) RCS_MCS_Corrector
+  PARAMS: L_mag=0.6972e-3 rGnd1=100e09 rGnd2=100e09 rGnd3=100e09 rGnd4=100e09
x_MCS154  ( MAG_In154 MAG_Mid154 MAG_Out154 0 ) RCS_MCS_Corrector
+  PARAMS: L_mag=0.6972e-3 rGnd1=100e09 rGnd2=100e09 rGnd3=100e09 rGnd4=100e09
*Spool-piece Busbars*********************************************
x_BusBar_1  ( MAG_In154 MAG_Out153 MAG_Out1 MAG_In2 BB3_In1 BB3_In2 ) RCS_BusBar_WithIron
x_BusBar_2  ( MAG_In153 MAG_Out152 MAG_Out2 MAG_In3 BB3_In2 BB3_In3 ) RCS_BusBar_WithIron
x_BusBar_3  ( MAG_In152 MAG_Out151 MAG_Out3 MAG_In4 BB3_In3 BB3_In4 ) RCS_BusBar_WithIron
x_BusBar_4  ( MAG_In151 MAG_Out150 MAG_Out4 MAG_In5 BB3_In4 BB3_In5 ) RCS_BusBar_WithIron
x_BusBar_5  ( MAG_In150 MAG_Out149 MAG_Out5 MAG_In6 BB3_In5 BB3_In6 ) RCS_BusBar_WithIron
x_BusBar_6  ( MAG_In149 MAG_Out148 MAG_Out6 MAG_In7 BB3_In6 BB3_In7 ) RCS_BusBar_WithIron
x_BusBar_7  ( MAG_In148 MAG_Out147 MAG_Out7 MAG_In8 BB3_In7 BB3_In8 ) RCS_BusBar_WithIron
```

```
x_BusBar_8  ( MAG_In147 MAG_Out146 MAG_Out8 MAG_In9 BB3_In8 BB3_In9 ) RCS_BusBar_WithIron
x_BusBar_9  ( MAG_In146 MAG_Out145 MAG_Out9 MAG_In10 BB3_In9 BB3_In10 ) RCS_BusBar_WithIron
x_BusBar_10  ( MAG_In145 MAG_Out144 MAG_Out10 MAG_In11 BB3_In10 BB3_In11 ) RCS_BusBar_WithIron
x_BusBar_11  ( MAG_In144 MAG_Out143 MAG_Out11 MAG_In12 BB3_In11 BB3_In12 ) RCS_BusBar_WithIron
x_BusBar_12  ( MAG_In143 MAG_Out142 MAG_Out12 MAG_In13 BB3_In12 BB3_In13 ) RCS_BusBar_WithIron
x_BusBar_13  ( MAG_In142 MAG_Out141 MAG_Out13 MAG_In14 BB3_In13 BB3_In14 ) RCS_BusBar_WithIron
x_BusBar_14  ( MAG_In141 MAG_Out140 MAG_Out14 MAG_In15 BB3_In14 BB3_In15 ) RCS_BusBar_WithIron
x_BusBar_15  ( MAG_In140 MAG_Out139 MAG_Out15 MAG_In16 BB3_In15 BB3_In16 ) RCS_BusBar_WithIron
x_BusBar_16  ( MAG_In139 MAG_Out138 MAG_Out16 MAG_In17 BB3_In16 BB3_In17 ) RCS_BusBar_WithIron
x_BusBar_17  ( MAG_In138 MAG_Out137 MAG_Out17 MAG_In18 BB3_In17 BB3_In18 ) RCS_BusBar_WithIron
x_BusBar_18  ( MAG_In137 MAG_Out136 MAG_Out18 MAG_In19 BB3_In18 BB3_In19 ) RCS_BusBar_WithIron
x_BusBar_19  ( MAG_In136 MAG_Out135 MAG_Out19 MAG_In20 BB3_In19 BB3_In20 ) RCS_BusBar_WithIron
x_BusBar_20  ( MAG_In135 MAG_Out134 MAG_Out20 MAG_In21 BB3_In20 BB3_In21 ) RCS_BusBar_WithIron
x_BusBar_21  ( MAG_In134 MAG_Out133 MAG_Out21 MAG_In22 BB3_In21 BB3_In22 ) RCS_BusBar_WithIron
x_BusBar_22  ( MAG_In133 MAG_Out132 MAG_Out22 MAG_In23 BB3_In22 BB3_In23 ) RCS_BusBar_WithIron
x_BusBar_23  ( MAG_In132 MAG_Out131 MAG_Out23 MAG_In24 BB3_In23 BB3_In24 ) RCS_BusBar_WithIron
x_BusBar_24  ( MAG_In131 MAG_Out130 MAG_Out24 MAG_In25 BB3_In24 BB3_In25 ) RCS_BusBar_WithIron
x_BusBar_25  ( MAG_In130 MAG_Out129 MAG_Out25 MAG_In26 BB3_In25 BB3_In26 ) RCS_BusBar_WithIron
x_BusBar_26  ( MAG_In129 MAG_Out128 MAG_Out26 MAG_In27 BB3_In26 BB3_In27 ) RCS_BusBar_WithIron
x_BusBar_27  ( MAG_In128 MAG_Out127 MAG_Out27 MAG_In28 BB3_In27 BB3_In28 ) RCS_BusBar_WithIron
x_BusBar_28  ( MAG_In127 MAG_Out126 MAG_Out28 MAG_In29 BB3_In28 BB3_In29 ) RCS_BusBar_WithIron
x_BusBar_29  ( MAG_In126 MAG_Out125 MAG_Out29 MAG_In30 BB3_In29 BB3_In30 ) RCS_BusBar_WithIron
```

```
x_BusBar_30  ( MAG_In125 MAG_Out124 MAG_Out30 MAG_In31 BB3_In30 BB3_In31 ) RCS_BusBar_WithIron
x_BusBar_31  ( MAG_In124 MAG_Out123 MAG_Out31 MAG_In32 BB3_In31 BB3_In32 ) RCS_BusBar_WithIron
x_BusBar_32  ( MAG_In123 MAG_Out122 MAG_Out32 MAG_In33 BB3_In32 BB3_In33 ) RCS_BusBar_WithIron
x_BusBar_33  ( MAG_In122 MAG_Out121 MAG_Out33 MAG_In34 BB3_In33 BB3_In34 ) RCS_BusBar_WithIron
x_BusBar_34  ( MAG_In121 MAG_Out120 MAG_Out34 MAG_In35 BB3_In34 BB3_In35 ) RCS_BusBar_WithIron
x_BusBar_35  ( MAG_In120 MAG_Out119 MAG_Out35 MAG_In36 BB3_In35 BB3_In36 ) RCS_BusBar_WithIron
x_BusBar_36  ( MAG_In119 MAG_Out118 MAG_Out36 MAG_In37 BB3_In36 BB3_In37 ) RCS_BusBar_WithIron
x_BusBar_37  ( MAG_In118 MAG_Out117 MAG_Out37 MAG_In38 BB3_In37 BB3_In38 ) RCS_BusBar_WithIron
x_BusBar_38  ( MAG_In117 MAG_Out116 MAG_Out38 MAG_In39 BB3_In38 BB3_In39 ) RCS_BusBar_WithIron
x_BusBar_39  ( MAG_In116 MAG_Out115 MAG_Out39 MAG_In40 BB3_In39 BB3_In40 ) RCS_BusBar_WithIron
x_BusBar_40  ( MAG_In115 MAG_Out114 MAG_Out40 MAG_In41 BB3_In40 BB3_In41 ) RCS_BusBar_WithIron
x_BusBar_41  ( MAG_In114 MAG_Out113 MAG_Out41 MAG_In42 BB3_In41 BB3_In42 ) RCS_BusBar_WithIron
x_BusBar_42  ( MAG_In113 MAG_Out112 MAG_Out42 MAG_In43 BB3_In42 BB3_In43 ) RCS_BusBar_WithIron
x_BusBar_43  ( MAG_In112 MAG_Out111 MAG_Out43 MAG_In44 BB3_In43 BB3_In44 ) RCS_BusBar_WithIron
x_BusBar_44  ( MAG_In111 MAG_Out110 MAG_Out44 MAG_In45 BB3_In44 BB3_In45 ) RCS_BusBar_WithIron
x_BusBar_45  ( MAG_In110 MAG_Out109 MAG_Out45 MAG_In46 BB3_In45 BB3_In46 ) RCS_BusBar_WithIron
x_BusBar_46  ( MAG_In109 MAG_Out108 MAG_Out46 MAG_In47 BB3_In46 BB3_In47 ) RCS_BusBar_WithIron
x_BusBar_47  ( MAG_In108 MAG_Out107 MAG_Out47 MAG_In48 BB3_In47 BB3_In48 ) RCS_BusBar_WithIron
x_BusBar_48  ( MAG_In107 MAG_Out106 MAG_Out48 MAG_In49 BB3_In48 BB3_In49 ) RCS_BusBar_WithIron
x_BusBar_49  ( MAG_In106 MAG_Out105 MAG_Out49 MAG_In50 BB3_In49 BB3_In50 ) RCS_BusBar_WithIron
x_BusBar_50  ( MAG_In105 MAG_Out104 MAG_Out50 MAG_In51 BB3_In50 BB3_In51 ) RCS_BusBar_WithIron
x_BusBar_51  ( MAG_In104 MAG_Out103 MAG_Out51 MAG_In52 BB3_In51 BB3_In52 ) RCS_BusBar_WithIron
```

```
x_BusBar_52  ( MAG_In103 MAG_Out102 MAG_Out52 MAG_In53 BB3_In52
    BB3_In53 ) RCS_BusBar_WithIron
x_BusBar_53  ( MAG_In102 MAG_Out101 MAG_Out53 MAG_In54 BB3_In53
    BB3_In54 ) RCS_BusBar_WithIron
x_BusBar_54  ( MAG_In101 MAG_Out100 MAG_Out54 MAG_In55 BB3_In54
    BB3_In55 ) RCS_BusBar_WithIron
x_BusBar_55  ( MAG_In100 MAG_Out99 MAG_Out55 MAG_In56 BB3_In55
    BB3_In56 ) RCS_BusBar_WithIron
x_BusBar_56  ( MAG_In99 MAG_Out98 MAG_Out56 MAG_In57 BB3_In56
    BB3_In57 ) RCS_BusBar_WithIron
x_BusBar_57  ( MAG_In98 MAG_Out97 MAG_Out57 MAG_In58 BB3_In57
    BB3_In58 ) RCS_BusBar_WithIron
x_BusBar_58  ( MAG_In97 MAG_Out96 MAG_Out58 MAG_In59 BB3_In58
    BB3_In59 ) RCS_BusBar_WithIron
x_BusBar_59  ( MAG_In96 MAG_Out95 MAG_Out59 MAG_In60 BB3_In59
    BB3_In60 ) RCS_BusBar_WithIron
x_BusBar_60  ( MAG_In95 MAG_Out94 MAG_Out60 MAG_In61 BB3_In60
    BB3_In61 ) RCS_BusBar_WithIron
x_BusBar_61  ( MAG_In94 MAG_Out93 MAG_Out61 MAG_In62 BB3_In61
    BB3_In62 ) RCS_BusBar_WithIron
x_BusBar_62  ( MAG_In93 MAG_Out92 MAG_Out62 MAG_In63 BB3_In62
    BB3_In63 ) RCS_BusBar_WithIron
x_BusBar_63  ( MAG_In92 MAG_Out91 MAG_Out63 MAG_In64 BB3_In63
    BB3_In64 ) RCS_BusBar_WithIron
x_BusBar_64  ( MAG_In91 MAG_Out90 MAG_Out64 MAG_In65 BB3_In64
    BB3_In65 ) RCS_BusBar_WithIron
x_BusBar_65  ( MAG_In90 MAG_Out89 MAG_Out65 MAG_In66 BB3_In65
    BB3_In66 ) RCS_BusBar_WithIron
x_BusBar_66  ( MAG_In89 MAG_Out88 MAG_Out66 MAG_In67 BB3_In66
    BB3_In67 ) RCS_BusBar_WithIron
x_BusBar_67  ( MAG_In88 MAG_Out87 MAG_Out67 MAG_In68 BB3_In67
    BB3_In68 ) RCS_BusBar_WithIron
x_BusBar_68  ( MAG_In87 MAG_Out86 MAG_Out68 MAG_In69 BB3_In68
    BB3_In69 ) RCS_BusBar_WithIron
x_BusBar_69  ( MAG_In86 MAG_Out85 MAG_Out69 MAG_In70 BB3_In69
    BB3_In70 ) RCS_BusBar_WithIron
x_BusBar_70  ( MAG_In85 MAG_Out84 MAG_Out70 MAG_In71 BB3_In70
    BB3_In71 ) RCS_BusBar_WithIron
x_BusBar_71  ( MAG_In84 MAG_Out83 MAG_Out71 MAG_In72 BB3_In71
    BB3_In72 ) RCS_BusBar_WithIron
x_BusBar_72  ( MAG_In83 MAG_Out82 MAG_Out72 MAG_In73 BB3_In72
    BB3_In73 ) RCS_BusBar_WithIron
x_BusBar_73  ( MAG_In82 MAG_Out81 MAG_Out73 MAG_In74 BB3_In73
    BB3_In74 ) RCS_BusBar_WithIron
```

```
x_BusBar_74  ( MAG_In81 MAG_Out80 MAG_Out74 MAG_In75 BB3_In74 BB3_In75 ) RCS_BusBar_WithIron
x_BusBar_75  ( MAG_In80 MAG_Out79 MAG_Out75 MAG_In76 BB3_In75 BB3_In76 ) RCS_BusBar_WithIron
x_BusBar_76  ( MAG_In79 MAG_Out78 MAG_Out76 MAG_In77 BB3_In76 BB3_In77 ) RCS_BusBar_WithIron

*Spool-piece Busbar spatial end******************************
v_Bb78_1 (MAG_Out77 MAG_In78) 0
v_Bb78_2 (MAG_Out77 BB3_In77) 0
.ends
```

A.2 Matlab Code for circut handling and analysis

A.2.1 Circuit file adaptation

```
function [] = changeModelERROR( fileNameOrigBB, fileName2owBB, ...
fileNameOrigCircuit, fileName2owCircuit, parameters, circuitnode)

  fid = fopen(fileNameOrigBB);
  txt = '';
  tline = fgetl(fid);
  while ischar(tline)
    disp(tline)
    tline = fgetl(fid);
    txt = [txt tline '\n'];
  end
  fclose(fid);
  for(k = 1:length(parameters))
    txt = strrep(txt,['varParam(',num2str(k),')'],num2str(parameters(k)));
  end
  disp(txt);
  fid = fopen(fileName2owBB, 'w');
  fprintf(fid,txt);
  fclose(fid);

  fid2 = fopen(fileNameOrigCircuit);
  txt2 = '';
  tline2 = fgetl(fid2);
  while ischar(tline2)
    disp(tline2)
    tline2 = fgetl(fid2);
    txt2 = [txt2 tline2 '\n'];
```

```
    end
    fclose(fid2);
    for(k = 1:length(circuitnode))
      txt2 = strrep(txt2,'varParamNode',num2str(circuitnode));
    end
    disp(txt2);
    fid2 = fopen(fileName2owCircuit, 'w');
    fprintf(fid2,txt2);
    fclose(fid2);

end
```

A.2.2 Error calculation simulation vs. measurement

```
function [e] = calcError (measurement, vch0, vch1, vch2, vch3,
    freq, fpoints)

    freq1 = measurement(:,1);
    mag_ch0_1 = measurement(:,2);
    mag_ch1_1 = measurement(:,3);
    mag_ch2_1 = measurement(:,4);
    mag_ch3_1 = measurement(:,8);

    ch0_meas_resamp_y = spline ( freq1, mag_ch0_1, fpoints);
    ch1_meas_resamp_y = spline ( freq1, mag_ch1_1, fpoints);
    ch2_meas_resamp_y = spline ( freq1, mag_ch2_1, fpoints);
    ch3_meas_resamp_y = spline ( freq1, mag_ch3_1, fpoints);

    ch0_sim_resamp_y = spline ( freq, vch0, fpoints);
    ch1_sim_resamp_y = spline ( freq, vch1, fpoints);
    ch2_sim_resamp_y = spline ( freq, vch2, fpoints);
    ch3_sim_resamp_y = spline ( freq, vch3, fpoints);

    e0 = 0;
    e1 = 0;
    e2 = 0;
    e3 = 0;

    for q= 1: 1 : 1451
      e0 = e0 + (((ch0_meas_resamp_y(1,q) -
     ch0_sim_resamp_y(1,q))^2)^(1/2));
      e1 = e1 + (((ch1_meas_resamp_y(1,q) -
     ch1_sim_resamp_y(1,q))^2)^(1/2));
      e2 = e2 + (((ch2_meas_resamp_y(1,q) -
     ch2_sim_resamp_y(1,q))^2)^(1/2));
```

```
    e3 = e3 + (((ch3_meas_resamp_y(1,q) -
   ch3_sim_resamp_y(1,q))^2)^(1/2));
  end
  e0 = e0/451;
  e1 = e1/451;
  e2 = e2/451;
  e3 = e3/451;
  eall = e0 + e1 + e2 + e3;
  e = [e0 e1 e2 e3 eall];

end
```